Linköping Studies in Science and Technology
Thesis No. 611

Experimental Design and Updating of Finite Element Models

Magnus Andersson

REGLERTEKNIK
AUTOMATIC CONTROL
LINKÖPING

Division of Automatic Control
Department of Electrical Engineering
Linköping University, S–581 83 Linköping, Sweden
WWW: `http://www.control.isy.liu.se`
Email: `magnusa@isy.liu.se`

Linköping 1997

Experimental Design and Updating of Finite Element Models

Department of Electrical Engineering,
Linköping University,
S–581 83 Linköping,
Sweden.

ISBN 91-7871-928-3
ISSN 0280-7971
LiU-TEK-LIC-1997:12

To my future wife,
-whoever she might be [1]

[1] Citation, found in [41].

Abstract

This thesis deals with two partly related topics: model updating and actuator/sensor placement concerning finite element (FE) models of large, flexible mechanical structures.

The importance of accurate dynamical FE models of mechanical structures in, e.g., aviation/aerospace applications are steadily increasing. For instance, a sufficient accurate model may reduce the expenses for ground vibration testing and wind-tunnel experiments substantially. It is therefore of high industrial interest to obtain accurate models of flexible structures. One approach is to improve a parameterized, initial FE model using measurements of the real structure, so-called model updating. For a fast, successful model updating, three requirements must be fulfilled. The model updating must be computationally cheap, which requires an efficient model reduction technique. The cost function describing the deviation between the model output and the measurements must have good convexity properties so that an estimation of the parameters corresponding to the global optimum is likely to be obtained. Finally, the optimization methods must be reliable. A novel mode-pairing free cost function is presented, and together with a proposed general procedure for model updating, a cheap model updating formulation with good parameter estimation properties is obtained.

Actuator and sensor placement is a part of the experimental design. It is performed in advance of the vibrational experiment in order to ensure high quality measurements. Using a nominal FE model of the structure, an actuator/sensor placement can be made. Actuator/sensor placement tasks are generally discrete, non-convex optimization problems of high complexity. One is therefore restricted to the use of sub-optimal algorithms in order to fulfill time and memory storage requirements. A computationally cheap algorithm for general actuator/sensor placement objectives are proposed. A generalization of an actuator/sensor placement criterion for model updating, and a novel noise-robust actuator placement criterion for experimental modal analysis are proposed.

Acknowledgment

First of all, I would like to thank Prof. Lennart Ljung for giving me the opportunity to join the control group. Together with Prof. Torkel Glad he has created a very stimulating atmosphere for research. Ever since the first minute here, I have become more and more impressed about their ability to engage people working around them. I would also like to thank our secretary Ulla Salaneck for keeping the administration on the right track.

The work presented in this licentiate thesis has been made as a part of a project initiated by the NFFP (Nationellt FlygForskningsProgram). Together with my advisor Prof. Lennart Ljung, Dr. Tomas McKelvey, and Dr. Thomas Abrahamsson at SAAB AB, as well as all other participants in the project, I have had many fruitful discussions concerning my work. Without them, I would probably not be sitting here writing this sentence for many years....

Today computers are inevitable, but with the superb help from Magnus Sundstedt and Mattias Olofsson, they have not become an insuperable problem. Thanks also to Mats Jirstrand for his patient answers about LaTeX.

The early versions of this thesis had not a high correlation with the actual copy in your hand, since there probably were more errors than words at that time. Thanks to Krister Edström and Dr. Peter Lindskog for giving me advice to improve the grammar as well as the contest. For the errors not being corrected, the responsibility is totally mine.

Besides the people mentioned above, there are many other people that contributes to the nice spirit always appearing in our *fika*-room. The lively discussions emerging there, are really becoming an addict. When nothing else helps, a stay there is often enough to clear up my mind.

Finally, I am indebted to my parents Inger and Carl-Eric for their love and support ever since my first staggering steps a long time ago, as well as my sister Malin who has been an invaluable encouragement for many, many times.

Linköping, March 1997

Magnus Andersson

Contents

Notation

Symbols

$\mathbb{R}$, $\mathbb{C}$	the sets of real and complex numbers
$\emptyset$	the empty set
A_s, B_s, C_s, D_s	the matrices defining the state space model
B, C, C_a, D	matrices defining the I/O model for an FE model
G	FRF of an I/O model
M, L, K	the system matrices of an FE model, modeling the mass, stiffness and damping, respectively
N_{dof}	the number of dof (degrees of freedom) of a model
N_q	the number of computed modes of the FE model
N_q^x	the number of measured modes of the structure
N_{tm}	number of target modes for design of actuator/sensor placement
N_ω	the number of frequency points of the FRF
N_θ	the number of parameters in the parameterization
P	objective criterion for actuator/sensor placement
$\bar{U}_i$	input force pattern for mode ϕ_i
V	cost function for model updating

Y	FROF of an I/O-model
$\bar{Y}_i$	FROF for the input force pattern $\bar{U}_i$
j	the imaginary unit
m	the number of actuators
q	the generalized coordinates of a FE model
p	the number of sensors
v	the difference vector between the the measurements v^x and the model output v^a
$\mathcal{A}_a$, $\mathcal{S}_a$	the artificial sets of actuators and sensors, respectively
$\mathcal{A}_c$, $\mathcal{S}_c$	the candidate sets of actuators and sensors, respectively
$\mathcal{A}_o$, $\mathcal{S}_o$	the optimal sets of actuators and sensors, respectively
$\mathcal{A}_r$, $\mathcal{S}_r$	the resulting sets of actuators and sensors, respectively
$\mathcal{C}$	complexity of actuator/sensor placement algorithms
$\mathcal{M}$	a FE model
$\mathcal{M}^x$	a mechanical structure
$\mathcal{M}^r$	a reference model
$\mathcal{M}^\theta$	the open set of feasible models
$\mathcal{T}$	kinetic energy
$\mathcal{V}$	strain energy
C_k	COMAC-value for sensor nr. k
M_{ij}	the MAC-value for normal mode ϕ_i and measured mode $\hat{\phi}_j^x$
M_i^d	the dMAC-value for mode ϕ_i and estimated mode $\hat{\phi}_i^d$
$\mathsf{M}_{*,i}^{nd}$	approximated ndMAC-value for mode ϕ_i and $\hat{\phi}_i^{nd}$, $* = a, b$
Φ_r	basis for reduction of the system matrices
Θ	the open set of feasible parameter values
$\check{\Theta}$	the closed set of initial parameter values giving a consistent estimation, $\hat{\theta} = \check{\theta}$
ω	the frequency variable
ϕ_i, ξ_i, ω_i	the respective mode, damping ratio, and resonance frequency of the FE model
$\hat{\phi}_i^x$, $\hat{\xi}_i^x$, $\hat{\omega}_i^X$	the respective estimated mode, estimated damping ratio, and estimated resonance frequency of the structure
θ	parameterization, parameter vector
θ_k	parameter nr. k
θ^i	parameter values at iteration i

Operators and Functions

$A \subset B$	A is a subset of B
$A \setminus B$	the set $\{x \mid x \in A \text{ and } x \notin B\}$
∂	derivation operator.
$\dot{x}, \ddot{x}$	First and second derivative of x w.r.t. time
x', x''	first and second derivative of x w.r.t. spatial position
$\mathrm{E}[x]$	expectation of x
$\mathrm{Cov}[x]$	covariance matrix of x
$\check{\theta}$	minimizing argument of $V(\theta)$
$\hat{\theta}$	estimated value of $\check{\theta}$
$\tilde{\theta}$	parameter bias, $\check{\theta} - \hat{\theta}$
$\mathrm{Im}\{x\}$	imaginary part of x
$\mathrm{Re}\{x\}$	real part of x
$\|X\|_{Fro}$	Frobenius norm of matrix X

Abbreviations

dof	Degrees Of Freedom
FE	Finite Element
FEM	Finite Element Method
FRF	Frequency Response Function
FROF	Frequency Response Output Function
Garteur	Group of Aeronautical Research and technology in EURope
LLS	Linear Least Squares
MAC	Modal Assurance Criterion
ML	Maximum-Likelihood
MMIF	Multi-variate Mode Indicator Function
NLLS	Non-linear LLS
ODE	Ordinary Differential Equation
PDE	Partial Differential Equation

1

Introduction

1.1 Finite Element Modeling

The Finite Element Method (FEM) is a standard tool for solving many problems in engineering science. Basically, the FE models are approximations of more complex models. By dividing a structure of general geometry into small sub-geometries, the PDE (partial differential equation) describing the dynamical behavior of the structure can be approximated by ODEs (ordinary differential equations) valid in the different sub-geometries. Since the ODEs are derived once and for all, the actual modeling reduces to a division of the structure into sub-geometries and choices of ODEs for these sub-geometries. For mechanical structures, the sub-geometries may be long, slender volumes, thin plates etc., and the corresponding finite elements are beams and shells with known properties. The grid points are characteristic for finite elements where the movements of the corresponding sub-geometry are computed/approximated. One may therefore state that the FE model is a spatially discretization of the PDE model.

FE modeling of mechanical structures yields a stiffness matrix K and a mass matrix M. These so-called system matrices are approximations of the corresponding distributions of stiffness and mass in the structure. Notice that even if the FE model is an approximation, it may become extremely large for complex, flexible structures. Damping also exist in a structure, but there is no corresponding FE modeling of a damping matrix L available, due to the diverse origins of damping. Therefore *ad hoc* modeling of damping is inevitable.

When the system matrices M, L, K are obtained, an input/output (I/O) model describing the measured effects from the applied forces can be constructed through the knowledge of the geometry of the structure as well as the corresponding model.

1.2 Model Updating

FE models are known to be sufficiently accurate in many applications, in particular when the primary purpose of the model is to quantify the behavior of a structure in the design stage. For instance, the behavior of a bridge is simulated in order to detect critical resonance frequencies and shapes of vibration in advance of the construction work. When the model has sufficiently good properties, the bridge is built and the model becomes of less value.

In aviation/aerospace applications it is for several reasons important that the FE model is accurate, i.e., that the model has a dynamical behavior close to the real structure. For instance, the security aspects on aero-planes require an experimental ground-test verification of the construction in a test set-up. The verification includes measuring of the low-frequency dynamical behavior of the structure for several configurations, e.g., for different amount of fuel in the wing-tanks. This measuring is very expensive and time-consuming. If an initial model of the structure can be updated/improved from the measurements of a single configuration, the other configurations can be simulated using the improved model. In order for these simulations to be valid, it is assumed that the improved model for the measured configuration is accurate, and that the differences between the configurations are easily accounted for in the model. This is mostly the case since the differences between the configurations are often known masses located to known positions. At some velocities the wings of an aero-plane may break down due to the vibrations (wing flutter). With an accurate model, the critical velocities yielding wing flutter can be estimated from an initial model with different configurations. This will reduce the expenses for the high-velocity aero-dynamic experiments in wind tunnels. Another application for model updating is to reduce a large-scaled model aimed for sizing, to a small model aimed for dynamic simulations. Since a small FE model is compared to a larger FE model, many of the problems encountered with real measurements can be avoided.

The complexity of FE models implies that the model updating formulation must be made carefully. The physical interpretation of the FE model may be used to construct a small and efficient parameterization θ of the initial model. If the parameters reflect the major errors/uncertainties of the initial model, a greatly improved model can be obtained. However, it is not only the parameterization that is critical for a successful model updating. It is also important that the cost function V describing the deviation between the model and the structure has good properties, i.e., that the estimation of the parameter values is fast and convex for a large domain in the parameter space. Even if the parameterization and the cost function V are constructed appropriately, robust and reliable optimization methods are required in order to obtain valid models. These aspects, together with the computational expenses of the model updating formulation form the most important considerations.

The physical interpretation of the parameters is also valuable when validating the updated model, i.e., when determining whether the updated model is valid for its intended purposes or not. If the parameter values are physically unrealistic and/or if the improvement of the model is not sufficient, then one may have to discard the updated model and start all over again.

1.3 Actuator and Sensor Placement

In order to measure the dynamical behavior of a dynamic structure, the actuators yielding the applied forces and the sensors measuring the vibrations of the structure must be placed on the structure. Traditionally, the purpose of actuator/sensor placement is for experimental modal analysis, i.e., the estimation and analysis of the resonance frequencies, the modes (shapes of vibration), and the damping of the structure. The major objective is to locate the actuators/sensors so that the dominating vibrations are properly excited/measured. However, there are also other objectives such as placement for control and model updating.

The discrete optimization problem arising in actuator/sensor placement tasks is in general non-convex. To find the optimal locations of actuators and sensors requires a full search among all possible combinations. However, such an extensive search is in general computationally too expensive. It is therefore important that the objective function has good convexity properties and that the optimization algorithm is a well-balanced trade-off between computational expenses and sub-optimality.

Moreover, the measuring of the dynamical behavior of the structure is expensive. It is therefore not possible to collect different measurements for different purposes. As a consequence, one must use a criterion being able to place actuators and sensors fulfilling several objectives.

1.4 Contributions

The major contributions of this thesis are

- the mode-pairing free cost function $\bar{V}$ in Section 3.8.5,

  where the discrete optimization problem of pairing modes is avoided. The cost function minimizes the deviations in resonance frequencies and quantities of the frequency response function.
- the noise-robust actuator placement criterion P^{nd} in Section 4.4.1,

  where a minor reduction of the corresponding noise-free objective yields a major improvement of the robustness against noise. A consequence of this is an improved signal-to-noise ratio (SNR) of the measurements.

The high computational expenses when dealing with FE models of large, flexible structures is inevitable. It is therefore important to reduce the time and memory storage needed. The objectives to minimize the computational expenses are

- the general model updating procedure in Section 3.8.2,
  where a reduction, and a linearization of the FE model is kept fixed for several iterations.
- Algorithm 4.4 in Section 4.2,
  where an iterative improvement of the actuator and sensor positions is found to be near optimal in simulations.

The minor contributions includes

- the reliable optimization method in Section 3.8.2.
- the mode-pairing cost function V_{mp} in Section 3.8.4.
- the notes on the choice of design variables in Section 3.10.
- the alternative derivation of the EI-method in Section 4.4.2.
- the overall good properties of actuator placement based on the controllability Gramian in Section 4.4.3.
- the generalization of the actuator/sensor placement criterion for model updating in Section 4.5.

1.5 Tour of the Thesis

In Chapter 2, an introduction to FEM and related topics is given. The chapter provides an insight into FE modeling, FE models and their basic properties. Chapter 2 includes a derivation of a three-dimensional beam element, the assembly of finite element system matrices into FE models, and some approaches to model damping. I/O-models based on a FE model are constructed. Finally, boundary conditions on the structure are accounted for. Readers familiar with FE modeling, properties of mechanical structures, and the construction of I/O-models from FE models, may turn directly to Chapter 3.

In Chapter 3 the concept of estimating physical parameters from measurements is treated. Readers not familiar with the field of estimation/system identification may value the first introducting section. The important model reduction technique is presented, and a short introduction to linear/non-linear least-squares optimization methods is given. The multiple mode indicator function (MMIF) is also discussed. In Section 3.8 an inexpensive model updating formulation and the novel mode-pairing free cost function are proposed. Some details on the choice of the design variables when updating FE models are presented in Section 3.10.

In Chapter 4 the topic of placement of actuators and sensors is studied. After a brief discussion of optimality, trade-offs, and robustness in Section 4.1, general placement algorithms and their computational complexity are presented in Section 4.2. Placement for the purpose of modal analysis is discussed in Section 4.4, where the novel noise-robust actuator placement criterion is proposed. Placement for model updating is also treated before the final section where comparison and validation issues are discussed.

2

Finite Element Models

In this chapter an introduction to the concept of Finite Element (FE) modeling is presented. Starting with a verbal description of the idea behind FE modeling in Section 2.1, a derivation of a three-dimensional finite beam element, and a mass point element are performed in Sections 2.2 and 2.3, respectively. The assembly of the elements into an FE model of the entire structure is presented in Section 2.4. Some properties of FE models are presented in Section 2.5, and in Section 2.6 the modeling of damping is described. The construction of input-output models arising from FE modeling is treated in Section 2.7, and boundary conditions on the structure are discussed in Section 2.8. Finally, some concluding remarks are given in Section 2.9.

2.1 Introduction to the Finite Element Method

In engineering sciences, nearly all physical phenomena can be described by differential equations. These differential equations are often complex and hard (impossible) to solve analytically and may therefore be solved approximately using a numerical method. One of these numerical methods is the Finite Element Method (FEM). In the late 1960's the computers became powerful enough in order to use the FEM in industrial applications and the development of the FEM therefore increased rapidly. Today, FEM is a standard tool for solving a wide range of problems encountered in industry and science. For instance, many mechanical structures, e.g., buildings and vehicles have a very complex mechanical design. The partial differential equations (PDE) describing the behavior of a mechanical structure are often to complex to be solved analytically, even for structures with non-complex geometry. The solution of the PDE must therefore be approximated using numerical methods. Instead of approximate a model of the entire structure numerically in one giant step, the FEM is based on the approximation of small parts of the structure with *finite elements* yielding a more easy-used model. When all parts of the structure are approximated by elements, a model of the entire structure may be obtained by putting the elements together. The idea behind the FEM is thus to approximate a structure with many standard finite elements, where each element is a model of a small part of the structure. The finite elements are often standard elements with known characteristics, and a fast solution of the considered problem can therefore be computed.

The approximation of a structure with small elements gives the opportunity to solve the PDE numerically. Basically, the FEM approximates the PDE with an ODE (Ordinary Differential Equation). The infinite dimensional model corresponding to the PDE is thus approximated with a finite dimensional model corresponding to the ODE. However, one must keep in mind that also the PDE is a model of the real structure, i.e., the finite dimensional FE model is an approximation of an infinite dimensional model of the real structure.

In Fig. 2.1 the basic steps of FE modeling are visualized. It is seen that the FE modeling of the real structure incorporates two steps: first a modeling step to obtain a PDE and then an FE modeling step to obtain an ODE. In practice the modeling of the real structure is made directly by the standard finite elements available in the FEM software packages. The first modeling step is then inherent in the FE modeling step visualized by the dashed arrow in Fig. 2.1.

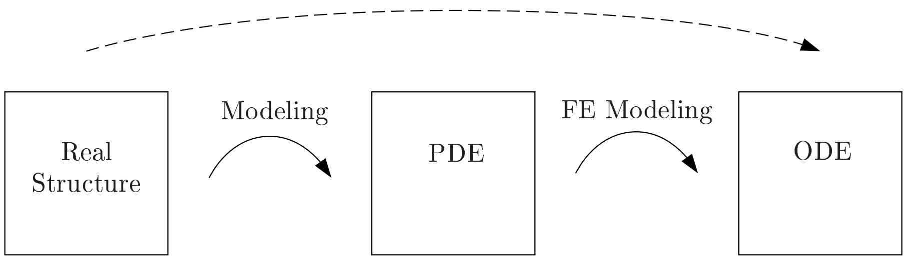

Figure 2.1 *The basic steps of the FE modeling.*

FE modeling of mechanical structures yield a mass matrix M and a stiffness matrix K representing the distribution of mass and stiffness in the structure. M and K are the *system matrices* of the FE model.

The finite elements are characterized by *grid points* where the coordinates are assumed to be known exactly. Using the grid points of the finite element, an interpolation can be made such that the coordinates of any point on the finite element can be determined approximately. The finite element is thus a spatially discretization of the part it is modeling. Putting the finite elements together, a spatially discrete model describing the behavior of the structure is obtained.

The coordinates of an arbitrary point of the structure can be computed using the assumptions made about the finite elements of the model. One must keep in mind that the finite element is often an approximation of the corresponding PDE for static forces/displacements. However, this approximation is known to also be valid in the low frequency region.

In Fig. 2.2 a mechanical structure is divided into two separated regions, and then a finite element model is constructed (here represented by its finite element mesh).

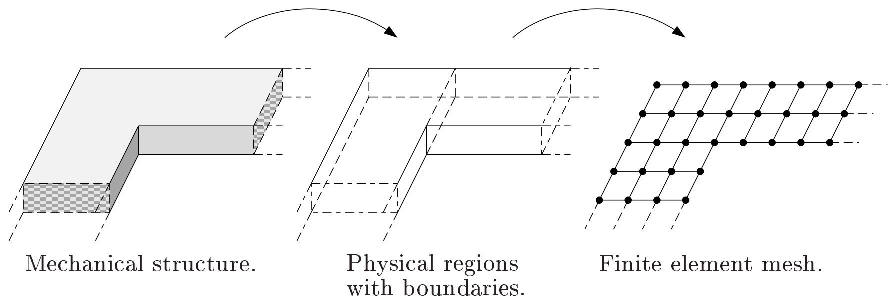

Figure 2.2 *FE modeling of a mechanical structure.*

The *degrees of freedom* (dof), denotes the types of movement a grid point can do. If no constraints is put on a grid, it has 6 dof, i.e., 3 translational dof and 3 rotational dof. A structure modeled with N_{gp} grid points has $N_{dof} = 6N_{gp}$ dof (if no constraints on the movements of the grid points are present).

We are thus able to construct a spatially discrete (finite dimensional) model (ODE) of a structure physically modeled by a spatially continuous (infinite dimensional) model (PDE). The obtained FE model is a collection of finite elements, where each element represents a small part of the structure.

In the literature there are a vast number of publications describing the FEM, structural mechanics and related topics. In [44] an analysis of mechanical structures is presented, including the equations of motion for several beam types. An analysis of finite elements can be found in [37]. The theory of the FEM is presented in [7, 33], and in [4] the numerics of the FEM is treated. The dynamics of mechanical structures is highlighted in [14, 26], and an introduction to the specific topic of model updating can be found in [12].

2.2 A Beam Element

In this section the system matrices for a uniform slender three-dimensional beam element are derived, see Fig. 2.6. The derivation is divided into three separate ones. The axial deformation of an one-dimensional element is first considered, see Fig. 2.3. Then one-dimensional transverse motion, see Fig. 2.4, and torsional motion, see

Fig. 2.5, are also treated. Combining the system matrices of these three motions, the system matrices of a three-dimensional uniform beam element are obtained. The derivation basically follows the presentation in [26], but a derivation can also be found in [14]. In [37] the system matrices for a beam element including shear deformation and rotatory inertia effects are derived. However, for a slender beam the effects of shear deformation is negligible and will therefore not be considered here.

The method used to obtain the system matrices is the *displacement method* since the displacements of the element are approximated. Other methods exists, e.g., the *force method* where the stresses of the element are approximated, as well as various *mixed methods*.

The FE modeling technique presented here is based on an energy approach. The main idea is that the strain and kinetic energy should be preserved, when the finite element is constructed.

2.2.1 Axial Motion

The axial motion of a slender, linearly elastic beam of mass density ρ, elastic modulus E, and cross-sectional area A may be expressed as

$$\frac{\partial}{\partial x}\left(EA\frac{\partial u(x,t)}{\partial x}\right) + h(x,t) = \rho A\frac{\partial^2 u(x,t)}{\partial t^2} \tag{2.1}$$

where $h(x,t)$ denotes the applied force per unit length, $u(x,t)$ the displacement, x the spatial variable and t time, see Fig. 2.3. Approximating the solution $u(x,t)$

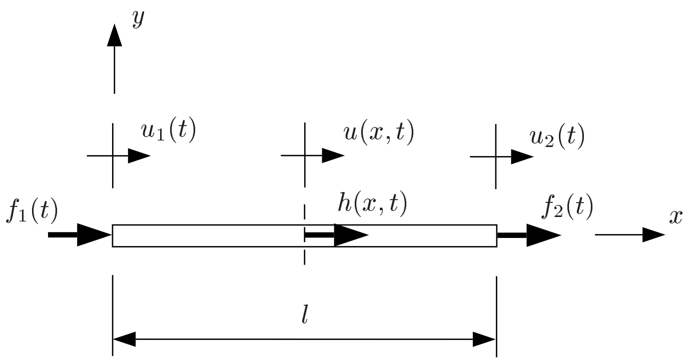

Figure 2.3 *The axial displacement of a uniform element, where $u(x,t)$ denotes the displacement as a function of x, and where $u_1(t)$, $u_2(t)$ are the axial displacements in the respective end points.*

in (2.1) as

$$u(x,t) = \psi_1(x)u_1(t) + \psi_2(x)u_2(t) \tag{2.2}$$

where the coordinates are defined as in Fig. 2.3, the axial motion of a uniform element of length l can be obtained. Since $u(0,t) = u_1(t)$, and $u(L,t) = u_2(t)$, the *shape functions* ψ_i must satisfy the boundary conditions

$$\begin{aligned} \psi_1(0) = 1, \quad \psi_1(l) = 0 \\ \psi_1(0) = 0, \quad \psi_2(l) = 1 \end{aligned} \tag{2.3}$$

Assuming static forces $f_2 = -f_1$ in Fig. 2.3, i.e., $h(x,t) \equiv 0$, the shape functions in (2.2) become

$$\psi_1(x) = 1 - \frac{x}{l}, \quad \psi_2(x) = \frac{x}{l} \tag{2.4}$$

since $(EAu')' = 0$, where u' is shorthand for $\partial u/\partial x$. The strain energy $\mathcal{V}$ in the beam due to the axial displacement is given by

$$\mathcal{V} = \frac{1}{2}\int_0^l EA(u')^2 dx = \frac{1}{2}\sum_{i=1}^{2}\sum_{j=1}^{2} k_{ij}u_i u_j \tag{2.5}$$

for the assumptions made on u in (2.2), yielding

$$k_{ij} = \int_0^l EA\psi_i'\psi_j' dx \tag{2.6}$$

if the equality in (2.5) holds. The corresponding kinetic energy $\mathcal{T}$ is given by

$$\mathcal{T} = \frac{1}{2}\int_0^L \rho A(\dot{u})^2 dx = \frac{1}{2}\sum_{i=1}^{2}\sum_{j=1}^{2} m_{ij}\dot{u}_i\dot{u}_j \tag{2.7}$$

where $\dot{u}$ is shorthand for $\partial u/\partial t$, and where

$$m_{ij} = \int_0^l \rho A\psi_i\psi_j dx \tag{2.8}$$

if the equality in (2.7) holds. Using the expressions in (2.4), (2.6) and (2.8) the stiffness matrix k and mass matrix m for the element are obtained as

$$k = \frac{AE}{l}\begin{bmatrix} 1 & -1 \\ -1 & 1 \end{bmatrix} \tag{2.9}$$

and

$$m = \frac{\rho Al}{6}\begin{bmatrix} 2 & 1 \\ 1 & 2 \end{bmatrix} \tag{2.10}$$

In (2.9) and (2.10), the entries at position ij in k and m are defined by k_{ij} and m_{ij} in (2.6) and in (2.8), respectively.

2.2.2 Transverse Motion

To derive the equation of transverse motion the well-known Bernoulli-Euler theory may be applied, see [26]. The transverse motion of a slender beam neglecting shear deformation is described by

$$\frac{\partial^2}{\partial x^2}\left(EI_x\frac{\partial^2 u(x,t)}{\partial t^2}\right)+\rho A\frac{\partial^2 u(x,t)}{\partial t^2}=h(x,t) \tag{2.11}$$

where I_x denotes the moment of inertia of the cross section, $h(x,t)$ the applied transverse force per unit length, and $u(x,t)$ is the transverse displacement, see Fig. 2.4. Since the PDE in (2.11) is of fourth order, the solution $u(x,t)$ of (2.11) be approximated by

$$u(x,t)=\sum_{i=1}^{4}\psi_i(x)u_i(t) \tag{2.12}$$

where the displacement coordinates u_i are defined as in Fig. 2.4. The shape functions ψ_i satisfy the boundary conditions

$$\begin{aligned}
\psi_1(0)=1, &\quad \psi_1'(0)=\psi_1(l)=\psi_1'(l)\\
\psi_2'(0)=1, &\quad \psi_2(0)=\psi_2(l)=\psi_2'(l)\\
\psi_3(l)=1, &\quad \psi_3'(0)=\psi_3(l)=\psi_3'(l)\\
\psi_4'(l)=1, &\quad \psi_4(0)=\psi_4'(0)=\psi_4(l)
\end{aligned} \tag{2.13}$$

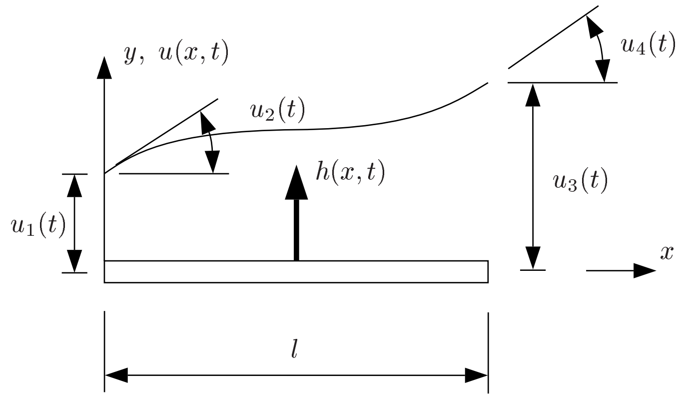

Figure 2.4 *The transverse displacement $u(x,t)$ of a uniform element, where $u_1(t)$ and $u_3(t)$ denote the transverse displacement in the respective end points, and where $u_2(t)$ and $u_4(t)$ denote the rotation in the respective end points. $h(x,t)$ denotes the external transverse force per unit length.*

Consider the case of static external forces on the beam. Then appropriate shape functions obeying (2.13) can be derived since the displacements are also static. The transverse motion of the element is described by $(EIu'')'' = 0$, having a third order polynomial as a solution:

$$\psi(x) = \sum_{i=0}^{3} c_i \left(\frac{x}{l}\right)^i \tag{2.14}$$

Substituting the boundary conditions in (2.13) into (2.14) the shape functions become

$$\begin{aligned} \psi_1 &= 1 - 3\left(\frac{x}{l}\right)^2 + 2\left(\frac{x}{l}\right)^3, \quad & \psi_2 &= x - 2l\left(\frac{x}{l}\right)^2 + L\left(\frac{x}{l}\right)^3 \\ \psi_3 &= 3\left(\frac{x}{l}\right)^2 - 2\left(\frac{x}{l}\right)^3, & \psi_4 &= -L\left(\frac{x}{l}\right) + L\left(\frac{x}{l}\right)^3 \end{aligned} \tag{2.15}$$

For the Bernoulli-Euler beam, the strain energy $\mathcal{V}$ and the kinetic energy $\mathcal{T}$ are given by

$$\mathcal{V} = \frac{1}{2}\int_0^l EI(u'')^2 dx = \frac{1}{2}\sum_{i=1}^{4}\sum_{j=1}^{4} k_{ij} u_i u_j \tag{2.17a}$$

$$\mathcal{T} = \frac{1}{2}\int_0^l \rho A(\dot{u})^2 dx = \frac{1}{2}\sum_{i=1}^{4}\sum_{j=1}^{4} m_{ij} \ddot{u}_i \ddot{u}_j \tag{2.17b}$$

leading to the expressions

$$k_{ij} = \int_0^l EI\psi_i''\psi_j'' dx \tag{2.18}$$

and

$$m_{ij} = \int_0^l \rho A\psi_i\psi_j dx \tag{2.19}$$

if the equalities in (2.17) hold. The stiffness matrix k and the mass matrix m for the Bernoulli-Euler beam element thus become

$$k = \frac{EI}{l^3}\begin{bmatrix} 12 & 6l & -12 & 6l \\ 6l & 4l^2 & -6l & 2l^2 \\ -12 & -6l & 12 & -6l \\ 6l & 2l^2 & -6l & 4l^2 \end{bmatrix} \tag{2.20}$$

and

$$m = \frac{\rho A l}{420}\begin{bmatrix} 156 & 22l & 54 & -13l \\ 22l & 4l^2 & 13l & -3l^2 \\ 54 & 13l & 156 & -22l \\ -13l & -3l^2 & -22l & 4l^2 \end{bmatrix} \tag{2.21}$$

2.2.3 Torsional Motion

The equation of torsional motion for a uniform torsion element of length l is described by

$$\frac{\partial}{\partial x}\left(GJ\frac{\partial u(x,t)}{\partial x}\right) + h(x,t) = \rho I_p \frac{\partial^2 u(x,t)}{\partial t^2} \tag{2.22}$$

where GJ is the torsional stiffness, I_p the polar moment of inertia and $h(x,t)$ the applied torque per unit length, see Fig. 2.5. Assuming that the applied forces are

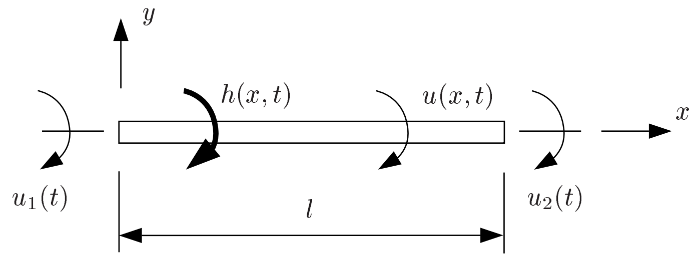

Figure 2.5 *The torsional displacement $u(x,t)$ of a beam element. $u_1(t)$ and $u_2(t)$ denote the torsional displacement in the respective end points, and $h(x,t)$ is the torque per unit length.*

static, i.e., $h(x,t) \equiv 0$ in (2.22), the solution u of $(GJu')' = 0$ is

$$u(x,t) = \psi_1(x)u_1(t) + \psi_2(x)u_2(t) \tag{2.23}$$

Since (2.2) equals (2.23), the shape functions are identical with those in (2.4). The strain energy $\mathcal{V}$ and the kinetic energy $\mathcal{T}$ for torsional motion in the beam are given by

$$\mathcal{V} = \frac{1}{2}\int_0^l GJ(u')^2 dx \quad \text{and} \quad \mathcal{T} = \frac{1}{2}\int_0^l \rho I_p(\dot{u})^2 dx \tag{2.24}$$

The expressions for the stiffness and mass thus become

$$k_{ij} = \int_0^l GJ\psi_i'\psi_j' dx \quad \text{and} \quad m_{ij} = \int_0^l \rho I_p \psi_i \psi_j dx \tag{2.25}$$

The mass and stiffness matrix for the uniform torsion element then become

$$k = \frac{GJ}{l}\begin{bmatrix} 1 & -1 \\ -1 & 1 \end{bmatrix} \tag{2.26}$$

and the mass matrix

$$m = \frac{\rho I_p l}{6}\begin{bmatrix} 2 & 1 \\ 1 & 2 \end{bmatrix} \tag{2.27}$$

2.2.4 System Matrices of a Three-Dimensional Beam Element

The stiffness and mass matrices for a slender uniform three-dimensional beam element can be constructed if the corresponding system matrices of the axial, transverse and torsional beam elements are combined. In Fig. 2.6 the local reference frame of the three-dimensional beam, and the coordinates $(u_1, \dots, u_{12})$ are visualized. The x-axis coincides with the centroidal axes of the element, and the y-axis

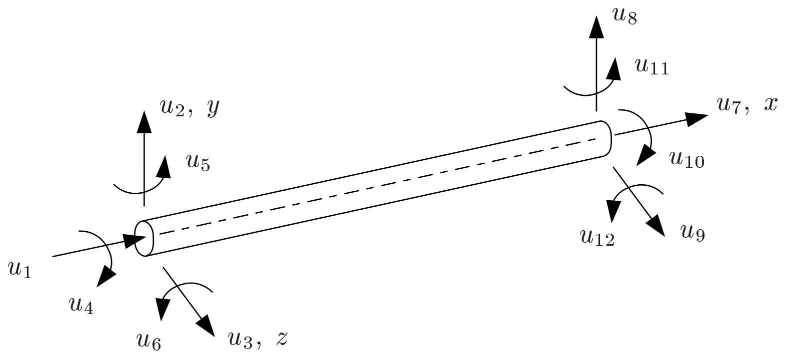

Figure 2.6 *The three-dimensional beam element.* $u_1 - u_6$ *and* $u_7 - u_{12}$ *denote the coordinates of the respective end points, and* xyz *denotes the reference frame of the three-dimensional beam element.*

and the z-axis are the principal axes of the cross sections. The coordinates u_1 and u_7 concern the axial motion of the element, see Section 2.2.1. The transversal motion in the xy-plane is represented by u_2, u_6, u_8, u_{12}, and in the xz-plane by u_3, u_5, u_9, u_{11}, see section 2.2.2. Finally, the coordinates u_4 and u_{10} represent the torsional motion of the element, see section 2.2.3.

Identifying the coordinates of the element in Fig. 2.6, the stiffness matrix k and the mass matrix m for the three-dimensional beam may be constructed from the stiffness and mass matrices in (2.9), (2.10), (2.20), (2.21), (2.26) and (2.27), representing the axial, transverse, and torsional motion, respectively.

The stiffness matrix k and the mass matrix m for the three dimensional beam element thus become

$$
k = \begin{bmatrix}
\frac{EA}{l} & 0 & 0 & 0 & 0 & 0 & \frac{-EA}{l} & 0 & 0 & 0 & 0 & 0 \\
0 & \frac{12EI_z}{l^3} & 0 & 0 & 0 & \frac{6EI_z}{l^2} & 0 & \frac{-12EI_z}{l^3} & 0 & 0 & 0 & \frac{6EI_z}{l^2} \\
0 & 0 & \frac{12EI_y}{l^3} & 0 & \frac{-6EI_y}{l^2} & 0 & 0 & 0 & \frac{-12EI_y}{l^3} & 0 & \frac{-6EI_y}{l^2} & 0 \\
0 & 0 & 0 & \frac{GJ}{l} & 0 & 0 & 0 & 0 & 0 & \frac{-GJ}{l} & 0 & 0 \\
0 & 0 & \frac{-6EI_y}{l^2} & 0 & \frac{4EI_y}{l} & 0 & 0 & 0 & \frac{6EI_y}{l^2} & 0 & \frac{2EI_y}{l} & 0 \\
0 & \frac{6EI_z}{l^2} & 0 & 0 & 0 & \frac{4EI_z}{l} & 0 & \frac{-6EI_z}{l^2} & 0 & 0 & 0 & \frac{2EI_z}{l} \\
\frac{-EA}{l} & 0 & 0 & 0 & 0 & 0 & \frac{EA}{l} & 0 & 0 & 0 & 0 & 0 \\
0 & \frac{-12EI_z}{l^3} & 0 & 0 & 0 & \frac{-6EI_z}{l^2} & 0 & \frac{12EI_z}{l^3} & 0 & 0 & 0 & \frac{-6EI_z}{l^2} \\
0 & 0 & \frac{-12EI_y}{l^3} & 0 & \frac{6EI_y}{l^2} & 0 & 0 & 0 & \frac{12EI_y}{l^3} & 0 & \frac{6EI_y}{l^2} & 0 \\
0 & 0 & 0 & \frac{-GJ}{l} & 0 & 0 & 0 & 0 & 0 & \frac{GJ}{l} & 0 & 0 \\
0 & 0 & \frac{-6EI_y}{l^2} & 0 & \frac{2EI_y}{l} & 0 & 0 & 0 & \frac{6EI_y}{l^2} & 0 & \frac{4EI_y}{l} & 0 \\
0 & \frac{6EI_z}{l^2} & 0 & 0 & 0 & \frac{2EI_z}{l} & 0 & \frac{-6EI_z}{l^2} & 0 & 0 & 0 & \frac{4EI_z}{l}
\end{bmatrix}
\tag{2.28}
$$

and

$$
m = \frac{\rho A l}{420} \begin{bmatrix}
140 & 0 & 0 & 0 & 0 & 0 & 70 & 0 & 0 & 0 & 0 & 0 \\
0 & 156 & 0 & 0 & 0 & 22l & 0 & 54 & 0 & 0 & 0 & -13l \\
0 & 0 & 156 & 0 & -22l & 0 & 0 & 0 & 54 & 0 & -13l & 0 \\
0 & 0 & 0 & \frac{140I_p}{A} & 0 & 0 & 0 & 0 & 0 & \frac{70I_p}{A} & 0 & 0 \\
0 & 0 & -22l & 0 & 4l^2 & 0 & 0 & 0 & 13l & 0 & -3l^2 & 0 \\
0 & 22l & 0 & 0 & 0 & 4l^2 & 0 & 13l & 0 & 0 & 0 & -3l^2 \\
70 & 0 & 0 & 0 & 0 & 0 & 140 & 0 & 0 & 0 & 0 & 0 \\
0 & 54 & 0 & 0 & 0 & 13l & 0 & 156 & 0 & 0 & 0 & -22l \\
0 & 0 & 54 & 0 & -13l & 0 & 0 & 0 & 156 & 0 & -22l & 0 \\
0 & 0 & 0 & \frac{70I_p}{A} & 0 & 0 & 0 & 0 & 0 & \frac{140I_p}{A} & 0 & 0 \\
0 & 0 & 13l & 0 & -3l^2 & 0 & 0 & 0 & -22l & 0 & 4l^2 & 0 \\
0 & -13l & 0 & 0 & 0 & -3l^2 & 0 & -22l & 0 & 0 & 0 & 4l^2
\end{bmatrix}
\tag{2.29}
$$

2.3 A Point Mass Element

The beam element derived in Section 2.2 can be used for the modeling of slender beams with negligible shear deformation. If the structure has parts that cannot be properly modeled by this element, other elements must be introduced. In FE software packages there are many different types of finite elements available, see [37]. Here, the simple point mass element is constructed. It is capable to model a significant amount of mass concentrated to a small part of the structure.

In Fig. 2.7 the coordinates of the point mass element are defined. The masses

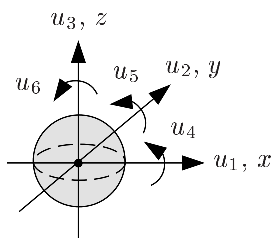

Figure 2.7 *The coordinates u and the reference frame xyz of the point mass element.*

corresponding to the axial motion become

$$m_1 = m_2 = m_3 = \int_X \int_Y \int_Z \rho \, dxdydz \tag{2.30}$$

where X, Y and Z describe the geometry of the part to be modeled. The masses corresponding to the rotatory of inertia are

$$m_4 = \int_{x \in X} \rho I_x \, dx, \quad m_5 = \int_{y \in Y} \rho I_y \, dy, \quad m_6 = \int_{z \in Z} \rho I_z \, dz \tag{2.31}$$

where I_x, I_y, I_z denote the moments of inertia around the corresponding principal axes x, y, z. The mass matrix m of the point mass element becomes

$$m = \begin{bmatrix} m_1 & 0 & 0 & 0 & 0 & 0 \\ 0 & m_2 & 0 & 0 & 0 & 0 \\ 0 & 0 & m_3 & 0 & 0 & 0 \\ 0 & 0 & 0 & m_4 & 0 & 0 \\ 0 & 0 & 0 & 0 & m_5 & 0 \\ 0 & 0 & 0 & 0 & 0 & m_6 \end{bmatrix} \tag{2.32}$$

and the stiffness matrix k is a zero-matrix of appropriate size.

2.4 Constructing Finite Element Models

In this section we will describe a procedure for constructing the system matrices K and M for the entire structure from the system matrices k and m of the separate elements. Since every element has its own local reference frame (coordinate system), the transformation of the system matrices k and m in the local reference frame to the system matrices k_e, m_e in the corresponding coordinates of the global reference frame is considered first. Then the actual construction will be treated, i.e., the assembly of k_e and m_e of the separate elements into the system matrices K and M of the entire structure.

The local coordinates and the local reference frame for a single element are denoted by u and xyz, respectively, while the corresponding global coordinates for the element are denoted by U_e. The global coordinates and the global reference frame of the entire structure are denoted by U and XYZ, respectively, see Fig. 2.8. Thus, u and U_e are related via a rotation, and the coordinates U_e form a subset of the coordinates U.

2.4.1 Transformation of System Matrices

In the finite element method the structure is approximated locally by finite elements. In order to obtain a model of the entire structure, the elements must be connected. This can be done if the conditions on the displacements in the common grid points of the elements are considered. These conditions require that the local reference frames of the elements coincide, i.e., that the coordinate systems are equal for elements connected in a grid point. The local reference frames of the elements are therefore transformed into the global reference frame for the entire structure. After a transformation of the coordinates, the elements can be connected in terms of the global reference frame.

Assume that the transformation matrix between the local frame and the global frame is denoted T_e, i.e., $u = T_e U_e$. Then the relation between the system matrices k, m in the local reference frame, and the corresponding matrices k_e, m_e in the global reference frame can be derived. It is clear that the strain energy $\mathcal{V}$, and the kinetic energy $\mathcal{T}$ must be preserved during the transformation:

$$\mathcal{V} = \frac{1}{2}u^T k u = \frac{1}{2}U_e^T (T_e^T k T_e) U_e = \frac{1}{2}U_e^T k_e U_e \tag{2.33a}$$

$$\mathcal{T} = \frac{1}{2}\dot{u}^T m \dot{u} = \frac{1}{2}\dot{U}_e^T (T_e^T m T_e) \dot{U}_e = \frac{1}{2}\dot{U}_e^T m_e \dot{U}_e \tag{2.33b}$$

This yield the relations

$$k_e = T_e^T k T_e \tag{2.33a}$$

$$m_e = T_e^T m T_e \tag{2.33b}$$

In order to construct the transformation matrix between a local reference frame xyz and the global reference frame XYZ, a reference grid point is introduced, see point P_3 in Fig. 2.8. The reference point is used to define the relation between the coordinates u of the local reference frame, and the coordinates U_e of the global reference frame. It can be shown that the local reference frame of an element is redundant if a reference grid (point) P_3 is specified. The orthonormal vectors $\vec{x}$, $\vec{y}$, $\vec{z}$ may be determined if $\vec{x}$ is defined parallel with the x-axis, and if $\vec{z}$ is in the plane defined by P_1, P_2 and P_3.

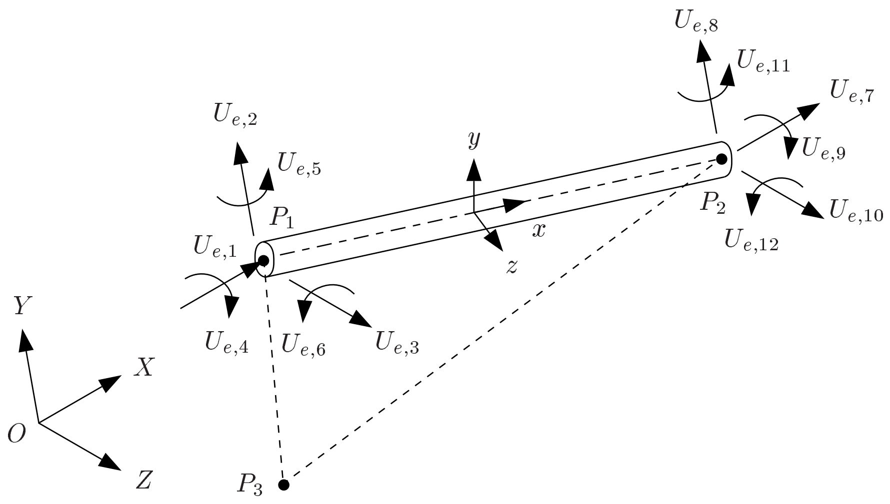

Figure 2.8 *A three-dimensional beam in the local reference frame xyz and the global reference frame XYZ.*

The transformation matrix T_e, $u = T_e U_e$, may now be constructed as follows:

$$T_e = \begin{bmatrix} \bar{T} & 0 & 0 & 0 \\ 0 & \bar{T} & 0 & 0 \\ 0 & 0 & \bar{T} & 0 \\ 0 & 0 & 0 & \bar{T} \end{bmatrix} \tag{2.34}$$

where

$$\bar{T} = \begin{bmatrix} \vec{X} \cdot \vec{x} & \vec{Y} \cdot \vec{x} & \vec{Z} \cdot \vec{x} \\ \vec{X} \cdot \vec{y} & \vec{Y} \cdot \vec{y} & \vec{Z} \cdot \vec{y} \\ \vec{X} \cdot \vec{z} & \vec{Y} \cdot \vec{z} & \vec{Z} \cdot \vec{z} \end{bmatrix} \tag{2.35}$$

In (2.35), is $\cdot$ the scalar product between the unit vectors $\vec{x}$, $\vec{y}$, $\vec{z}$ parallel with x, y, z of the local reference frame, and the unit vectors $\vec{X}$, $\vec{Y}$, $\vec{Z}$ parallel with the axes X, Y, Z of the global reference frame.

2.4.2 Assembly of System Matrices

After the transformation of k and m into k_e and m_e as shown in Section 2.4.1, it remains to assemble these matrices into the system matrices K and M of the entire structure. Let U denote the coordinates of the entire structure in the global reference frame, and U_e the coordinates of a single finite element. The relation between U and U_e for a finite element can then be expressed via a locator matrix L_e, $U_e = L_e U$, picking out the coordinates U_e from U. The assembly of k_e

and m_e into K and M can be performed as

$$K = \sum_{e=1}^{N_e} K_e \quad \text{where} \quad K_e = L_e^T k_e L_e \tag{2.36}$$

if the strain energy $\mathcal{V}$ of the structure is preserved:

$$\mathcal{V} = \frac{1}{2} U^T K U = \frac{1}{2} \sum_{e=1}^{N_e} U_e^T k_e U_e, \quad U_e = L_e U \tag{2.37}$$

where N_e denotes the number of elements in the FE model. In the same fashion the mass matrix M of the structure becomes

$$M = \sum_{e=1}^{N_e} M_e \quad \text{where} \quad M_e = L_e^T m_e L_e \tag{2.38}$$

However, an efficient construction of K and M does not involve the expensive pre- and post- multiplication by the large sized locator matrix L_e as in (2.36) and (2.38). Instead, the values of k_e and m_e are directly put into the corresponding entries of K and M, respectively.

2.5 Some Properties of Finite Element Models

The system matrices of the structure obtained in the FE modeling have substantial internal structure. They are built up by small sub-matrices corresponding to the elements of the FE model. These sub-matrices are symmetric, frequently repeated, and sparse, see (2.29) and (2.28). The construction of K and M as in Section 2.4 therefore clearly shows their symmetry, i.e., $K^T = K$ and $M^T = M$. The sparsity of the system matrices depends on the geometry of the structure and the type of finite elements, and is due to the fact that a grid is generally connected to only a few other grids. The high amount of sparsity and the symmetry of the system matrices are used to minimize the memory storage needed and the computation time in FE software packages. In Appendix A, the sparsity of the FE Garteur (Group for Aeronautical Research and Technology in EURope) model is visualized, see Fig. A.2.

Furthermore, the system matrices are positive semi-definite since they are closely associated with the strain energy $\mathcal{V}$, and the kinetic energy $\mathcal{T}$ of the structure,

$$\mathcal{V} = \frac{1}{2} x^T K x \quad \text{and} \quad \mathcal{T} = \frac{1}{2} \dot{x}^T M \dot{x} \tag{2.39}$$

where x is the displacement of the dof in the FE model.

If the model has *rigid body modes*, i.e., if the displacements are described by pure translations or pure rotations of the structure, then the stiffness matrix K will be positive semi-definite since the kinetic energy $\mathcal{T}$ vanishes in (2.39) due to the absence of deflection in the structure. An FE model in three dimensions have up to 6 rigid body modes, 3 translational and 3 rotational ones. The rank of the stiffness matrix equals the number of dof N_{dof} minus the number of rigid body modes. In Section 2.8, some boundary conditions on the structure are included in the model. If the structure is connected to another structure (as assumed in Example 2.1), some or all of the rigid body modes may vanish depending on the boundary conditions. The mass matrix M may also become singular, but the modeling of the mass distribution using the finite elements in Section 2.4 always yield a positive definite mass matrix M.

The preservation of energy in a spatially discrete mechanical system may be formulated as

$$\mathcal{V} + \mathcal{T} - \int \dot{x}^T f \; d\tau = 0 \tag{2.40}$$

where f is the externally applied forces. Differentiating the expression in (2.40) w.r.t. time, the equation of motion for an undamped mechanical system may be written

$$M\ddot{x} + Kx = f \tag{2.41}$$

where x denotes the dof. Characteristic for mechanical structures is that the vibrations are dominated by resonance frequencies and their corresponding modes describing the shape of vibration. The *normal modes* ϕ_i and *resonance frequencies* ω_i of (2.41) are determined via the generalized eigenvalue problem

$$(K - \omega_i^2 M)\phi_i = 0, \quad i = \{1, \ldots, N_{dof}\}, \quad \phi_i \in \mathbb{R}^{N_{dof}} \tag{2.42}$$

where N_{dof} is the number of dof. The interpretation of ω_i, ϕ_i in (2.42) is as the harmonic solution of (2.41),

$$x(t) = \sum_{i=1}^{N_{dof}} \phi_i \sin(\omega_i t + \alpha_i) \tag{2.43}$$

where α_i is a constant phase shift. In Appendix A the modes of the Garteur model are visualized, see Fig. A.3.

The modes ϕ_i are orthogonal to ϕ_j, $\forall i \neq j$,both w.r.t. M and K,

$$\phi_i^T M \phi_j = 0 \quad \text{and} \quad \phi_i^T K \phi_j = 0, \quad \forall i \neq j, \quad i, j \in \{1, \ldots, N_{dof}\} \tag{2.44}$$

Notice that the *orthogonality property* in (2.44) is also valid for the case of mode multiplicity, i.e., when $\omega_i = \omega_j$ for the modes ϕ_i and ϕ_j, see [14].

The quantities $\phi_i^T M \phi_i$ and $\phi_i^T K \phi_i$ in (2.46) are often referred to as the *modal mass* and the *modal stiffness* of mode ϕ_i, respectively. The *modal mass matrix* and the *modal stiffness matrix* are in the same fashion defined as

$$\Phi^T M \Phi, \quad \Phi^T K \Phi \tag{2.44}$$

where the *modal matrix* Φ is defined as

$$\Phi = [\phi_1, \ldots, \phi_{N_{dof}}] \tag{2.45}$$

The modes ϕ_i, computed via (2.42), are unique except for a scaling. The modes ϕ_i are usually scaled to become *mass normalized*:

$$\phi_i^T M \phi_i = 1, \quad \phi_i^T K \phi_i = \omega_i^2 \tag{2.46}$$

From now on it is assumed that the modes have the property (2.46).

For a vector ψ of appropriate size the Rayleigh quotient R in [14] is defined as

$$R(\varphi) = \frac{\varphi^T K \varphi}{\varphi^T M \varphi} \tag{2.47}$$

revealing the close relationship between R and ω^2, compare with (2.46) and (2.47). Thus, R may be interpreted as the square of the resonance frequency if the mode is φ.

In all mechanical structures there is damping. Usually it is modeled as viscous damping L_v, see Section 2.6. For the viscously damped structure the equation of motion becomes

$$M\ddot{x} + L_v\dot{x} + Kx = f \tag{2.48}$$

where $L_v \geq 0$. Assuming that the damping is under-critical, the corresponding *complex modes* ϕ_i^c of the damped model in (2.48) are defined as

$$(K + j\omega_i^c L_v - (\omega_i^c)^2 M)\phi_i^c = 0, \quad i = \{1, \ldots, N_{dof}\}, \quad \phi_i^c \in \mathbb{C}^{N_{dof}} \tag{2.49}$$

where ω_i^c denotes the damped resonance frequencies, see [14]. In view of (2.49) the *dynamic stiffness* Z is defined as

$$Z(\omega) = K + j\omega L_v - \omega^2 M \tag{2.50}$$

In general, the normal modes ϕ_i not coincides with the complex modes ϕ_i^c. If the viscous damping is so-called *proportional*, then $\phi_i^c = \phi_i$. The *modal damping* of mode ϕ_i is then defined as

$$\gamma_i = \phi_i^T L_v \phi_i \tag{2.51}$$

However, for structures being highly flexible, the concern of the damping is usually not addressed and ϕ_i^c, ω_i^c is approximated with ϕ_i, ω_i. Further aspects on complex modes are presented in, e.g., [12, 14]. The *modal damping matrix* is defined as $\Phi^T L \Phi$. For subsequent use the *modal damping ratio* is defined as

$$\xi_i = \frac{\gamma_i}{2\omega_i} \tag{2.52}$$

Notice that the *modal parameters* ϕ_i, ξ_i, ω_i are an alternative form of representing a model M, L, K:

$$\{M, L, K\} \quad \Leftrightarrow \quad \big\{(\phi_1, \xi_1, \omega_1), \ldots, (\phi_{N_{dof}}, \xi_{N_{dof}}, \omega_{N_{dof}})\big\} \tag{2.53}$$

where $(\phi_i, \xi_i, \omega_i)$ is the triple of *modal parameters.*

2.6 Modeling of Damping

The modeling of damping is probably the most critical issue when constructing FE models used to predict the behavior of flexible mechanical structures: when the structure is vibrating in resonance, the damping plays a major role in the response of the structure. Notice that flexible structures are totally dominated by the resonance vibrations. A good damping model for the structure is therefore of vital importance.

Damping is a phenomenom inherent in all structures and arises for many different reasons, e.g., (dry) friction between sub-structures, material damping, added local dampers etc., see [26, 31]. Moreover, damping may be significantly non-linear (in fact, dry friction is always non-linear) and the modeling of damping is therefore difficult. The variety of damping mechanisms constituting the damping in a structure makes the modeling of damping as a matrix L of proper dimension $N_{dof} \times N_{dof}$ infeasible. Therefore hardly no support for a proper modeling of damping is today available in commercial FE software packages.

In order to model the damping, some assumptions about the damping distribution must be made. These assumptions are often based upon prior knowledge of the characteristics of the structure and for ease of use. The construction of the damping model is often done by fitting some parameters in the damping model to measurements of the damping in the structure. However, we will not consider the actual fit of the parameters, only present the most common damping models used in FE applications.

The two most commonly used damping models are viscous and hysteretic damping, here denoted L_v and L_s, respectively. They are both based on simple assumptions made about the damping distribution, and their validity must be determined in the specific application. In [31] a comparison between hysteretic damping and viscous damping is made.

2.6.1 Viscous Damping

Recall that damping is proportional if $\Phi^T L_v \Phi$ is diagonal. In [6] it is shown that

$$L_v M^{-1} K = K M^{-1} L_v \tag{2.54}$$

is a sufficient condition for a viscous damping L_v to be proportional.

One approach to model damping is to assume the damping matrix L_v to be a linear combination of the element mass and stiffness matrices, see [43]:

$$L_v = \sum_{i=1}^{N_e} (a_i m_{e,i} + b_i k_{e,i}) \tag{2.55}$$

where a_i and b_i are the parameters to fit, and N_e is the number of elements in the FE model. In practice though, the assumption of constant damping in sub-structures is appropriate. Then a_i and b_i become constant in the separate sub-structures. If a_i and b_i are assumed to be constant in the entire structure, the special case of the so-called Rayleigh damping is achieved. Notice that L_v in (2.55) is in general only proportional when $a_i = a$, $b_i = b$, $\forall e$, i.e., for Rayleigh damping. The drawback with the Rayleigh damping is that only two parameters are available to be fitted to the measured damping of the model.

Another attractive damping modeling approach [22] is to constrain L_v to be proportional,

$$\Phi^T L_v \Phi = \operatorname{diag}(\ldots, 2\omega_i \xi_i, \ldots) \tag{2.56}$$

so-called *modal damping*. Using the property $\Phi^T M \Phi = I$, L_v becomes

$$L_v = M\Phi \operatorname{diag}(\ldots, 2\omega_i \xi_i, \ldots)\Phi^T M \tag{2.57}$$

There are however methods not relying on the assumption of modal damping. In [18] a generally non-proportional viscous damping matrix L_v is obtained through modal measurements made on the structure. An analysis of the error when a non-proportional damping matrix is approximated by a proportional matrix is made in [35].

2.6.2 Hysteretic Damping

Hysteretic (or structural) damping [43] arises if there is stress-strain hysteresis in the material. If the structure is forced to harmonic motion, the damping is proportional to the displacement x, but in phase with the velocity $\dot{x}$. The equation of motion becomes

$$M\ddot{x} + (jL_s + K)x = f \tag{2.58}$$

where L_s is the hysteretic damping matrix.

2.7 Input/Output Models

The input/output (I/O) behavior of a mechanical structure modeled with a mass matrix M, stiffness matrix K, and a damping matrix L (all of dimension $N_{dof} \times N_{dof}$) may be written

$$\begin{aligned} M\ddot{x}(t) + L\dot{x}(t) + Kx(t) &= Bu(t) \\ y(t) &= Cx(t) + C_a\ddot{x}(t) + Du(t) \end{aligned} \tag{2.59}$$

where x is the vector of dof, u is the vector of m input forces and y the vector of p outputs. In (2.59), B (of dimension $l \times m$) describes the positions of the actuators yielding the input forces and C ($p \times l$) the positions of the sensors measuring the output. C_a ($p \times l$) and D ($p \times m$) appear if acceleration measurements are made. Normally, y represents acceleration measurements, but displacement measurements are also common.

The frequency response function (FRF) of (2.59) is defined as the transfer function $G(s)$ evaluated on the imaginary axis, $s = j\omega$,

$$G(\omega) = (C + j\omega C_a)\left(K + j\omega L - \omega^2 M\right)^{-1} B + D \tag{2.60}$$

where ω denotes frequency, and where $G(\omega)$ denotes $G(j\omega)$ for simplicity. The frequency domain input $u(\omega)$ and output $y(\omega)$ are obtained as

$$u(\omega) = \mathcal{F}u(t), \quad y(\omega) = \mathcal{F}y(t) \tag{2.61}$$

where $\mathcal{F}$ denotes the Fourier transform. If G_{kl} denotes the entry at row k and column l of G, then the FRF can be determined as

$$G_{kl}(\omega) = y_k(\omega)/u_l(\omega), \quad \text{if} \quad u_i(\omega) = 0, \quad \forall i \neq l \tag{2.62}$$

where $y_k(\omega)$ denotes the k-th entry of $y(\omega)$, and where $u_l(\omega)$ denotes the l-th entry of $u(\omega)$, respectively.

Notice that a sinusoidal input force

$$u(t) = [U_1 \sin(\omega t + \alpha_1), \dots, U_m \sin(\omega t + \alpha_m)]^T \tag{2.63}$$

of appropriate size yields (in stationarity) a sinusoidal output response

$$y(t) = [y_1(t), \dots, y_p(t)]^T, \quad y_i(t) = |G_*(\omega)| \sin\left(\omega t + \arg\{G_*(\omega)\}\right) \tag{2.64}$$

for some $G_*(\omega) \in \mathbb{C}^p$.

Using the modal matrix Φ from (2.45) for a transformation of coordinates, $q = \Phi x$, and a pre-multiplication with Φ^T, the equations of motion for the *generalized coordinates* q become

$$\begin{aligned} \ddot{q}(t) + \Gamma\dot{q} + \Omega q(t) &= \Phi^T B u(t) \\ y(t) &= C\Phi q(t) + C_a \Phi \dot{q}(t) + Du(t) \end{aligned} \tag{2.64}$$

where

$$\Gamma = \Phi^T L \Phi \tag{2.65a}$$

$$\Omega = \text{diag}(\omega_1^2, \dots, \omega_l^2) \tag{2.65b}$$

If Γ is diagonal,

$$\Gamma = \text{diag}(\dots, 2\omega_i\xi_i, \dots) \tag{2.65}$$

the FRF of (2.64) can be written conveniently as

$$G(\omega) = \sum_{i=1}^{N_{dof}} \frac{(C + j\omega C_a)\phi_i\phi_i^T B}{\omega_i^2 - \omega^2 + j2\xi_i\omega_i\omega} + D \tag{2.66}$$

where ξ_i is the modal damping ratio defined in (2.52). Without going into computational details, it holds that solving the eigenvalue problem (2.42) followed by the computation of the FRF using (2.66) is cheaper than to compute (2.60) directly, at least when the number of frequency points ω is large.

A state space model

$$\begin{aligned} \dot{z}(t) &= A_s z(t) + B_s u(t) \\ y(t) &= C_s z(t) + D_s u(t) \end{aligned} \tag{2.67}$$

of (2.59) may be obtained as

$$A_s = \begin{pmatrix} 0 & I \\ -M^{-1}K & M^{-1}L \end{pmatrix}, \quad B_s = \begin{pmatrix} 0 \\ B \end{pmatrix}, \quad C_s = \begin{pmatrix} C & C_a \end{pmatrix}, \quad D_s = D \tag{2.68}$$

where $z = [x^T \, \dot{x}^T]^T$. For a similarity transformation $z = T\bar{z}$, the state space realization of (2.67) becomes

$$\begin{aligned} \dot{\bar{z}}(t) &= T^{-1}A_s T\bar{z}(t) + T^{-1}B_s u(t) \\ y(t) &= C_s T\bar{z}(t) + D_s u(t) \end{aligned} \tag{2.69}$$

The state space model corresponding to (2.64) can be written

$$\begin{aligned} \dot{z} &= \begin{pmatrix} 0 & I \\ -\Omega & -\Gamma \end{pmatrix} z + \begin{pmatrix} 0 \\ \Phi^T B \end{pmatrix} u \\ y &= \begin{pmatrix} C\Phi & C_a\Phi \end{pmatrix} z + Du \end{aligned} \tag{2.70}$$

With some extra demands on the construction of Φ, the state space model in (2.70) can be verified to be a canonical representation of the I/O-model in (2.59), whether the damping is proportional or not.

The *frequency response output function* (FROF) denoted $Y(\omega)$ is defined as

$$Y(\omega) = G(\omega)U, \quad U = [U_1, \ldots, U_m]^T \tag{2.71}$$

where G is the FRF in (2.60), and where U is the vector of the *mono-phase amplitudes* of the input $u(t) = U\sin(\omega t)$, i.e., some entries in U may be negative. The interpretation of $Y(\omega)$ is as the FRF for the single input/multiple output system defined by $G(\omega)U$. Thus, the output $y(t)$ corresponding to $Y(\omega)$ is sinusoidal, where the amplitudes and phases of $y_i(t)$, $i = 1, \ldots, p$, are determined by $Y(\omega) \in \mathbb{C}^p$.

2.8 Boundary Conditions and Constraints

In Section 2.4.2, the system matrices are assembled as if the structure is unaffected by the surroundings, i.e., as if no boundary conditions are present. However, in practice there are always boundary conditions turning up as prescribed forces f_b acting on the structure, or as prescribed displacements x_c constraining the motion of the structure. Partitioning the model into active (not constrained) dof x_a and constrained dof x_c, the equation of motion corresponding to (2.41) becomes

$$\begin{bmatrix} M_{aa} & M_{ac} \\ M_{ca} & M_{cc} \end{bmatrix} \begin{bmatrix} \ddot{x}_a \\ \ddot{x}_c \end{bmatrix} + \begin{bmatrix} K_{aa} & K_{ac} \\ K_{ba} & K_{bc} \end{bmatrix} \begin{bmatrix} x_a \\ x_c \end{bmatrix} = \begin{bmatrix} f_a + f_{b_a} \\ f_c + f_{b_c} \end{bmatrix} \tag{2.72}$$

where f_c denotes the reactive forces appearing due to the constrained displacements x_c.

Example 2.1 *An important case of boundary condition is when the modeled structure is connected to a larger structure which can be considered as a rigid body due to its much higher mass and stiffness. The constrained dof x_c in the intersection between the FE model and the (modeled) surroundings is prescribed to be zero. If $x_c \equiv 0$ in (2.72), the corresponding equation of motion can be partitioned as*

$$M_{aa}\ddot{x}_a + K_{aa}x_a = f_a + f_{b_a} \tag{2.73a}$$
$$M_{ca}\ddot{x}_a + K_{ca}x_a = f_c + f_{b_c} \tag{2.73b}$$

where f_a denotes the commanded input forces.

Another important case introducing boundary conditions is the effect of gravity on the structure. The gravity may be seen as a prescribed force f_b and causes a pre-stress of the structure. The pre-stress can change the shape of the structure and therefore also its dynamic behavior. Assuming no externally applied forces, i.e., $f_a = 0$, and assuming that the structure is in stationarity, $\ddot{x} = 0$ (since the gravity force f_b is constant), the displacements in the active dof x_a can be computed as

$$x_a = K_{aa}^{-1} f_b \tag{2.74}$$

according to (2.72). Notice that the gravity force on a structure is distributed and must therefore be made spatially discrete in the same fashion as the distribution of mass in the structure. The gravity force f_b may therefore be computed [26] as

$$f_{b,e} = \sum_i \int_0^L f(x)\psi_{e,i}\, dx \tag{2.75}$$

where ψ_i are the shape functions of the finite element, and $f(x)$ is the distributed gravity force on the structure. f_b is then obtained as the sum of $f_{b,e}$ for all elements. The displacements ($\times 20$) due to the gravity on the Garteur model are visualized in Fig. 2.9, where the dots ($\cdot$) is the grids of the model for a zero-gravity force, and where the prescribed displacements ($x_c \equiv 0$) are the translational coordinates of the grids 6, 10 and 18 denoted by $\circ$.

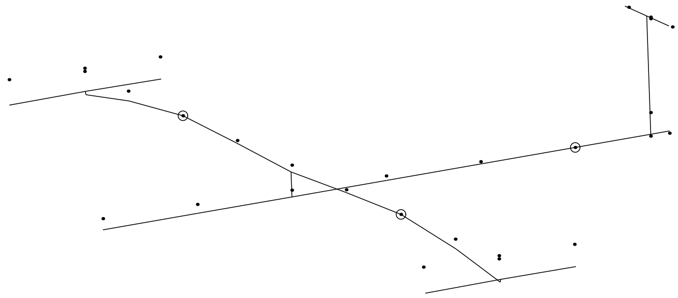

Figure 2.9 *The effect of gravity (×20) on the Garteur model. The constrained grids are marked by ∘.*

There is also a need for imposing dependency between the dof x in a model. For instance, when a sub-structure of the model is considered to be a rigid body some dof x_d is linearly dependent on the active dof x_a, i.e., $x_d = T_{da}x_a$. The dependency between x and x_a may therefore be written

$$x = T_a x_a \quad \text{where} \quad T_a = \begin{bmatrix} I \\ T_{da} \end{bmatrix} \tag{2.76}$$

The equation of motion for the active dof x_a then becomes

$$M_a \ddot{x}_a + K_a x_a = f_a \tag{2.77}$$

where

$$M_a = T_a^T M T_a, \quad K_a = T_a^T K T_a, \quad f_a = T_a^T f \tag{2.78}$$

If N_{dof} and $N_{dof,a}$ denote the number of dof in x and x_a, respectively, it is readily seen that the transformation matrix T_a can be used to reduce the size of the model. This is basically the idea behind the most common model reduction techniques applied to FE models, see [22, 32]. The drawback is the difficulty to select the "master" dof x_a and the "slave" dof x_d in order to achieve a reduced model valid in the whole frequency range of interest. Another drawback is that the sparsity of the matrices K_a and M_a is not preserved. Therefore, a reduction of the system matrices must be substantial if a gain in computation time and memory storage is to be achieved.

2.9 Summary

In this chapter, we made an introduction to FE modeling of mechanical structures. One can conclude that FE models are approximations (to ODEs) of more complete models (PDEs). The idea is to divide the structure into small parts, and then to let a finite element with known characteristics model the part in question. When the structure is modeled by the finite elements, the system matrices of the separate elements are combined into the system matrices of the entire structure. FE modeling of a mechanical system yield the system matrices M and K, representing the mass and stiffness distribution of the structure, respectively. However, there is no equivalent strategy to model the damping distribution of the structure. One is therefore restricted to *ad hoc* approaches to construct the corresponding damping matrix L. Some important properties of the FE models were also surveyed. The view of an FE model in terms of modal quantities was introduced. When the system matrices M, L, K are constructed, an I/O-model of the structure can be made once the positions of the actuators and sensors are known. It was also shown how the influence from the surroundings can be accounted for.

3

Model Updating

In Section 3.1, an introduction to model updating is given, and in Section 3.2 some recent proposed cost functions for model updating are surveyed. The multivariate mode indicator function used to detect/excite modes from measurements is presented in Section 3.3. A model reduction technique suitable for model updating can be found in Section 3.4, and in Sections 3.6 and 3.5 correlating techniques and a noise model are presented. In Section 3.7 optimization methods for various least-squares problems are surveyed. In Section 3.8, the major results of this chapter are presented. A general, inexpensive model updating formulation is presented in Section 3.8.3, and its implementation is given in Section 3.8.2. The mode-pairing free cost function is derived in Section 3.8.5. A convergence analysis is then detailed in Section 3.9. For the choice of design variables, a guideline is given in Section 3.10.

3.1 Introduction

Model updating is the established name of improving an initial (FE) model of a mechanical structure using measurements. It will be assumed that a parameterization of the model is performed. The objective is to estimate these parameters in order to improve/update the initial model. When making the parameterization of the model, the parameters represent the major errors/uncertainties of the model compared to the real structure. A good parameterization will therefore make a substantial improvement of the initial model possible.

Measurements

The type of measurements vary with the type of structure. Here it is assumed that the mode estimates $\hat{\phi}_i^x$, the estimated resonance frequencies $\hat{\omega}_i^x$, and the estimated damping ratios $\hat{\xi}_i^x$ of the structure are available. The low-frequency part of the FRF in (2.62)-(2.61) is also assumed to be estimated. The measuring of these quantities are common, e.g., in aviation applications.

The FRF is measured in specified frequency points in every channel, i.e., for every actuator-sensor combination. This is a very time-consuming task due to the number of actuators m, the large number N_ω of frequency points where the FRF are measured, and the low level of damping in aviation/aerospace structures. However, when the FRF is measured, a proper input signal can be computed to excite a single mode of the structure, see Section 3.3. The measuring of the modes $\hat{\phi}_i^x$ is also very time-consuming, since a long time period is needed to bring the structure to vibrate in stationarity due to the low level of damping. If a proportional damping model is valid, the damping ratio may be estimated from the FRF. Hence, the modal parameters along with measurements of the FRF can be assumed to be available when updating FE models of flexible structures.

For simplicity, it is assumed that displacement measurements are collected from the structure. Displacements can be measured by the use of lasers and laser-cameras placed in the surroundings of the structure. However, in practice it is more common to measure accelerations using small and accurate accelerometers attached to the structure. These accelerometers are of extremely low weight and their influence on the structure's behavior may therefore be neglected during the model updating.

FE Models

FE models of complex industrial structures may be extremely large. Sizes of up to 10,000-100,000 dof are not uncommon. These large models make the model reduction a significant issue for the model updating to become practical. The reduction of size must be up to 1000 times for the reduction to yield any sufficient gain in computation time and/or memory storage (since the reduced system matrices in general are not sparse). However, it is not only the degree of reduction that is important, the model reduction technique must also be able to preserve the effects of a deviation in the parameter values in order for an appropriate estimate of the parameters to be possible.

In Section 2.6 a few different damping modeling techniques were surveyed. The most attractive approach is to assume the damping to be proportional (modal), i.e., to every normal mode ϕ_i of the model a damping ratio ξ_i are assigned. Correlating the estimated modes of the structure $\hat{\phi}_i^x$ with the normal modes ϕ_i of the model, the estimated damping ratios $\hat{\xi}_i^x$ of the structure may be assigned to the damping ratios ξ_i of the model. The assumption that the damping is proportional is by no means valid for all applications. However, in aerospace/aviation applications where the structures are flexible, the assumption of proportional, damping is found to be valid in practice as well as in theory, see [14].

Model Updating

In order to improve an FE model, the system matrices are usually parameterized by a set of parameters θ:

$$M = M(\theta), \quad L = L(\theta), \quad K = K(\theta) \tag{3.1}$$

and an open set Θ of feasible values for θ. A parameterization θ, together with Θ define a model set $\mathcal{M}^\theta$,

$$\mathcal{M}^\theta = \{M(\theta), L(\theta), K(\theta) \,|\, \theta \in \Theta\} \tag{3.2}$$

containing all the feasible models. Denoting $\mathcal{M}^x$ as the real structure, the objective of the model updating is to minimize the deviation $|\mathcal{M} - \mathcal{M}^x|$ between the model $\mathcal{M} \in \mathcal{M}^\theta$ and $\mathcal{M}^x$ in some sense. The deviation is based on the difference between the measurements of the structure and the corresponding outputs of the model. Usually the degree of deviation is described by a scalar cost function $V = V(\theta) \geq 0$. The objective may therefore be formulated as a minimization problem,

$$\check{\theta} = \arg\min_{\theta \in \Theta} V(\theta) \tag{3.3}$$

where $\check{\theta}$ should be interpreted as the minimizing argument of V,

$$V(\check{\theta}) \leq V(\theta), \quad \forall \theta \in \Theta \tag{3.4}$$

A choice of cost function may be

$$V(\theta) = |v(\theta)|_b, \quad v(\theta) = v^a(\theta) - v^x \tag{3.5}$$

where b denotes a vector norm, v^x the vector of measurements, and v^a the corresponding output vector obtained from the model. In order to minimize V, a sequence of parameter values are computed,

$$\theta^{i+1} = \theta^i + \Delta\theta^i, \quad \theta^0 = \theta^{init} \tag{3.6}$$

where $\Delta\theta^i$ is the parameter step of iteration i. The iterative computation of $\hat{\theta}$ is a consequence of that the parameters are normally nonlinear in v. In order to compute $\Delta\theta^i$ the Jacobian J of $v(\theta)$ is needed

$$J_k = \frac{\partial v}{\partial \theta_k}, \quad k = 1, \ldots, N_\theta \tag{3.7}$$

where J_k is the k-th column of J, and N_θ is the number of parameters. Notice that v's dependency of θ is seldom explicitly available. For instance, the resonance frequencies ω_i are not explicitly expressed as $\omega_i = \omega_i(\theta)$. One is therefore restricted to the use of numerical difference approximations of $\partial v / \partial \theta$, and the Jacobian J is approximated by a numerical difference quotient, like

$$J_k \approx \frac{v(\theta_k + \delta\theta_k) - v(\theta_k)}{\delta\theta_k} \tag{3.8}$$

where $\delta\theta_k$ is the difference quotient step. Henceforth, J denotes the Jacobian computed as the numerical difference quotient in (3.8).

The limiting solution of (3.6) is defined by

$$\hat{\theta} = \lim_{i\to\infty} \theta^i \tag{3.9}$$

and is an estimate of $\check{\theta}$. If $\check{\theta} = \hat{\theta}$, then the parameter estimate is consistent. The bias of the parameter estimate $\tilde{\theta}$ is defined as $\tilde{\theta} = \check{\theta} - \hat{\theta}$.

Parameterization

The parameterization is today still based on engineering skills and prior knowledge, but some guidelines for the choice of parameterization exist, see Section 3.6.2 and Section 3.10.2. Here, the parameterization is assumed to be given, and the parameterization issues of the model are therefore not considered. The FE model is often physically parameterized, i.e., the parameters θ_i have a clear physical interpretation in terms of the FE model and the real structure, e.g., stiffnesses and material properties of a beam. There are some advantages using a physically parameterized model. The skills and knowledge of the engineer may be used to create a parameterization with good properties: (a) the parameterization determines a model set $\mathcal{M}^\theta$ including a model with small deviation from the structure, (b) the estimated parameter values are instructive for the engineer constructing the initial models, and (c) the validation of the updated model can partly be made in terms of the physical interpretation of the estimated parameters. There also exist some drawbacks. The formulated estimation problem is with nearly no exception non-linear. This means that the algorithm minimizing V may end up in a local minimum where $\hat{\theta} \neq \check{\theta}$. Another drawback may be the ill-conditioned optimization problem due to both "hard" and "easy" estimated parameters.

The Model Updating Challenge

It is clear that model updating of large FE models is a task of very high complexity. The main reasons are the large size of the FE models, the large number of parameters N_θ, but also the many actuators m, and sensors p yielding a large amount of measurements. This makes the computation of the Jacobians J the by far most time-consuming part of the model updating procedure. If J is not further approximated, every computation of J will need $N_\theta + 1$ computations of v which in general is too expensive. Every iteration in (3.9) during the model updating may take hours (or even days) in computation time for a large FE model, indicating that several days (weeks) might be needed to compute $\hat{\theta}$. It is therefore very important to formulate a computationally cheap minimization problem.

However, the complexity is not the main obstacle in order to successfully update the FE model. The non-linear estimation problem in (3.3)-(3.6) may have many local minima if it is not formulated with care. These local minima may spoil a successful model updating:

$$V(\hat{\theta}) \ll V(\theta^{init}) \quad \text{and} \quad \hat{\theta} \approx \check{\theta} \tag{3.10}$$

It is therefore of vital importance that the cost function has a large domain of attraction $\check{\Theta}$ to the global minimum $\check{\theta}$,

$$\check{\Theta} = \{\theta^0 \,|\, \theta^0 \in \Theta,\ \hat{\theta} = \check{\theta}\} \tag{3.11}$$

The set $\check{\Theta}$ is in general not computable, but simulations may indicate its properties.

Moreover, in order to minimize the risk of ending up in a local minimum, reliable optimization methods must be used. The optimization method must be able to deal with large and ill-conditioned formulations, having various constraints on the parameters. In particular, the optimization algorithms must be able to deal with highly non-linear problems.

Since there are many design variables inherent in the updating procedure, interactivity may be used, i.e., an engineer may act as a supervisor during the model updating procedure adjusting the design variables whenever it is needed. The engineer's knowledge and skills may then be used to determine an appropriate parameterization, cost function, as well as other design variables. However, the need for interactivity is caused by the drawbacks of the formulated problem. One of the objectives is therefore to minimize the need for interactivity, since it is not a fail-safe solution to the problems mentioned above, e.g., local minima.

We have found that the most important requirements on a model updating formulation includes

- Low computational complexity
- Good convergence properties of the cost function
- Reliable optimization methods

If all the requirements above are considered, the model updating task will be relatively fast and accurate.

Validation of Model Updating Formulations

In order to evaluate the properties of a model updating formulation, a reasonable choice is to use a reference model $\mathcal{M}^r$ representing a typical structure $\mathcal{M}^x$. The simulated measurements from $\mathcal{M}^r$ represents then the measurements from the structure $\mathcal{M}^x$. The advantage with this is that the model $\mathcal{M}$ minimizing $|\mathcal{M} - \mathcal{M}^r|$ is known (if $\mathcal{M}^r \in \mathcal{M}^\theta$). If the common problems appearing in a real model updating environment are simulated, the sensitivity of the parameter estimates against measurement noise, process noise, mode estimate errors, etc., may be studied.

In a real model updating context there does not exist a parameterization θ such that $\mathcal{M}^x \in \mathcal{M}^\theta$. This is due to several reasons. The FE modeling of a structure is an approximation no matter how fine the grid of the model is or what elements being used, the structure is always nonlinear, and so on. It is therefore not adequate to define a "true" model of a real structure. However, since FE models may be very accurate the deviation $|\mathcal{M}^x - \mathcal{M}|$ for a good parameterization θ is assumed to be small. What remains is the choice of a parameterization which is here assumed to be available.

From the discussion above it is motivated that an analysis of a model updating formulation can be made using simulated measurements from an FE model of a typical structure in a model updating application.

3.2 Literature Overview

The model updating strategies are historically divided into *direct methods* and *iterative methods*. The direct methods provide explicit solutions to the formulated minimization problem. These methods usually only require measurements of the modes, and the resonance frequencies of the structure. The iterative methods do not have an explicit solution to the formulated problems, requiring an iterative optimization method. Since the research on model updating techniques is more focused on the iterative methods, only a brief introduction to the direct methods is given here.

3.2.1 Direct Methods

The direct methods are usually based on modal measurements of the system, i.e., on the mode estimates $\hat{\phi}_i^x$, resonance frequency estimates $\hat{\omega}_i^x$, and different properties of the FE model, e.g., (2.42), (2.44), and/or the symmetry of the system matrices, $M = M^T$ and $K = K^T$. Using this type of knowledge of the model as constraints together with the measurements, different direct methods can be derived.

One of the recent direct methods based on measured modal data is proposed in [42], where it is assumed that the mass matrix is correct, and where the stiffness matrix is updated as

$$K_{new} = K_{init} + \Delta K \tag{3.12}$$

where K_{new} is the updated stiffness matrix and K_{init} the initial stiffness matrix. The matrix ΔK is obtained through minimizing

$$||M_{init}^{-0.5} \Delta K M_{init}^{-0.5}||_2 \tag{3.13}$$

under the constraints

$$(K_{new} - (\hat{\omega}_i^x)^2 M_{init})\hat{\phi}_i^x = 0, \quad K_{new} = K_{new}^T \tag{3.14}$$

for $i = 1, \dots, N_q^x$. The solution to the minimization problem is obtained directly as

$$\Delta K = M_{init}\hat{\phi}_x\hat{\Omega}_x\hat{\phi}_x^T M_{init} - K_{init}\hat{\phi}_x\left(\hat{\phi}_x^T K_{init}\hat{\phi}_x\right)^{-1}\hat{\phi}_x^T K_{init} \tag{3.15}$$

where $\hat{\Omega}_x = \mathrm{diag}\big(\dots, (\hat{\omega}^x)^2, \dots\big)$ is a diagonal matrix containing the square of the measured resonance frequencies. Notice the dimension problem between the measured modes $\hat{\phi}^x$ and the system matrices M_{init} and K_{init} in (3.15). The measured mode $\hat{\phi}_i^x \in \mathbb{R}^p$ and the matrix $K_{init} \in \mathbb{R}^{N_{dof}\times N_{dof}}$. There exist various mode expansion techniques to solve this problem, see [12].

The main advantage with the direct methods is the direct computation of the updated matrices. Another advantage may be the small number of design-variables present. However, the updated matrices cannot be interpreted in terms of the initial model since all entries of M_{init} and K_{init} may be changed by ΔM and ΔK. This fact complicates the highly important validation of the updated model.

An excellent presentation of the direct methods can be found in [12]. Reviews of the direct methods may also be found in [22, 29, 45].

3.2.2 Iterative Methods

The iterative methods have the advantage of being much more flexible in the problem formulation. For instance, any kind of measurements of the structure can be used, the models emerging in different applications can be individually parameterized, the updated matrices have a physical interpretation, prior knowledge such as pre-stresses on the structure can be included,etc.

The idea behind the iterative methods is to minimize a scalar cost function V describing the deviation between the measurements and the model. This cost function is traditionally based on either modal data or frequency response data, but other formulations exist, see, e.g., [20] for an overview of relations governing the model updating formulations.

Iterative Methods Based on Modal Data

A thorough presentation of the iterative methods based on modal data is made in [12]. The aim of these methods is to minimize the deviations in the resonance frequencies and mode shapes. However, the explicit use of mode shapes introduces extra difficulties that has to be taken care of. A proper scaling of the measured mode shapes must be made. The pairing of measured modes $\hat{\phi}_i^x$ and normal modes ϕ_i of the model is also important. In [9], the cost function

$$V_{EC}(\theta) = \sum_i \nu_{1,i}^2\left|\frac{\omega_i(\theta) - \hat{\omega}_i^x}{\hat{\omega}_i^x}\right|_2^2 + \sum_i \nu_{2,i}^2\left|\phi_i(\theta) - \hat{\hat{\phi}}_i^x\right|_2^2 + \sum_i \nu_{3,i}^2\left|\theta_i - \theta_i^0\right|_2^2 \tag{3.16}$$

is proposed. The cost function V_{EC} in (3.16) includes relative deviation in resonance frequencies, deviation in mode shapes, and a regularization term: the deviation of the parameters from their initial value. The second term in (3.16) requires a scaling of the measured mode $\hat{\phi}_i^x$, i.e.,,

$$\hat{\hat{\phi}}_i^x = \frac{\phi_i^T \hat{\phi}_i^x}{\phi_i^T \phi_i} \hat{\phi}_i^x \tag{3.17}$$

for a comparison of the modes (3.16) to make sense. Notice also that a differentiation of the normal modes ϕ_i w.r.t. θ is necessary. This might be troublesome for (near) multiple modes, and/or large models.

Other techniques to update an FE model from modal data have been presented, see, e.g., [8]. In [36] many of the drawbacks of the iterative methods based on modal measurements are highlighted and reduced. However, many of the drawbacks are inherent in the formulated problem and can therefore not be completely avoided.

Iterative Methods Based on Frequency Domain Data

Following [12], the frequency domain model updating methods can essentially be divided into input error methods and output error methods. The input error methods uses

$$v_{IE}(\theta) = u^x(\omega) - G^{-1}(\theta, \omega) y^x(\omega) \tag{3.18}$$

to update the system matrices, where $u^x(\omega)$ is the measured frequency domain input, G the FRF of the model, and $y^x(\omega)$ the measured frequency domain output of the structure, see (2.60), (2.62) and (2.61). The output error methods uses

$$v_{OE}(\theta) = y^x(\omega) - G(\theta, \omega) u^x(\omega) \tag{3.19}$$

to update the model. The corresponding time domain input error/output error equations may be expressed using (2.64) or (2.67).

In [23], cost functions based on the input error and output error formulations in (3.18) and (3.19) are studied. It is stated that measurements of forced vibrations form a complement to the more commonly used measurements of the modal parameters. Moreover, the ill-conditioned numerical properties of the parameter estimation problem are highlighted.

The choice of norm is discussed in [3], where the FRF-based cost functions

$$V_{LS}(\theta) = \sum_{\omega_i} \left\| G(\theta, \omega_i) - G^x(\omega_i) \right\|_2^2 \tag{3.20}$$

and

$$V_{LogLS}(\theta) = \sum_{\omega_i} \left\| \log G(\theta, \omega_i) - \log G^x(\omega_i) \right\|_2^2 \tag{3.21}$$

are compared. It is there found from test cases that V_{LogLS} have better properties than V_{LS}: the domain of convergence $\check{\Theta}$ to the global minimum $\check{\theta}$ increases, and the deviation in the modes is considered to be minimized since the anti-resonances of the measurements become more important due to that

$$|\log G_{kl}| \rightarrow \infty, \quad \text{as} \quad |G_{kl}| \rightarrow 0 \tag{3.22}$$

where G_{kl} denotes the entry at row k and column l in G.

Formulations based on the output error equation in (3.19), and the damping modeling approaches in Section 2.6 are presented in [22]. A mixed static-dynamic reduction technique is proposed to reduce the size of the model. The problem of modeling he damping is also highlighted.

3.3 The Multivariate Mode Indicator Function

The Multivariate Mode Indicator Function (MMIF) in [46] is used to detect (multiple) modes of the structure. It is also used to determine the amplitudes and phases (force patterns) of the sinusoidal input forces applied to the structure. The force patterns are computed in order to excite the structure for accurate mode estimations. This technique is called normal mode force appropriation (or phase resonance testing), and is today a well-established technique to excite a single mode of the structure. Normally, multiple actuators are used.

Recall that a sinusoidal input of the form (2.63) yields a sinusoidal output according to (2.64). It should therefore be possible to excite a single mode if the sinusoidal input force has a frequency that equals a resonance frequency of the structure. Assuming the resonance frequency ω_i is known, the *force pattern* $\bar{U}_i$ is chosen as

$$u(t) = \bar{U}_i \sin(\omega_i t), \quad \bar{U}_i = \begin{bmatrix} \bar{U}_{i,1} \\ \vdots \\ \bar{U}_{i,m} \end{bmatrix} \tag{3.23}$$

the response of the structure will be highly dominated by the single target mode ϕ_i of the structure.

The frequency response output function (FROF) $Y(\omega)$ in (2.71) is defined as $Y(\omega) = G(\omega)U$ for a force amplitude vector U. Henceforth, the FROF is only of interest in the resonance frequencies ω_i:

$$\bar{Y}_i = G(\omega_i)\bar{U}_i \tag{3.24}$$

where $\bar{Y}$ is the FROF for the force pattern in (3.23) for a resonance frequency ω_i, and where G is the FRF in (2.60). Notice that with $u(t)$ according to (3.23), the m inputs are reduced to one combined single input, since the product $B\bar{U}_i$ is a vector.

A mode is considered to be excited "cleanly" if the displacements (or accelerations) of all measured dof of the structure are out of phase $\pm 90°$ with the applied force. This is readily seen from (2.66) where the FRF becomes

$$G(\omega) = \sum_i \frac{C\phi_i\phi_i^T B}{\omega_i^2 - \omega^2 + j2\xi_i\omega_i\omega} \tag{3.25}$$

in case displacements are measured. Assuming that a force pattern $\bar{U}_i$ at a resonance frequency ω_i is applied to the structure so that only the mode ϕ_i makes a contribution to (3.25). The FROF then becomes

$$\bar{Y}_i = -j\frac{1}{2\xi_i\omega_i^2}C\phi_i\phi_i^T B\bar{U}_i \tag{3.26}$$

and the direction of the vector $C\phi_i$ can be estimated accurately, since $\phi_i^T B\bar{U}_i$ is a scalar. Henceforth, the notation $C\phi_i$ is suppressed, and the notation ϕ_i is used instead.

However, the perfect frequency response output in (3.26) is an idealized situation, since one can never guarantee that only the single mode ϕ_i is excited. This would require that

$$\phi_l^T B\bar{U}_i = 0, \quad \forall l \neq i \tag{3.27}$$

Thus, the modes estimated from the measurements will not be exactly out of phase $\pm 90°$ even if the damping is proportional.

An estimate $\hat{\phi}_i$ of mode ϕ_i may therefore be

$$\hat{\phi}_i = \mathrm{Im}\{\bar{Y}_i\} \tag{3.28}$$

where $\bar{Y}_i$ is defined as in (3.24).

The frequency response output $\bar{Y}_i$ can be written as

$$\bar{Y}_i = \bar{Y}_i^{re} + j\bar{Y}_i^{im} = G^{re}(\omega_i)\bar{U}_i + jG^{im}(\omega_i)\bar{U}_i \tag{3.29}$$

where superscripts re and im denote the real and imaginary part of G, respectively. Notice that $\bar{U}_i$ is real. If a single mode ϕ_i is to be excited at resonance frequency ω_i, then the real part of $\bar{Y}(\omega)$ in (3.29) should be small in comparison with the total response, due to (3.28). The objective is therefore to find the force pattern $\bar{U}_i$ minimizing

$$\lambda_{i,\min} = \min_{\|\bar{U}_i\|=1} \frac{\|\bar{Y}_i^{re}\|^2}{\|\bar{Y}_i\|^2} \tag{3.30}$$

where $\|\bar{Y}\|^2 = \bar{Y}^H\bar{Y}$, and $\bar{Y}^H$ is the complex conjugate of $\bar{Y}$, see [46].

It follows that $\lambda_{i,\min}$ in (3.30) is the smallest eigenvalue $\lambda_{i,k}$ of the generalized eigenvalue problem

$$\left(A_i - \lambda_{i,k}(A_i + B_i)\right)\bar{U}_{i,k} = 0, \quad k = 1, \dots, m \tag{3.31}$$

where $A_i = G^{re}(\omega_i)^T G^{re}(\omega_i)$, and $B_i = G^{im}(\omega_i)^T G^{im}(\omega_i)$. The eigenvalue problem in (3.31) is of small dimension, $m \times m$, if m actuators are used. Now, the set of m eigenvalues $\lambda_{i,k}$ in (3.31) can for each index i be used to detect a single mode ϕ_i. A single mode is detected if $\lambda_{i,1} = \lambda_{i,\min} \approx 0$, two near multiple modes if also $\lambda_{i,2} \approx 0$, etc. Moreover, the eigenvectors $\bar{U}_{i,k}$ in (3.31) are candidates as input force patterns to the structure at frequency ω_i. For a measured FRF G^x the MMIF is a method to obtain a force pattern that excites the single modes of the structure properly.

In Example 3.1, the eigenvalues λ_i and the force pattern $\bar{U}$ are computed for the reference Garteur model in Appendix A.

Example 3.1 *The reference Garteur model in Appendix A has four near multiple modes at 41 Hz. One may therefore suspect that it is troublesome to detect all these modes with any sets of actuator and sensor positions. Here the actuators are positioned at*

$$\mathcal{A}_r = \{13_x,\, 10_z,\, 14_z\}$$

and the sensors at

$$\mathcal{S}_r = \{12_x,\, 13_x,\, 14_x,\, 21_y,\, 22_y,\, 23_y,\, 27_y,\, 5_z,\, 6_z,\, 9_z,\, 10_z,\, 12_z,\, 13_z,\, 15_z\}$$

The notation x_k denotes the grid point x and the direction k of the input force/measured output, see Fig. A.1 in Appendix A. In Fig. 3.1 the eigenvalues λ of (3.31) *are presented as functions of the frequency. Since the eigenvalues λ_{min} are very low* (≈ 0) *for nearly all modes, they are detected by the MMIF. The eigenvalues of mode nr. 7* (≈ 0.15) *and mode nr. 8* (≈ 0.05) *are also low. See also Example 4.2 where the possibility to excite the modes appropriately are studied.*

In Table 3.1 the mono-phase amplitudes of the input force pattern are presented. It is seen that the amplitude of the force from the actuators can differ substantially. This means that the actuators must be able to yield forces linearly in a wide range of frequency as well as force levels in order to excite the modes appropriately.

Table 3.1 *The input force patterns from the actuators.*

Force Pattern $\bar{U}_{i,j}$	Mode i								
	1	2	3	4	5	6	7	8	9
$\bar{U}_{i,1}$	.527	.916	.236	.910	.994	.771	-.959	.836	.943
$\bar{U}_{i,2}$	.189	.275	-.760	.311	.041	-.057	.190	-.330	-.215
$\bar{U}_{i,3}$	-.828	.007	-.605	.276	-.100	.635	.209	.439	-.255

3.4 Model Reduction

FE models of complex flexible structures may be huge. Model reduction is therefore necessary. However, it is not only the size of the reduced model that affects the choice of the model reduction technique. Many other properties are valuable. For instance, it is important that a minor change of the full size model is reflected in the reduced size model (invariance of the model reduction technique). Otherwise the

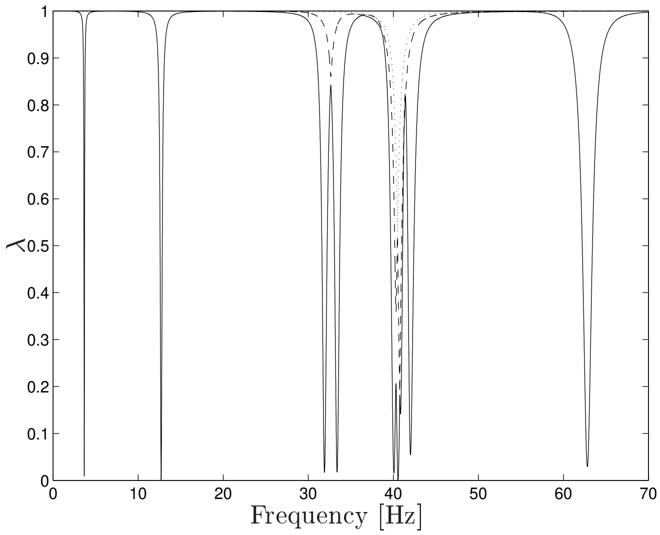

Figure 3.1 *The eigenvalues λ of (3.31) as a function of frequency, where λ_1 is denoted by a straight line (—), λ_2 a dashed line (- -), and λ_3 a dotted line ($\cdots$).*

parameter estimation techniques based on small perturbations in the parameters may fail to update the model. Moreover, the reduction must be substantial if the memory storage needed for the reduced model is to be decreased. This is due to the fact that the system matrices M, K are sparse, but that the system matrices M_r, K_r of the reduced model are not. The reduction of size must therefore be up to 1000 times if computation time and memory storage is to be sufficiently decreased.

Modal Basis Reduction Technique

Recall that a transformation of the dof x in the I/O-model (2.59) into the generalized dof $q = \Phi x$ in (2.64) is obtained via the modal matrix Φ defined in (2.45). The corresponding frequency domain I/O-models (2.60) and (2.66) suggest that a reduced I/O-model valid in a specific frequency range ω_R^x can be achieved by approximating

$$G(\omega) = \sum_{i=1}^{N_{dof}} \frac{(C + j\omega C_v)\phi_i \phi_i^T B}{\omega_i^2 - \omega^2 + j2\xi_i\omega_i\omega} + D, \quad \omega \in \omega_R^x \tag{3.32}$$

with

$$G_r(\omega) = \sum_{i=r_1}^{r_2} \frac{(C + j\omega C_v)\phi_i \phi_i^T B}{\omega_i^2 - \omega^2 + j2\xi_i \omega_i \omega} + D, \quad \omega \in \omega_R^x \tag{3.33}$$

where $r_1 \leq i \leq r_2$ denotes the modes ϕ_i used in the model reduction. The basis Φ_r of reduction contains the modes ϕ_i having a significant influence on G in the frequency area ω_R of interest,

$$\Phi_r = [\phi_{r_1}, \ldots, \phi_{r_2}], \quad \omega_{r_i} \in \omega_R \tag{3.34}$$

where $\omega_R^x \subset \omega_R$.

The reduced system matrices M_r, L_r and K_r then become

$$M_r = \Phi_r^T M \Phi_r, \quad L_r = \Phi_r^T L \Phi_r, \quad K_r = \Phi_r^T K \Phi_r \tag{3.35}$$

where Φ_r is defined by (3.34). The corresponding I/O-model becomes

$$\begin{aligned} M_r \ddot{q}(t) + L_r \dot{q} + K_r q(t) &= \Phi_r^T B u(t) \\ y(t) &= C\Phi_r q(t) + C_v \Phi_r \dot{q}(t) + Du(t) \end{aligned} \tag{3.36}$$

In a model updating context where the parameters θ in the parameterized model may change, a good property of Φ_r is invariance w.r.t. θ. If Φ_r is nearly invariant w.r.t. θ, the basis of reduction Φ_r is valid in a large domain Θ_r around the value of θ. It is then possible to omit the computation of Φ_r as long as $\theta \in \Theta_r$. Since the computation of Φ_r may be extremely expensive, this leads to that the computational expenses can be reduced substantially.

If the mass and stiffness matrices M and K are parameterized with the parameters θ,

$$M = M(\theta), \quad K = K(\theta) \tag{3.37}$$

then one can use the eigenvalue problem in (2.42) to derive the sensitivities of the modes, see [17]. For FE models with no multiple modes, the derivative of mode ϕ_i w.r.t. θ_k is

$$\frac{\partial \phi_i}{\partial \theta_k} = \sum_{j=1}^{N_{dof}} c_{ij}\phi_j, \quad \text{where} \quad c_{ij} = \begin{cases} \frac{\phi_j^T \left(\frac{\partial K}{\partial \theta_k} - \omega_i^2 \frac{\partial M}{\partial \theta_k}\right)\phi_i}{(\omega_i^2 - \omega_j^2)}, & \text{if } i \neq j \\ -\sum_{j \neq i} c_{ij} |\phi_j|_\infty, & \text{if } i = j \end{cases} \tag{3.38}$$

where $\omega_i \neq \omega_j$, $\forall i \neq j$. In (3.38), $|\phi_j|_\infty$ denotes the maximum value of $|\phi_j|$.

In [17] the derivatives of the modes for the case of a parameterized damping matrix $L = L(\theta)$ are also computed. Studying the coefficients c_{ij} of the series expansion in (3.38), it is seen that the influence of ϕ_j on $\frac{\partial \phi_i}{\partial \theta_k}$ is likely to be small if the difference in resonance frequency $|\omega_i^2 - \omega_j^2|$ is large. This indicates that the subspace spanned by the modes in a particular frequency range have good invariance properties w.r.t. θ_k, $k = 1, \ldots, N_\theta$ (if the term $\phi_j^T \left(\frac{\partial K}{\partial \theta_k} - \omega_i^2 \frac{\partial M}{\partial \theta_k}\right)\phi_i$ is neglected).

3.5 A Noise Model

The frequency domain output $y(\omega)$ may be written

$$y(\omega) = G(\omega)u(\omega) + y^n(\omega) \tag{3.39}$$

where $y(\omega)$ is the measured quantity, G denotes the FRF, $u(\omega)$ is the commanded input signal from the actuators, and $y^n(\omega)$ is a noise model.

A sufficiently general noise model for our purpose is

$$y^n(\omega) = y^{mn}(\omega) + G^{pn}(\omega)u^{pn}(\omega) \tag{3.40}$$

where $y^{mn}(\omega)$ is the modeled measurement noise generated by the sensors, $G^{pn}(\omega)$ the FRF from the process noise sources to the sensor positions, and $u^{pn}(\omega)$ the process noise input forces acting on the structure.

The measurement noise generated by the sensors can be modeled as complex independent Gaussian random variables,

$$y^{mn}(\omega) = \big[\dots, y_k^{mn}(\omega), \dots\big]^T \sim N_c\big(0, \mathrm{diag}(\dots, \sigma_k^{mn}(\omega), \dots)\big) \tag{3.41}$$

where the variance $(\sigma^{mn})^2$ of each sensor s_k may be frequency dependent. The notation N_c in (3.41) specifies a complex normal distribution. We will not further discuss complex random variables here. In [27] a complex Gaussian distribution is presented. The assumption of independent sensor noise is considered to be valid in almost all modeling applications. The measurement noise variance $(\sigma_k^{mn})^2$ may be estimated from measurements of a vibration-free surface.

Often one knows the positions of the process noise sources acting on the structure, e.g., the interface between the structure and its surrounding, the position of vibrating engines or pumps. Based on the frequency response function $G^{pn}(\omega)$ from the noise source together with a process noise source model, a model of the measured process noise can be obtained. Therefore, a modeling of the process noise source as an actuator a_k^{pn} exciting the structure with the random frequency dependent force U_k^{pn} may be done,

$$u^{pn}(\omega) = \big[\dots, u_k^{pn}(\omega), \dots\big]^T \sim N_c\big(0, \mathrm{diag}(\dots, \sigma_k^{pn}(\omega), \dots)\big) \tag{3.42}$$

where the noise sources a_k^{pn} are assumed to be independent. If the process noise sources are distributed, an equivalent modeling of the process noise sources as discrete actuators can be made. Notice that the assumption of independency between the process noise sources in (3.42) is no restriction since dependent noise sources always can be turned into an equivalent, independent one. A model of the influence of the process noise on the structure based on the FE model is thus possible to obtain.

The noise model discussed here is later on used as a tool for analyzing noise properties of the input error and output error equations in (3.19) and (3.18), respectively. In Section 4.4.1 a slightly modified noise model (only the imaginary part) is used for noise-robust actuator placement.

3.6 Correlation Techniques

Correlation is an important topic in experimental modal analysis, where the modal parameters of the model are compared with the modal parameters of the structure.

Here two correlation techniques are presented: the modal assurance criterion (MAC) correlating mode shapes, and the co-ordinate modal assurance criterion (COMAC) correlating dof. Other correlation techniques used for validation purposes can be found in [12, 22].

3.6.1 The Modal Assurance Criterion, MAC

The modal assurance criterion (MAC) is used to correlate the normal modes ϕ_i with the measured modes $\hat{\phi}_j^x$ of the structure, see [2]. The MAC-value M_{ij} is defined as

$$\mathsf{M}_{ij} = \frac{|\phi_i^T \hat{\phi}_j^x|^2}{|\phi_i|^2 |\hat{\phi}_j^x|^2} \tag{3.43}$$

where ϕ_i is the vector corresponding to the measured dof, and M_{ij} the entry at row i and column j of the MAC-matrix M. A MAC-value between 0.9 and 1 is in practice considered as high, and the modes may be thought of as pairs, even though the corresponding resonance frequencies differ.

Using M in (3.43), and an algorithm for finding pair of modes in the MAC-matrix it is possible to pair the measured triple of modal parameters,

$$\{\hat{\phi}_j^x, \hat{\omega}_j^x, \hat{\xi}_j^x\}, \quad j \in \{1, \ldots, N_q^x\} \tag{3.44}$$

of modal parameters to the corresponding triple of the model,

$$\{\phi_i, \omega_i, \xi_i\}, \quad i \in \{1, \ldots, N_q\} \tag{3.45}$$

where N_q^x and N_q denote the number of measured modes of the structure and the computed target modes of the model, respectively. In particular, measured damping ratios $\hat{\xi}_j^x$ can be assigned to the corresponding damping ratios ξ_i of the model. Also, deviations in resonance frequencies $\omega_i - \hat{\omega}_i^x$ may constitute a part of the cost function.

To ensure a reliable mode pairing, all possible combinations $\phi_i \leftrightarrow \hat{\phi}_j^x$ must be checked. This is a complex problem (growing exponentially in complexity), and sub-optimal algorithms must be used. Here the trade-off between sub-optimality and computational complexity for mode-pairing algorithms is not investigated. Instead a simple mode pairing algorithm is presented as Algorithm 3.1 below.

Algorithm 3.1 (Mode Pairing Algorithm)

Input: M, *MAC-matrix of dimension* $N_q \times N_q^x$.

Output: *column-row pairs* $\{c_i,\, r_i\},\ i = 1, \ldots, \min\{N_q, N_q^x\}$

1. *Let* $k = 1$*, and denote* $\mathsf{M}_t = \mathsf{M}$.
2. *Determine the entry* (r_k, c_k) *of the maximum value of* M_t.
3. *Let all elements in row* r_k *and column* c_k *of* M_t *be* 0.
4. *Let k=k+1.*
5. *If* $k < \max\{N_q^x,\, N_q\}$ *: go to 2.*
   Else : end.

Notice that only a tiny part of the entries of ϕ_i in (3.43) are used since the p number of sensors used during the measurements in practice is a fraction of N_{dof}. This means that the quotient N_{dof}/p commonly is in the interval between 10^2 and 10^4.

3.6.2 The Co-Ordinate Modal Assurance Criterion

In [24], the co-ordinate modal assurance criterion (COMAC) is presented. The COMAC correlates the measured dof of the structure with the corresponding dof of the model:

$$\mathsf{C}_k = \frac{\sum_{i=1}^{N_q^x} \left|\phi_{i,s_k} \hat{\phi}^x_{i,s_k}\right|^2}{\left(\sum_{i=1}^{N_q^x} |\phi_{i,s_k}|^2\right)\left(\sum_{i=1}^{N_q^x} |\hat{\phi}^x_{i,s_k}|^2\right)}, \quad k = 1, \ldots, p \tag{3.46}$$

where ϕ_{i,s_k} and $\hat{\phi}^x_{i,s_k}$ is the dof of ϕ_i and $\hat{\phi}^x_i$ measured by sensor s_k, respectively. A high C_k-value (≈ 1) indicates high correlation between the physical region of the structure around the sensor and the region around the corresponding dof of the model. Since the COMAC correlates measured dof with dof in the model, it may be used to validate spatially separated regions of the model.

3.7 Numerical Optimization Methods

In this section a short introduction to the method of least squares will be given. In Section 3.7.1 the constrained and unconstrained linear least squares (LLS) are treated. Methods to solve the non-linear least squares (NLLS) problem are discussed in Section 3.7.2. See also Section 3.8.3 where the implemented NLLS is presented. The main reference for LLS and NLLS is [5]. Additional treatment of NLLS problems can be found in [11, 39, 47].

3.7.1 Linear Least Squares

For a cost function V, linear in its parameters:

$$V(\theta) = v(\theta)^T v(\theta), \quad v(\theta) = v^a(\theta) - v^x, \quad v^a(\theta) = S\theta \tag{3.47}$$

the estimation of θ is straightforward in most applications. The computation of the estimate $\hat{\theta}$ in order to minimize $V(\theta)$, can be seen as the solution of the overdetermined problem

$$S\theta = d, \quad d = d^\star + n \tag{3.48}$$

where $S \in \mathbb{R}^{N_x \times N_\theta}$, and $d \in \mathbb{R}^{N_x}$. In (3.48), $S\theta$ is the model, $d^\star$ denotes the corresponding noise-free measurements, and n denotes the measurement errors/noise. It is assumed that the noise can be modeled as a vector of random variables with the statistical properties:

$$\mathrm{E}[n] = 0, \quad \mathrm{Cov}[n] = W \tag{3.49}$$

where W is a positive definite matrix. The best estimate $\check{\theta}$ of θ in (3.48) is given by

$$\begin{aligned} \check{\theta} &= \arg\min_{\theta} \left\| W^{-1/2}(S\theta - d) \right\|_2 \\ &= \left(S^T W^{-1} S\right)^{-1} S^T W^{-1} d \end{aligned} \tag{3.50}$$

where W is the covariance matrix of the noise in (3.49), see [5]. Thus, the best linear estimate is obtained if the set of overdetermined equations in (3.48) is weighted with the square root of W^{-1}. If W is positive definite it is no restriction to skip the notation of W, letting W be implicitly included in (3.48):

$$\check{\theta} = \arg\min_{\theta} \|S\theta - d\|_2 \tag{3.51}$$

Including Linear Inequality Constraints

If prior knowledge of the parameters such as

$$\theta^{min} \le \theta \le \theta^{max} \tag{3.52}$$

is available, this information can be accounted for when computing $\hat{\theta}$. The constrained minimization problem arising can be formulated as

$$\check{\theta} = \arg\min_{\theta} \left\| S\theta - d \right\|_2 \quad \text{subject to} \quad \theta^{min} \le \theta \le \theta^{max} \tag{3.53}$$

It can be shown that the minimization problem in (3.53) is convex if S has full rank N_θ, see [5].

The algorithms solving (3.53) are iterative. One type of algorithms are based on the division of the parameters into the set of free parameters θ^{free} and the set of fixed parameters θ^{fix}. During one iteration the fixed parameters will not change, and can temporarily be removed from the problem.

The iterative computation of $\check{\theta}$ in (3.53) can be written

$$\check{\theta} = \lim_{i\to\infty} \theta^i, \quad \theta^{i+1} = \theta^i + \Delta\theta^i, \quad \theta^0 = \theta^{init} \tag{3.54}$$

where $\Delta\theta^i$ is the vector of parameter changes in one iteration, and superscript i denotes the iteration number. The free parameters θ^{free} in an iteration fulfills one of the conditions

$$C_1 \;:\; \theta_k^{min} < \theta_k^i < \theta_k^{max} \tag{3.55a}$$

$$C_2 \;:\; \theta_k^i = \theta^{min}, \quad \Delta\theta_k^i > 0 \tag{3.55b}$$

$$C_3 \;:\; \theta_k^i = \theta^{max}, \quad \Delta\theta_k^i < 0 \tag{3.55c}$$

If the parameter step $\Delta\theta^i$ for the free parameters θ^{free} is too large so that

$$\theta_k^{min} \leq \theta_k^i + \Delta\theta_k^i \leq \theta_k^{max} \quad \forall\theta_k \in \theta^{free} \tag{3.56}$$

is violated, the parameter step $\Delta\theta^i$ must be reduced:

$$\theta^{i+1} = \theta^i + \alpha{\cdot}\Delta\theta^i, \quad \alpha = \min_k\{\alpha_k\} \quad \text{where} \tag{3.57}$$

$$\alpha_k = \begin{cases} (\theta_k^{max} - \theta_k^i)/\Delta\theta_k^i, & \theta_k^i + \Delta\theta_k^i > \theta_k^{max} \\ (\theta_k^{min} - \theta_k^i)/\Delta\theta_k^i, & \theta_k^i + \Delta\theta_k^i < \theta_k^{min} \end{cases}$$

Letting the free parameters be determined by the conditions $C_1 - C_3$ in (3.55), adjusting the solution $\Delta\theta^i$ as in (3.57), the minimization of the constrained problem in (3.53) may be performed properly, see [5] for the details.

Including Quadratic Inequality Constraints

The quadratic inequality constrained minimization problem can be formulated as

$$\check{\theta} = \arg\min_\theta \left\|S\theta - d\right\|_2 \quad \text{subject to} \quad \left\|F\theta - h\right\|_2 \leq \gamma_\theta \tag{3.58}$$

The interpretation of F, h and γ_θ are as scaling of θ, mean value of $F\theta$, and deviation factor for $F\theta$ from h, respectively. It can be shown that the solution of (3.58) is

$$\check{\theta}(\mu) = (S^TS + \mu_\theta^2 F^TF)^{-1}(S^Td + \mu F^Th) \tag{3.59}$$

for some $\mu > 0$. It can also be shown that

$$\left\|S\check{\theta}(\mu) - d\right\|_2 \tag{3.60}$$

is a function monotonically increasing in μ. Thus, the larger μ is, the larger the deviation from the unbiased minima $\check{\theta}$ in (3.50) is.

If the prior knowledge about the parameters in (3.52) only are vague, i.e.,

$$\theta^{min} \lesssim \theta \lesssim \theta^{max} \tag{3.61}$$

one may restate (3.61) as the quadratic inequality

$$\|F\theta - h\|_2 \leq \gamma_\theta \tag{3.62}$$

for some F, h and γ_θ. There are some advantages with the formulation in (3.58) compared to the formulation in (3.53). First, the division of the parameters into the free and fixed parameters are avoided. Moreover, a design variable μ is obtained, that may be used to form a well-balanced solution between the deviation in the parameters $\|\check{\theta}(\mu) - \theta^{init}\|$, and the minimization of the cost function $V = \|S\check{\theta}(\mu) - d\|_2$. Notice that every $\mu > 0$ corresponds to the solution of the minimization problem in (3.58) for some F, h and γ_θ.

Regularization

If S in (3.48) is ill-conditioned, a regularization term μ can be added in order to decrease the condition number of S^TS:

$$\check{\theta} = \arg\min_\theta \left\{ \left\|S\theta - d\right\|_2^2 + \mu^2 \left\|F\theta\right\|_2^2 \right\} \tag{3.63}$$

where $F \in \mathbb{R}^{N_\theta \times N_\theta}$, compare with (3.58). If μ and F are properly chosen, physically unrealistic values of $\check{\theta}$ may be avoided. The formulated minimization problem in (3.63) can be reformulated as

$$\check{\theta} = \arg\min_\theta \left\| \begin{bmatrix} S \\ \mu F \end{bmatrix} \theta - \begin{bmatrix} d \\ 0 \end{bmatrix} \right\|_2 = \arg\min_\theta \left\| \begin{bmatrix} R \\ \mu F \end{bmatrix} \theta - \begin{bmatrix} Q^T d \\ 0 \end{bmatrix} \right\|_2 \tag{3.64}$$

where $S = QR$ is the QR-factorization of S. The well-known regularization of (3.51) made in (3.63) can be regarded as a special case of the quadratic inequality constraint in (3.58).

3.7.2 Non-Linear Least Squares

In (3.48) it was assumed that the underlying statistical model defined by $v(\theta)$ is linear in the parameters. For a statistical model being nonlinear in the parameters, a linearization can be made:

$$v(\theta + \delta\theta) = v(\theta) + J(\theta)\delta\theta + \mathcal{O}(\|\theta\|_2^2) \tag{3.65}$$

Compare this with (3.7) and (3.8). The approximating solution of the NLLS

$$\check{\theta} = \arg\min_\theta V(\theta) \tag{3.66}$$

can thus be formulated as

$$\hat{\theta} = \lim_{i\to\infty} \theta^i, \quad \theta^{i+1} = \theta^i + \Delta\theta^i, \quad \Delta\theta_i = \left(J^T J\right)^{-1} J^T d \tag{3.67}$$

where $d = v(\theta^i) - v^x$ and $J = J(\theta^i)$ are parameter-varying, compare with (3.50). There are also methods relying on the Hessian H, $H_{kl} = \partial^2 v / \partial\theta_k \partial\theta_l$ of v, but a numerical computation of H is here too expensive to be practical.

A convenient validation of the parameter step $\Delta\theta^i$ is to check if the condition

$$C_v \quad : \qquad V(\theta^i + \Delta\theta^i) < V(\theta^i) \tag{3.68}$$

holds. If not, a new parameter step $\Delta\theta^i$ should be determined, or the algorithm should terminate if an appropriate $\Delta\theta^i$ cannot be found.

Trust Region Methods

Often the NLLS problems are ill-conditioned. To overcome this problem, regularization may be used to decrease the condition number κ of $(J^T J)^{-1}$. This is the idea behind the Levenberg-Marquardt method:

$$\begin{aligned} \Delta\theta^i &= F(\theta^i)^{-1} \Delta\theta^i_F, \\ \Delta\theta^i_F &= \arg\min_{\Delta\theta_F} \left\{ \left\| J(\theta^i) F(\theta^i) \Delta\theta_F - d(\theta^i) \right\|_2^2 + \mu^2 \left\| F(\theta^i) \Delta\theta_F \right\|_2^2 \right\} \end{aligned} \tag{3.69}$$

where F is a scaling matrix. A common choice of F is to let $F\Delta\theta$ reflect the relative parameter step,

$$F = \mathrm{diag}(\dots, 1/\theta_k, \dots) \tag{3.70}$$

see [28]. Henceforth, it is assumed that the scaling F of $\Delta\theta$ is tacitly understood in the formulation of the NLLS problem, i.e., $\Delta\theta$ denotes $\Delta\theta_F$:

$$\Delta\theta^i = \arg\min_{\Delta\theta} \left\{ \left\| J(\theta^i)\Delta\theta - d(\theta^i) \right\|_2^2 + \mu^2 \left\| \Delta\theta \right\|_2^2 \right\} \tag{3.71}$$

If $\overline{\sigma}(J) \gg \mu \gg \underline{\sigma}(J)$, the condition number κ of $J_\mu^T J_\mu$, where $J_\mu = [J^T \; \mu I]^T$ approximately becomes

$$\kappa(J_\mu^T J_\mu) = \frac{\overline{\sigma}(J)^2 + \mu^2}{\underline{\sigma}(J)^2 + \mu^2} \approx \frac{\overline{\sigma}(J)^2}{\mu^2} \tag{3.72}$$

where $\overline{\sigma}(\cdot)$ and $\underline{\sigma}(\cdot)$ denote the largest and smallest singular value of J, respectively. Thus, the regularization term μ may therefore be interpreted as a pre-conditioner of the NLLS problem in (3.71).

Fletcher's Method

The Levenberg-Marquardt approach to solve the NLLS is often feasible in practice. However, for highly non-linear problems, the value of μ can be the difference between failure and success. The very important choice of μ must therefore be made carefully. A method to adaptively select a value of μ is given in [47], see also [39].

The NLLS is based on the assumption that the cost function $V(\theta^i)$ is quadratic in its parameters, see (3.65). This is true only in some small neighborhood Θ_r around θ^i, since otherwise the linearization of $v(\theta^i)$ is not valid. Therefore, the quotient

$$r = \frac{V(\theta^i) - V(\theta^i + \Delta\theta^i)}{V(\theta^i) - \|v(\theta^i) + J(\theta^i)\Delta\theta^i\|_2^2} \tag{3.73}$$

may be used to determine if the linearization in (3.65) is valid or not. If $r \approx 1$ the linearization is valid but due to the non-linearity of v, the parameter-step $\Delta\theta^i$ is probably to small to yield a sufficient minimization of V. If r is small, the linearization is not valid, and the parameter step $\Delta\theta^i$ is probably not appropriate. A strategy to adaptively choose the value μ may be to increase μ when $r < r_{min}$, and decrease μ when $r > r_{max}$. This idea is put forward in [47] where the values $r_{min} = 0.25$ and $r_{max} = 0.75$ is proposed.

Let the scalar function

$$\chi(\alpha) = V(\theta^i + \alpha\cdot\Delta\theta^i) \tag{3.74}$$

be the value of the cost function along the parameter step $\Delta\theta^i$. Since the values

$$\chi(0), \quad \chi(1), \quad \chi'(0) = J^T d \tag{3.75}$$

are known, $\chi(\alpha)$ may be approximated with a quadratic function $\hat{\chi}(\alpha)$. It can be shown that the minimizing argument $\hat{\alpha}$ of $\hat{\chi}(\alpha)$ equals

$$\hat{\alpha} = \frac{J^T d}{V(\theta^i) - V(\theta^i + \Delta\theta^i) + 2\Delta\theta^i J^T d} \tag{3.76}$$

Notice that

$$\Delta\theta^i \text{ and } \mu^2 \quad \leftrightarrow \quad \frac{\Delta\theta^i}{\beta} \text{ and } \mu^2\cdot\beta \tag{3.77}$$

when μ^2 is sufficiently large compared to $\|J^T J\|_2$. In (3.76), $\leftrightarrow$ should be interpreted "approximately correspond to". The regularization term μ is then altered as

$$r > r_{max}: \quad \mu_{i,j+1} = \frac{\mu_{i,j}}{c} \tag{3.78a}$$

$$r < r_{min}: \quad \mu_{i,j+1} = c\mu_{i,j} \tag{3.78b}$$

where subscript i, j denotes the parameter iteration i, and the regularization iteration j, and where

$$c = \max\Big\{c_{min}, \min\{c_{max}, 1/\hat{\alpha}\}\Big\} \tag{3.79}$$

If $r_{min} < r < r_{max}$, $\mu_{i,j}$ is left unaltered. In [47], the values 2 and 10 of c_{min} and c_{max} is proposed.

3.8 Model Updating Using Frequency Domain Measurements

In this section the proposed model updating formulations are presented. After some introductory remarks in Section 3.8.1, a computationally cheap and general model updating procedure is proposed in 3.8.2. Using the proposed procedure, the computational burden is reduced substantially. The reduction of computation time is obtained through a semi-fixed basis of reduction, and a semi-fixed linearization of the system matrices are kept fixed for several parameter estimation iterations, see Fig. 3.2. In Section 3.8.4, a cost function V_{mp} using mode pairing, with enhanced convergence properties is presented. A mode-pairing free cost function $\bar{V}$ corresponding to V_{mp} is proposed in Section 3.8.5. The absence of mode-pairing minimizes the drawbacks of the mode-pairing, and therefore also the risk of ending up in a local minimum.

3.8.1 Prerequisites

Several frequency domain model updating formulations have been proposed recently, see Section 3.2.2. Essentially they rely on the input error equations (3.18), or the output error equations (3.19). The main advantage using frequency domain (FRF) measurements in the cost function is that spatial information of the structure is included in it. Another advantage is that scaling is not necessary since G is an I/O-property of the structure. Compare with the scaling of modes in (3.16)-(3.17).

Moreover, minimizing the deviation in the FRF corresponds to the maximum likelihood (ML) estimate, see [27]. Basically, the ML-estimate is the best estimate if the noise of the measurements are Gaussian distributed. However, we have found that there also exist some drawbacks using the FRF in the cost function. Cost functions only based on the FRF have a small domain of attraction $\check{\Theta}$, due to the frequent appearance of local minima. But the drawbacks of the FRF can be reduced substantially if the deviations in the resonance frequencies are included in the cost function.

If a combined resonance frequency/FRF cost function is used, a cost function with better parameter estimate properties than both the traditional modal domain formulations, and the more recent FRF-based formulations is achieved. This is the main idea of the proposed cost functions: to include both the deviation in the resonance frequencies, and the deviation in the FRF. Compared to the traditional frequency domain cost functions, enhanced convergence properties are obtained, and compared to the traditional modal domain cost functions, the problems with scaling are minimized.

The normal modes ϕ_i corresponding to the measured modes $\hat{\phi}_i^x$ must be computed in order to ensure a reliable model updating. Denoting ω_R^x and ω_R as the frequency areas for the resonance frequencies $\hat{\omega}_i^x$ and ω_i, respectively, it is necessary that $\omega_R^x \subset \omega_R$. For instance,

$$\omega_R^x = \{\omega \,|\, 2 \leq \omega \leq 80\} \text{ Hz}$$

and

$$\omega_R = \{\omega \,|\, 1 \leq \omega \leq 120\} \text{ Hz}$$

are frequency regions typical for model updating. For large flexible structures, the number of normal modes N_q of the model may therefore be considerably higher than the number of measured modes N_q^x of the structure, i.e., $N_q \gg N_q^x$.

Here it is assumed that the estimate $\hat{\phi}_i^x$ is defined by (3.28). The estimates $\hat{\omega}_i^x$ and $\hat{\xi}_i^x$ are assumed to equal ω_i^x and ξ_i^x, respectively.

3.8.2 A Computationally Cheap Model Updating Procedure

FE models of large dynamical structures may be huge ($N_{dof} = 100,000$ is not uncommon in aviation applications). The computation of the modes ϕ_i and the corresponding resonance frequencies ω_i of the eigenvalue problem (2.42) may be time-consuming even if high-performing computers are used. The second most time-consuming part is the construction of the system matrices M and K. In order to reduce the computational burden, the number of times the modes are computed, and the number of times the system matrices are constructed should be alleviated.

In a model updating context, the computation of the Jacobian J may become extremely expensive if approximations are not made. To reduce the computational burden of the algorithms, it is therefore natural to focus on the expenses of computing J. Here, a computationally cheap, general procedure for model updating is proposed, see Fig. 3.2. The model updating procedure is based on the reduction and linearization of the system matrices. The basis for reduction is kept fixed for several iterations, i.e., *semi-fixed*. This reduces the number of times the modes of the model must be computed. In the same fashion, the linearization of the system matrices are kept semi-fixed. This reduces the number of times the system matrices must be constructed. Thus, an approximation v_r^{lin} of v is obtained:

$$v(\theta) = v\big(w(\theta)\big), \quad v_r^{lin}(\theta) = v\big(w_r^{lin}(\theta)\big) \tag{3.80}$$

where w denotes properties of the model, and v denotes the differences between the model and the measurements defined by the cost function V. In (3.80), lin and r are short for linearization and reduction, respectively. The validity of the approximation made depends on the parameterization, and the invariance properties of the basis of reduction.

The cost function $V = |v|_2^2$ to be minimized may be written

$$V(\theta) = v^T(\theta)v(\theta) \tag{3.81}$$

where v is the deviation vector between the properties of the model v^a and the measurements of the structure v^x,

$$v(\theta) = v^a(\theta) - v^x \tag{3.82}$$

The cost function V is not further specified here, see Section 3.8.4 and Section 3.8.5 for the choice of V. Here it suffices to know that the deviation between the model and the structure is represented by the vector v. The parameters θ in (3.81) defines a parameterization of the system matrices:

$$M = M(\theta), \quad L = L(\theta), \quad K = K(\theta) \tag{3.83}$$

where

$$\theta = \left[\theta_1, \dots, \theta_{N_\theta}\right]^T \tag{3.84}$$

is the vector of parameters. The damping matrix L is here assumed to be implicitly parameterized via M and K:

$$L(\theta) = L(M(\theta), K(\theta)) \tag{3.85}$$

The vector v^a in (3.82) may therefore be expressed as

$$v^a(\theta) = v^a(M(\theta), K(\theta)) \tag{3.86}$$

Assuming a basis Φ_r of reduction is selected as in Section 3.4,

$$\Phi_r = [\phi_{i_1}, \dots, \phi_{i_{N_q^x}}] \tag{3.87}$$

a reduction of M and K in (3.83) may be performed

$$M_r(\theta) = \Phi_r^T M(\theta)\Phi_r, \quad K_r(\theta) = \Phi_r^T K(\theta)\Phi_r \tag{3.88}$$

The size of the system matrices in (3.88) is reduced from $N_{dof} \times N_{dof}$ to $N_q^x \times N_q^x$. Notice that $\Phi_r = \Phi_r(\theta)$ in (3.87) and (3.88). If Φ_r is semi-fixed, i.e., kept fixed during several parameter estimate iterations, the computation time may be reduced substantially. When the invariance properties of the semi-fixed reduction basis Φ_r are no longer valid, Φ_r is recomputed, and kept semi-fixed until a new computation of Φ_r is necessary.

In commercial FE software packages, the differentiation of M and K w.r.t. θ_k is not available in symbolic form. One is therefore restricted to numerical difference quotient approximations:

$$\frac{\partial M}{\partial \theta_k} \approx \widehat{\frac{\partial M}{\partial \theta_k}} = \frac{M(\theta_k + \delta\theta_k) - M(\theta_k)}{\delta\theta_k} \tag{3.89a}$$

$$\frac{\partial K}{\partial \theta_k} \approx \widehat{\frac{\partial K}{\partial \theta_k}} = \frac{K(\theta_k + \delta\theta_k) - K(\theta_k)}{\delta\theta_k} \tag{3.89b}$$

The numerical differentiation of M and K w.r.t. θ as in 3.89 require $N_\theta + 1$ constructions of M and K, respectively.

In view of (3.35), (3.38), and (3.89), a linearization of M_r and K_r can be made:

$$M_r^{lin}(\theta + \Delta\theta) = M_r(\theta) + \sum_{k=1}^{N_\theta} \Phi_r^T \widehat{\frac{\partial M}{\partial \theta_k}} \Phi_r \Delta\theta_k + \mathcal{O}(|\Delta\theta|^2) \tag{3.90a}$$

$$K_r^{lin}(\theta + \Delta\theta) = K_r(\theta) + \sum_{k=1}^{N_\theta} \Phi_r^T \widehat{\frac{\partial K}{\partial \theta_k}} \Phi_r \Delta\theta_k + \mathcal{O}(|\Delta\theta|^2) \tag{3.90b}$$

where $\Delta\theta_k$ denotes entry k of $\Delta\theta$.

The frequency region ω_R^x of interest suggests that v in (3.86) may be approximated by v_r^{lin}:

$$v_r^{lin}(\theta) = v_r^{lin}\big(M_r^{lin}(\theta), K_r^{lin}(\theta)\big), \quad \theta \in \Theta_v \tag{3.91}$$

for an open subset Θ_v around θ. Recall the invariance properties of Φ_r discussed in Section 3.4. An approximation J_r^{lin} of the Jacobian J using (3.91) is obtained as

$$J_{r,k}^{lin} = \frac{v_r^{lin}(\theta_k + \delta\theta_k) - v_r^{lin}(\theta_k)}{\delta\theta_k} \tag{3.92}$$

where $J_{r,k}^{lin}$ is the k-th column of J_r^{lin}. Compare this with (3.8). Notice, the computation of $v_r^{lin}(\theta_k + \delta\theta_k)$ in (3.92) is made using the linearizations $M_r^{lin}(\theta)$, $K_r^{lin}(\theta)$ of M_r and K_r in (3.90). The computation of v_r^{lin} is very cheap whenever the linearizations of $M_r(\theta)$, $K_r(\theta)$ in (3.90) are available. Therefore the approximation J_r^{lin} of J is very inexpensive to compute. This can be used to obtain a cheap approximate estimate of $\check{\theta}$.

Using the semi-fixed basis Φ_r, and the linearization of M_r and K_r in (3.90), a computationally cheap model updating procedure may be formulated, see Fig. 3.2.

In Section 2.7 it is pointed out that diagonal representations of the system matrices are desirable for computational reasons. If M_r and K_r in (3.88) are not diagonal, the eigenvalue problem

$$(K_r - (\omega_i^r)^2 M_r)\phi_i^r, \quad (\phi_i^r)^T M_r \phi_i^r = 1, \quad i = 1, \ldots, N_q^x \tag{3.93}$$

is solved. Defining

$$\Phi_r^d = \Phi_r \Phi_d = [\phi_1^d, \ldots, \phi_{N_q^x}^d], \quad \Phi_d = [\phi_1^r, \ldots, \phi_{N_q^x}^r] \tag{3.94}$$

the reduced system matrices M_r and K_r become diagonal:

$$M_r^d = \Phi_d^T M_r \Phi_d = (\Phi_r^d)^T M \Phi_r^d = I \tag{3.95a}$$

$$K_r^d = \Phi_d^T K_r \Phi_d = (\Phi_r^d)^T K \Phi_r^d = \operatorname{diag}(\ldots, (\omega_i^r)^2, \ldots) \tag{3.95b}$$

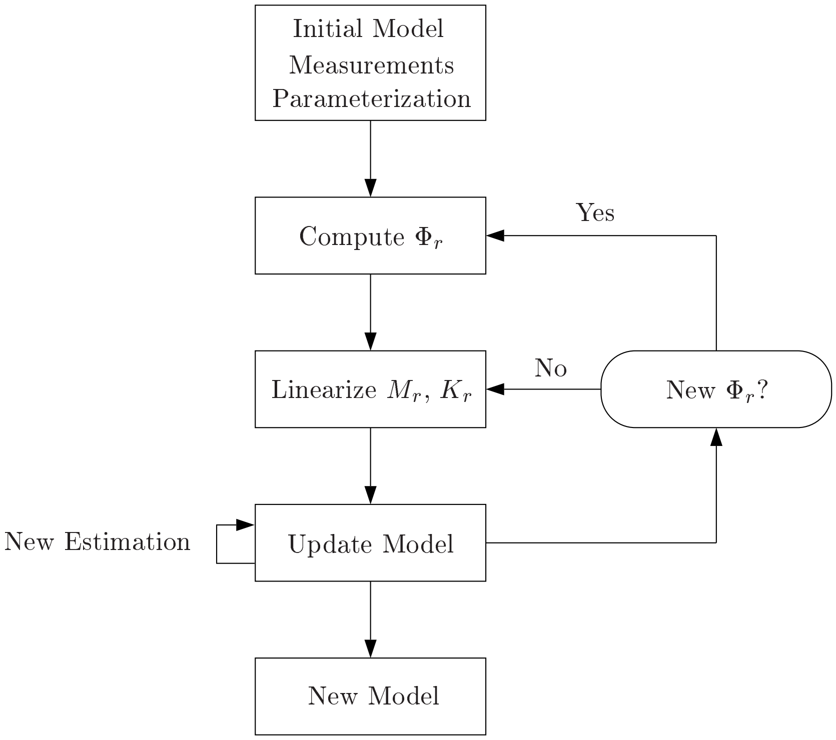

Figure 3.2 *A flow chart of the inexpensive model updating procedure.*

where Φ_r^d is a matrix of dimension $N_{dof} \times N_q^x$, and Φ_d is a matrix of dimension $N_q^x \times N_q^x$.

Henceforth, the notation v_r^{lin} and J_r^{lin} are suppressed: v, and J denote v_r^{lin}, and J_r^{lin}, respectively.

3.8.3 Description of the Optimization Method

In Fig. 3.2 it is seen that the model updating procedure has three loops, and therefore also three cost functions. One loop concerns the iterations when both the reduction basis Φ_r and the linearization in (3.90) are kept fixed, another when Φ_r is kept fixed but the linearization in (3.90) is computed, and the third when both Φ_r and the linearization in (3.90) are computed. The corresponding cost functions are denoted as

$$\begin{array}{llll} V_{um}: & \Phi_r \text{ fixed,} & M_r^{lin}, K_r^{lin} & \text{fixed} \quad (3.96a) \\ V_{mk}: & \Phi_r \text{ fixed,} & M_r^{lin}, K_r^{lin} & \text{computed} \quad (3.96b) \\ V_{rb}: & \Phi_r \text{ computed,} & M_r^{lin}, K_r^{lin} & \text{computed} \quad (3.96c) \end{array}$$

where subscripts um, mk, rb is "short" for update model, linearize M, K, and reduction basis, respectively. Since there are three cost functions, there are also three parameter trajectories denoted by

$$\theta_{um}, \quad \theta_{mk}, \quad \theta_{rb} \tag{3.97}$$

corresponding to the cost functions V_{um}, V_{mk}, V_{rb}. The differences are due to that V_{mk} and V_{rb} is not computed in every iteration. Since the approximations v_r^{lin}, J_r^{lin} are used, the following is a consequence:

$$\begin{aligned}
&V_{um} \not\equiv V_{mk} \not\equiv V_{rb} : && \Phi_r \ \text{fixed}, && M_r^{lin}, K_r^{lin} \ \text{fixed} && (3.98a)\\
&V_{um} = V_{mk} \not\equiv V_{rb} : && \Phi_r \ \text{fixed}, && M_r^{lin}, K_r^{lin} \ \text{computed} && (3.98b)\\
&V_{um} = V_{mk} = V_{rb} : && \Phi_r \ \text{computed}, && M_r^{lin}, K_r^{lin} \ \text{computed} && (3.98c)
\end{aligned}$$

Notice that due to (3.98):

$$\begin{aligned}
V_{um}(\theta^{i+1}) < V_{um}(\theta^{i}) \quad &\not\Rightarrow \quad V_{mk}(\theta^{i+1}) < V_{mk}(\theta^{i}) && (3.99a)\\
V_{um}(\theta^{i+1}) < V_{um}(\theta^{i}) \quad &\not\Rightarrow \quad V_{rb}(\theta^{i+1}) < V_{rb}(\theta^{i}) && (3.99b)\\
V_{mk}(\theta^{i+1}) < V_{mk}(\theta^{i}) \quad &\not\Rightarrow \quad V_{rb}(\theta^{i+1}) < V_{rb}(\theta^{i}) && (3.99c)
\end{aligned}$$

where $\not\Rightarrow$ should be interpreted as "does not necessarily imply that". Due to (3.99), the cost function condition C_v in (3.68) may be relaxed to:

$$\begin{aligned}
C_{um} &: \quad V_{um}(\theta_{um}^{i}) > V_{um}(\theta_{um}^{i} + \Delta\theta^{i}) && (3.100a)\\
C_{mk} &: \quad V_{mk}(\theta_{mk}^{i}) > \min_{l} V_{mk}(\theta_{mk}^{i+l}), \quad l = 1, \dots, N_{mk} && (3.100b)\\
C_{rb} &: \quad V_{rb}(\theta_{rb}^{i}) > \min_{l} V_{rb}(\theta_{rb}^{i+l}), \quad l = 1, \dots, N_{rb} && (3.100c)
\end{aligned}$$

where N_{mk} and N_{rb} are design variables. Besides the conditions in (3.100), other termination criteria may be used. A parameter step changes M and K. One may therefore use

$$C_{M_rK_r} \ : \quad \max\left\{ \frac{\|M_r(\theta_{um}^{i+1}) - M_r(\theta_{um}^{i})\|_{Fro}}{\|M_r(\theta_{um}^{i})\|_{Fro}}, \frac{\|K_r(\theta_{um}^{i+1}) - K_r(\theta_{um}^{i})\|_{Fro}}{\|K_r(\theta_{um}^{i})\|_{Fro}} \right\} > \Delta_{M_rK_r} \tag{3.101a}$$

$$C_{MK} \ : \quad \max\left\{ \frac{\|M(\theta_{mk}^{i+1}) - M(\theta_{mk}^{i})\|_{Fro}}{\|M(\theta_{mk}^{i})\|_{Fro}}, \frac{\|K(\theta_{mk}^{i+1}) - K(\theta_{mk}^{i})\|_{Fro}}{\|K(\theta_{mk}^{i})\|_{Fro}} \right\} > \Delta_{MK} \tag{3.101b}$$

as termination criteria for V_{um} and V_{mk}, respectively. The interpretation of $\Delta_{M_rK_r}$ and Δ_{MK} are as the largest relative differences for the linearization in (3.90) and for the reduction basis in (3.87) to be valid.

Notice that a termination of the loop corresponding to V_{um} only implies a new linearization of $M_r(\theta)$ and $K_r(\theta)$, see (3.90). A termination of the V_{mk}-loop implies a new selection of Φ_r, see (3.87). However, a termination of the V_{rb}-loop terminates the model updating procedure.

In Fletcher's original method, the regularization term μ was increased from zero until the condition

$$C_r \;:\quad r_{min} < r < r_{max} \tag{3.102}$$

was fulfilled. We have found that a more robust determination of μ is necessary in order to not accept a too small μ, i.e., to prevent a too large parameter step $\Delta\theta^i$. Recall that prior knowledge of the parameters are available, which implies that physically unrealistic values of θ should not be permitted. Also, a too big parameter step may increase the risk of ending up in an undesired local minimum. Starting with an initial value $\mu_{i,0}$, $\mu_{i,j}$ is adjusted according to (3.78). However, $r = r(\mu)$ is not monotonically decreasing with μ. One must therefore determine $\mu_{i,0}$ carefully. We have empirically found that relating μ to $\|J\|_2$ work well,

$$\mu_{i,0} = \alpha_\mu \cdot \bar{\sigma}, \quad \bar{\sigma} = \|J\|_2 \tag{3.103}$$

where α_μ is a function of the relative reduction of the cost function V_{rb}:

$$\alpha_\mu = \alpha_\mu(\Delta V_{rb}), \quad \alpha'_\mu(\Delta V_{rb}) > 0, \quad \Delta V_{rb} = \frac{V_{rb}(\theta^i_{rb})}{V_{rb}(\theta^0_{rb})} \tag{3.104}$$

in the iterations ending up with determining θ^{i+1}_{rb}. The strategy of choosing μ as in (3.103) and (3.104) can be motivated by that the closer θ^i is to $\check{\theta}$, the better is the assumption of V being quadratic in θ. If V really is quadratic in θ, then $\mu = 0$ is the best choice. Thus, the regularization μF in (3.69), are related to the parameter values through F, to the validity r of the assumption of V being quadratic in θ, to the spectral norm of J and to the relative improvement $V_{rb}(\theta^i_{rb})/V_{rb}(\theta^0_{rb})$, see (3.70), (3.73), (3.103), and (3.104).

The concern for a robust choice of μ, is the common situation of numerous local minima. Also the prior knowledge of the parameters influences the choice of μ. Furthermore, μ is the single most important design variable of the optimization method. If μ is not appropriately chosen, it is more likely that the estimate $\hat{\theta}$ ends up in an undesired local minimum.

The convergence of the parameter estimates can be slow if μ is chosen too conservative, but it is a prize one must pay for a consistent estimation of θ, i.e., for $\hat{\theta} = \check{\theta}$. However, the robustness requirements may be relaxed when the cost function improvement is significant, $V_{rb}(\theta^i_{rb})/V_{rb}(\theta^0_{rb}) < \gamma_{rb}$. Then the validity of the assumption of V being quadratic in θ is not considered, i.e., r is not affecting the choice of μ. Instead μ is only determined by $\Delta\theta^i$:

$$\mu \;:\quad \|\Delta\theta^i\| < \gamma_{\Delta\theta} \tag{3.105}$$

where $\gamma_{\Delta\theta}$ is the maximum relative parameter step length.

If the reduction of the step length via $\gamma_{\Delta\theta}$ in (3.105) fails to keep the parameter values θ^i_k so that $\theta^{min}_k < \theta^i_k < \theta^{max}_k$, an optimization method constraining the parameter estimate is used, see Section 3.7.1.

3.8.4 A Cost Function Using Mode Pairing

Here a cost function based on mode-pairing will be proposed. The cost function uses all the measurements assumed to be available, see Section 3.1. Assume that the normal modes ϕ_i corresponding to $M(\theta)$ and $K(\theta)$ for $\theta = \theta^n$ are computed. If a mode pairing algorithm has paired every measured mode

$$\hat{\phi}_i^x, \quad i = 1, \dots, N_q^x \tag{3.106}$$

of the structure to a normal mode

$$\phi_j, \quad j \in \{1, \dots, N_q\} \tag{3.107}$$

of the model, then the triples

$$\{\phi_i, \omega_i, \xi_i\} \leftrightarrow \{\hat{\phi}_i^x, \hat{\omega}_i^x, \hat{\xi}_i^x\}, \quad i = 1, \dots, N_q^x \tag{3.108}$$

may also be considered as pairs with reordered indices. In (3.108), the $\leftrightarrow$ denotes the paired triples corresponding to the pairs $\phi_i \leftrightarrow \hat{\phi}_i^x$.

Using the basis

$$\Phi_r = [\phi_1, \dots, \phi_{N_q^x}] \tag{3.109}$$

for reduction of the FE model, the reduced system matrices become

$$M_r = I \tag{3.110a}$$

$$L_r = \text{diag}(\dots, 2\omega_i \hat{\xi}_i^x, \dots) \tag{3.110b}$$

$$K_r = \text{diag}(\dots, \omega_i^2, \dots) \tag{3.110c}$$

where $\hat{\xi}_i$ is the measured damping ratios assigned to the model according to (3.108), i.e., $\xi_i = \hat{\xi}_i^x$. The reduced model becomes

$$\begin{aligned} M_r \ddot{q} + L_r \dot{q} + K_r q &= \Phi_r^T B u \\ y &= C \Phi_r q \end{aligned} \tag{3.111}$$

and the corresponding FRF

$$G_r(\omega) = C\Phi_r \big(\text{diag}(\dots, \omega^2 - \omega_i^2 + j2\hat{\xi}_i^x \omega_i \omega, \dots)\big)^{-1} \Phi_r^T B \tag{3.112}$$

Compare this with (3.33).

For a perturbation of the parameters,

$$\theta = \theta^n + \Delta\theta \tag{3.113}$$

the reduced system matrices M_r and K_r are no longer diagonal. Diagonalizing M_r and K_r as in (3.93)-(3.95), the reduced system matrices become

$$M_r^d = I \tag{3.110a}$$

$$L_r^d = \text{diag}(\dots, 2\omega_{r,i} \hat{\xi}_i^x, \dots) \tag{3.110b}$$

$$K_r^d = \text{diag}(\dots, \omega_{r,i}^2, \dots) \tag{3.110c}$$

where the measured damping $\hat{\xi}_i^x$ is paired to the damping ratio ξ_i of the model, via the pairing of $\phi_j^d = \Phi_r \phi_j^r$, and $\hat{\phi}_i^x$:

$$\{\phi_i^d,\, \omega_{r,i},\, \xi_{r,i}\} \leftrightarrow \{\hat{\phi}_i^x,\, \hat{\omega}_i^x,\, \hat{\xi}_i^x\}, \quad i = 1, \ldots, N_q^x \tag{3.115}$$

where the indices are reordered according to the outcome of a mode pairing algorithm.

The reduced, perturbed, and diagonalized model becomes

$$\begin{aligned} M_r^d \ddot{q} + L_r^d \dot{q} + K_r^d q &= (\Phi_r^d)^T B u \\ y &= C \Phi_r^d q \end{aligned} \tag{3.116}$$

and the corresponding FRF becomes

$$G_r^d(\omega) = C\Phi_r^d \big(\mathrm{diag}(\ldots, \omega^2 - \omega_{r,i}^2 + j2\hat{\xi}_i^x \omega_{r,i}\omega, \ldots)\big)^{-1} (\Phi_r^d)^T B \tag{3.117}$$

Notice that G_r^d equals G_r whenever M_r and K_r are diagonal.

Using all the commonly available measurements, a combined frequency/modal domain cost function can be constructed as

$$V_{mp}(\theta)|_{mp} = \nu_1^2 V_{mp,1}(\theta)|_{mp} + \nu_2^2 V_{mp,2}(\theta)|_{mp} + \nu_3^2 V_{mp,3}(\theta)|_{mp} \tag{3.118}$$

where ν_i are cost function weights, and where $|_{mp}$ denotes that a mode-pairing has been made in order to ensure that the cost function makes sense. In (3.118), the cost function parts $V_{mp,i}$ are defined as

$$V_{mp,1}(\theta) = \sum_{i=1}^{N_\omega} \left\| G_r^d(\theta, \omega_{R,i}^x) - G^x(\omega_{R,i}^x) \right\|_{Fro}^2 \tag{3.119a}$$

$$V_{mp,2}(\theta) = \sum_{i=1}^{N_q^x} \left| \frac{\omega_{r,i}(\theta) - \hat{\omega}_i^x}{\hat{\omega}_i^x} \right|_2^2 \tag{3.119b}$$

$$V_{mp,3}(\theta) = \sum_{i=1}^{N_q^x} \left\| G_r^d(\theta, \hat{\omega}_i^x) \bar{U}_i^x - \bar{Y}_i^x \right\|_2^2 \tag{3.119c}$$

where G_r^d in (3.119a) denotes the FRF of the reduced model, N_ω the number of measured frequency points $\omega_{R,i}^x$ of G^x, and Fro the Frobenius norm. In (3.119b), N_q^x denotes the number of measured modes of the structure, $\omega_{r,i}$ and $\hat{\omega}_i^x$ denote the resonance frequencies of the model and the structure, respectively. In (3.119c), $\bar{Y}_i^x$ denotes the measured frequency response output, see (3.24), and $\bar{U}_i^x$ is the commanded input force pattern generating $\bar{Y}_i^x$.

3.8.5 A Mode Pairing Free Cost Function

The proposed cost function in (3.118) uses all available information (measurements) of the structure but has a serious drawback which may introduce severe local minima. The drawback is the assumption that a successful mode pairing is made (the major drawback is perhaps the assumption that a good mode pairing is possible at all). In [1] it is shown that the pairing of modes is critical for a model updating task to be successful. For instance, all the proposed terms $V_{mp,i}$ of the cost function in (3.118) relies on a successful mode pairing. One may therefore search for cost functions where the influence of an unsuccessful mode pairing is minimized. Here a mode-pairing free cost function corresponding to V_{mp} in (3.118) is proposed. However, the proposed cost function requires accurate estimates of $\hat{\phi}_i^x$ for the estimate $\hat{\theta}$ to be consistent, i.e., for $\hat{\theta} = \check{\theta}$.

The traditional model updating formulations use the paired modes ϕ_i of the model as a basis for reduction of the system matrices M, L and K. This mode by mode view is relevant for experimental modal analysis when a validation of the model is desired. For model updating (model reduction) it is an unnecessary restriction, though.

The construction of Φ_r as in Section 3.8.4, may be viewed as an attempt to obtain a basis for the measured modes $\hat{\phi}_i^x$. However, this basis may not be appropriate if (near) multiple modes are present in the model and/or in the structure. For instance, suppose that ϕ_1 and ϕ_2 are modes of the model, and that $\phi^x = \alpha_1\phi_1 + \alpha_2\phi_2$ is a "true" mode of the structure. It is then clear that a successful mode pairing can not be guaranteed. A similar example for the case of multiple modes of the model may be constructed. These situations with multiple modes in the model and/or in the structure are considered as rather common in aviation applications, and must therefore be accounted for. This can be done if the basis vector $\bar{\phi} = \alpha_1\phi_1 + \alpha_2\phi_2$ is used to reduce the size of the model.

Defining $\hat{\phi}_i$ as

$$\hat{\phi}_i = \Phi_q \hat{a}_i, \quad \hat{a}_i = \underset{a \in \mathbb{R}^{N_q}}{\arg\min} \, \|\Phi_q a_i - \hat{\phi}_i^x\|_2, \quad i = 1, \ldots, N_q^x \tag{3.120}$$

where Φ_q is defined as the basis of all computed normal modes,

$$\Phi_q = [\phi_1, \ldots, \phi_{N_q}] \tag{3.121}$$

The column vectors $\hat{\phi}_i$ of the basis Φ_q is the projection of the measured modes $\hat{\phi}_i^x$ onto the subspace spanned by the basis Φ_q of computed modes of the model. The basis $\bar{\Phi}_r$ of reduction is then defined as

$$\bar{\Phi}_r = [\bar{\phi}_i, \ldots, \bar{\phi}_{N_q^x}], \quad \text{where} \quad \bar{\phi}_i = \frac{1}{\left((\hat{\phi}_i)^T M \hat{\phi}_i\right)^{1/2}} \hat{\phi}_i \tag{3.122}$$

where $\bar{\phi}_i$ is the mass-normalized version of $\hat{\phi}_i$. Notice that the mass-normalization of $\hat{\phi}_i$ in (3.122) is based on the assumption that the mass matrix M of the model is approximating the mass distribution of the structure accurately.

The resonance frequency $\bar{\omega}_i$ corresponding to $\bar{\phi}_i$ is defined by the Rayleigh quotient R,

$$R(\bar{\phi}_i) = (\bar{\omega}_i)^2 = \frac{\bar{\phi}_i^T K \bar{\phi}_i}{\bar{\phi}_i^T M \bar{\phi}_i}, \quad i = 1, \ldots, N_q^x \tag{3.123}$$

see (2.47). In [1], the enhanced parameter estimate convergence properties using the Rayleigh quotient in the cost function are studied.

The reduced system matrices $\bar{M}_r$ and $\bar{K}_r$ become

$$\bar{M}_r = \bar{\Phi}_r^T M \bar{\Phi}_r \tag{3.124a}$$
$$\bar{K}_r = \bar{\Phi}_r^T K \bar{\Phi}_r \tag{3.124b}$$

In order to obtain a reduced damping matrix $\bar{L}_r$, some assumptions about the damping distribution in the structure must be made. Let $\Phi_x = [\phi_1^x, \ldots \phi_{N_q^x}^x]$ denote the "true" modes of the structure, and L_x the "true" damping matrix of the structure. If the damping distribution in the structure are proportional, then $\Phi_x^T L \Phi_x$ will be diagonal. Assuming that $\hat{\phi}_i^x$ is parallel with ϕ_i^x, and that $\bar{\phi}_i^r$ is parallel with $\hat{\phi}_i^x$:

$$\hat{\phi}_i^x \parallel \phi_i^x, \quad \text{and} \quad \hat{\phi}_i^r \parallel \hat{\phi}_i^x, \quad i = 1, \ldots, N_q^x \tag{3.125}$$

then also $\bar{\Phi}_r^T L_x \bar{\Phi}_r$ will be diagonal. These assumptions indicate that $\bar{L}_r$ may be modeled as

$$\bar{L}_r = \text{diag}(\ldots, 2\hat{\xi}_i^x \bar{\omega}_i, \ldots) \tag{3.126}$$

where $\bar{\omega}_i$ is the square root of the Rayleigh quotient in (3.123).

However, the matrices $\bar{M}_r$ and $\bar{K}_r$ are in general not diagonal. A diagonalization of $\bar{M}_r$ and $\bar{K}_r$ using $\bar{\Phi}_r^d$ can then be performed as

$$\bar{M}_r^d = (\bar{\Phi}_r^d)^T \bar{M}_r \bar{\Phi}_r^d \tag{3.127a}$$
$$\bar{K}_r^d = (\bar{\Phi}_r^d)^T \bar{K}_r \bar{\Phi}_r^d \tag{3.127b}$$

where

$$\bar{\Phi}_r^d = [\bar{\phi}_1^r, \ldots, \bar{\phi}_{N_q^x}^r] \tag{3.128}$$

compare with (3.93)-(3.95). In (3.128), the basis vector $\bar{\phi}_i^r$ is defined by

$$(\bar{K}_r - (\bar{\omega}_i^r)\bar{M}_r)\bar{\phi}_i^r = 0, \quad (\bar{\phi}_i^r)^T \bar{M}_r \bar{\phi}_i^r = 1, \quad i = 1, \ldots, N_q^x \tag{3.129}$$

The damping matrix $\bar{L}_r^d$ may be constructed in (at least) two ways, depending on if a proportional damping is required during the model updating or not:

$$\bar{L}_r^d = \begin{cases} (\bar{\Phi}_r^d)^T \bar{L}_r \bar{\Phi}_r^d, & \text{non-proportional damping} \\ \text{diag}\big((\bar{\Phi}_r^d)^T \bar{L}_r \bar{\Phi}_r^d\big) = \text{diag}(\ldots, \bar{\zeta}_i, \ldots), & \text{proportional damping} \end{cases} \tag{3.129}$$

Notice that the damping of the updated model becomes proportional if the parameter estimation is consistent $\hat{\theta} = \check{\theta}$, and if the mode estimates are unbiased, i.e., $\hat{\phi}_i^x \parallel \phi_i^x$. This is true even if non-proportional damping is used during the model updating.

The reduced model becomes

$$\begin{aligned} \bar{M}_r^d \ddot{q} + \bar{L}_r^d \dot{q} + \bar{K}_r^d q &= (\bar{\Phi}_r^d)^T B u \\ y &= C \bar{\Phi}_r^d q \end{aligned} \tag{3.130}$$

and the corresponding FRF:

$$\bar{G}_r^d(\omega) = C\bar{\Phi}_r^d \big(\bar{Z}_r^d(\omega)\big)^{-1} (\bar{\Phi}_r^d)^T B \quad \text{where} \tag{3.131}$$

$$\bar{Z}_r^d(\omega) = \begin{cases} \bar{K}_r^d + j\omega \bar{L}_r^d - \omega^2 \bar{M}_r^d, & \text{non-proportional damping} \\ \operatorname{diag}\big(\ldots, (\bar{\omega}_i^r)^2 - \omega^2 + j\bar{\zeta}_i\omega, \ldots\big), & \text{proportional damping} \end{cases}$$

For a perturbation in the parameter value according to (3.113), a diagonalization of $\bar{M}_r^d$ and $\bar{K}_r^d$ in (3.127) may be performed as in (3.93)-(3.95).

Using the basis $\bar{\Phi}_r$ in (3.122) for reduction, the reduced model (3.130), the FRF in (3.131), and the defined resonance frequencies $\bar{\omega}_i^r$ in (3.123), a mode-pairing free cost function corresponding to V_{mp} in (3.118) can be constructed:

$$\bar{V}(\theta) = \nu_1^2 \bar{V}_1(\theta) + \nu_2^2 \bar{V}_2(\theta) + \nu_3^2 \bar{V}_3(\theta) \tag{3.132}$$

where ν_i are cost function weights, and where

$$\bar{V}_1(\theta) = \sum_{i=1}^{N_\omega} \left\| \bar{G}_r^d(\theta, \omega_{R,i}) - G^x(\omega_{R,i}) \right\|_{Fro}^2 \tag{3.133a}$$

$$\bar{V}_2(\theta) = \sum_{i=1}^{N_q^x} \left| \frac{\bar{\omega}_i^r(\theta) - \hat{\omega}_i^x}{\hat{\omega}_i^x} \right|_2^2 \tag{3.133b}$$

$$\bar{V}_3(\theta) = \sum_{i=1}^{N_q^x} \left\| \bar{G}_r^d(\theta, \hat{\omega}_i^x) U_i^x - \bar{Y}_i^x \right\|_2^2 \tag{3.133c}$$

Compare with (3.119).

Numerical Simulation Examples

In Examples 3.2 and 3.3 below, an updating of the Garteur model in Appendix A is made. The general updating procedure in Section 3.8.3, the optimization method in Section 3.8.2, and the mode-pairing free cost function in (3.132)-(3.133) are used. The cost function weights are determined so that for the initial parameter values θ^{init}, the following hold

$$\bar{V}_1 = \frac{1}{14}\bar{V}, \quad \bar{V}_2 = \frac{10}{14}\bar{V}, \quad \bar{V}_3 = \frac{3}{14}\bar{V} \tag{3.133}$$

The damping matrix L_r^d is chosen to be proportional, see (3.129).

We have experimently found that if the deviations in the resonance frequencies are sufficiently reduced, the estimation of the parameters from the spatial information has good properties, see Example 3.2.

The parameterizations are defined by

$$\theta = [\theta_1, \ldots, \theta_8, \theta_{10}, \ldots, \theta_{12}]^T \tag{3.134}$$

and

$$\theta = [\theta_1, \theta_5, \ldots, \theta_8, \theta_{10}, \ldots, \theta_{12}]^T \tag{3.135}$$

see Table A.7. The difference between the parameterizations in (3.134) and (3.135) is the parameters θ_2, θ_3, θ_4 representing the stiffness of the fuselage. Since the fuselage of the Garteur model in Appendix A is much stiffer than the wings and the stabilizers, the stiffness parameters of the fuselage is hard to estimate compared to the other stiffness parameters of the model. A parameterization with both "easy" and "hard" parameters to estimate is called ill-conditioned (due to the ill-conditioned Jacobian J). Notice that the condition of J depends on the actuator and sensor positions as well as on other design variables of the measuring. For the parameters θ_k in Table A.7 not being included in the parameterizations in (3.134)-(3.135), it holds that $\theta_k/\theta_k^{ref} = 1$. The actuators are placed at

$$\begin{aligned} \mathcal{A}_1 &= \{12_z,\, 14_x,\, 15_z,\, 20_y\} \\ \mathcal{A}_2 &= \{12_z,\, 15_z,\, 20_y\} \\ \mathcal{A}_3 &= \{6_z,\, 12_z,\, 14_x,\, 15_z,\, 20_y\} \end{aligned} \tag{3.136}$$

see Fig. A.1. The 30 sensors are placed at

$$\begin{aligned} \mathcal{S} = \{&4_x,\, 4_z,\, 5_z,\, 6_z,\, 7_z,\, 8_x,\, 9_z,\, 10_z,\, 11_z,\, 12_x,\, 12_z \\ &13_x,\, 13_z,\, 14_x,\, 14_z,\, 15_x,\, 15_z,\, 19_y,\, 20_y,\, 21_y,\, 21_z \\ &22_y,\, 22_z,\, 23_y,\, 25_x,\, 25_z,\, 26_x,\, 26_z,\, 27_y,\, 28_y\} \end{aligned} \tag{3.137}$$

Using the set of actuators $\mathcal{A}_1$ in (3.136) and the set of sensors $\mathcal{S}$ in (3.137), the MAC-values between ϕ_i^x and $\hat{\phi}_i^x$ become

$$\mathcal{A}_1 \;:\quad \{1.00,\, 1.00,\, 1.00,\, 1.00,\, 1.00,\, 1.00,\, 0.99,\, 0.99,\, 1.00\}$$

see Section 3.3 and Section 3.6.1. Compare this with the dMAC in (4.11)-(4.12) in Section 4.4.1. The corresponding MAC-values for $\mathcal{A}_2$ and $\mathcal{A}_3$ in (3.136) and $\mathcal{S}$ are

$$\mathcal{A}_2 \;:\quad \{1.00,\, 1.00,\, 1.00,\, 0.87,\, 1.00,\, 1.00,\, 0.99,\, 0.99,\, 1.00\}$$

and

$$\mathcal{A}_3 \;:\quad \{1.00,\, 1.00,\, 1.00,\, 1.00,\, 1.00,\, 1.00,\, 1.00,\, 1.00,\, 1.00\}$$

respectively. The low MAC-value (0.87) of mode nr. 4 for $\mathcal{A}_2$ is used below to indicate the sensitivity of the cost function $\bar{V}$ w.r.t. not "cleanly" excited modes of the structure.

It is found that the semi-fixed linearization M_r^{lin}, K_r^{lin} does not pay off in neither parameter estimation nor cost function decrease. This is due to that the assumption of $\bar{V}_{um}$ being quadratic in θ is highly valid. The estimation of the parameters is therefore only marginally improved by keeping the linearization of M_r, K_r fixed for more than one parameter estimation iteration. However, the basis of reduction Φ_r may be kept fixed for several iterations.

Here, the parameters are constrained to

$$\frac{\theta_k^{init}}{\alpha_\theta} < \theta_k^i < \alpha_\theta \theta^{init} \tag{3.138}$$

where $\alpha_\theta = 3$ in order to only influence the estimation of $\check{\theta}$ if θ_k^i for some i, k is obviously erroneous.

Notice, that noise in measurements are not included in the simulations.

Example 3.2 *Let the Garteur model in Appendix A be parameterized by* (3.134). *The position of the actuators and sensors are specified by* $\mathcal{A}_1$ *and* $\mathcal{S}$ *in* (3.136) *and* (3.137), *respectively. In Fig. 3.3(a), the parameter trajectories are visualized. The non-global minimum of parameter* θ_4 *is due to the not perfectly excited modes (the MAC-values differ from 1). However, using the actuator set* $\mathcal{A}_3$ *it can be found that also the estimate* $\hat{\theta}_4$ *of* θ_4 *equals* $\check{\theta}_4$, *see Fig. 3.3(b). The influence of not perfectly excited modes of the structure is further explored in Example 3.3. Henceforth in this example, the actuator positions are defined by* $\mathcal{A}_1$.

In Fig. 3.4 (a), the cost function history, i.e., the values of $\bar{V}$ *during the iteration are shown, and in (b) the values of the cost function parts* $\bar{V}_i = \bar{V}_{mu,i}$ *in* (3.133) *are shown. The cost function* $\bar{V}_{um}$ *is approximating* $\bar{V}_{mk}$, *compare the solid line and the circles in Fig. 3.4(a). This indicates that the linearization of* M_r, K_r *is valid. It can also be seen in Fig. 3.4(b) that the deviations in the resonance frequencies of* $\bar{V}_1$ *play a major role when estimating the parameters during the first iterations and that the spatial information about the structure becomes more important after a few iterations.*

In Fig. 3.5, the history of the regularization term μ *in* (3.71), *and the singular values of* J *are visualized. It is seen that the stabilizing effect of* μ *is basically reduced as the cost function is minimized. However, when a new basis of reduction* Φ_r *is computed, the regularization is temporarily increased. An interpretation of the regularization compared to the singular values may be as the number of linear combinations of the parameters that are changed in one iteration. The number of singular values being larger than the regularization term, is the number of linear combinations of the parameters that are adjusted in one parameter estimation iteration.*

The history of the generalized resonance frequencies $\bar{\omega}_i$ *in* (3.123) *are shown in*

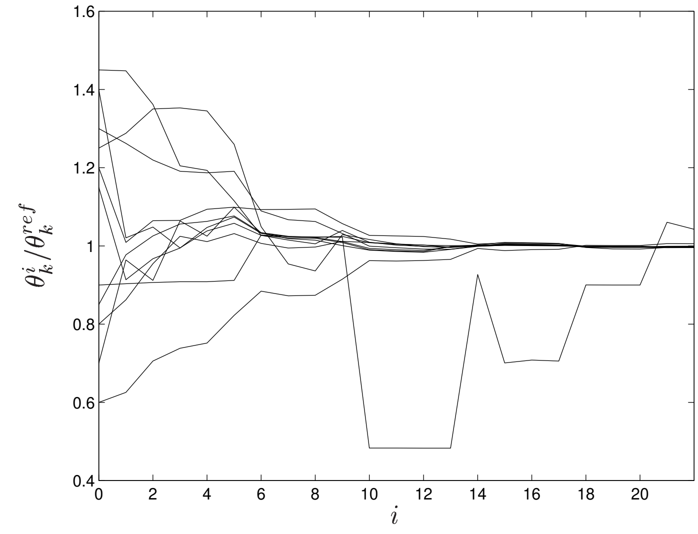

(a) Parameter history for actuator positions $\mathcal{A}_1$.

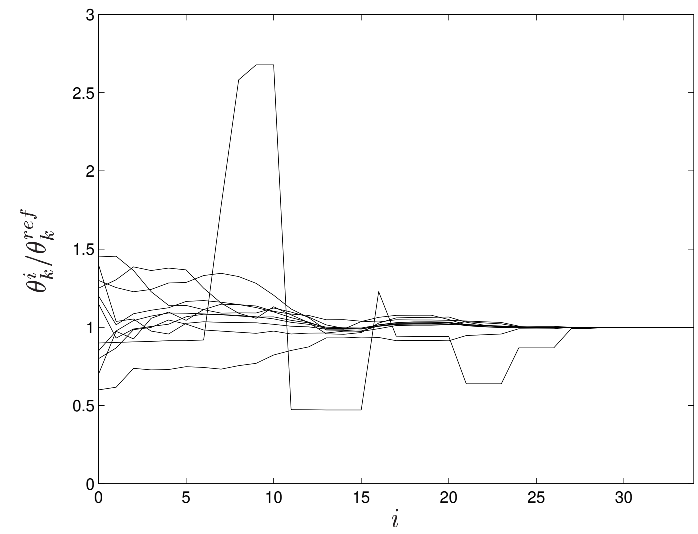

(b) Parameter history for actuator positions $\mathcal{A}_3$.

Figure 3.3 *The parameter trajectory of the updating in Example 3.2. The i on the x-axis denotes the parameter estimation iteration. The y-axis represents the quotient $\theta_k^i/\theta_k^{ref}$ between the value of the parameters θ_k^i and the true value of θ_k^{ref}.*

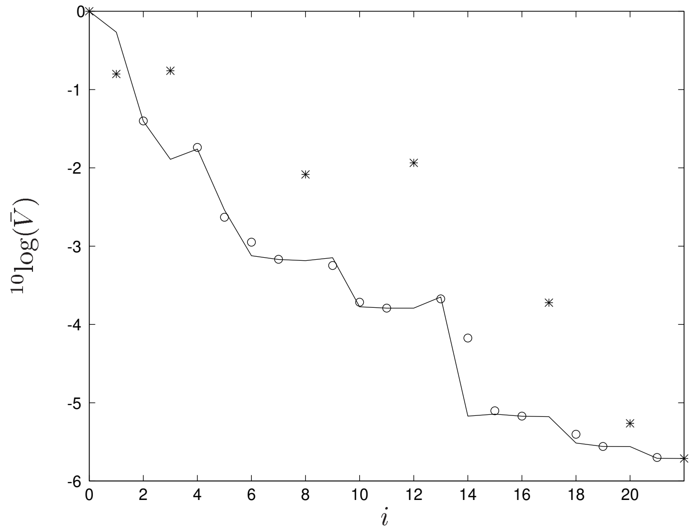

(a) Solid line (—) corresponds to $\bar{V}_{um}$, $\circ$ corresponds to $\bar{V}_{mk}$, and $*$ corresponds to $\bar{V}_{rb}$.

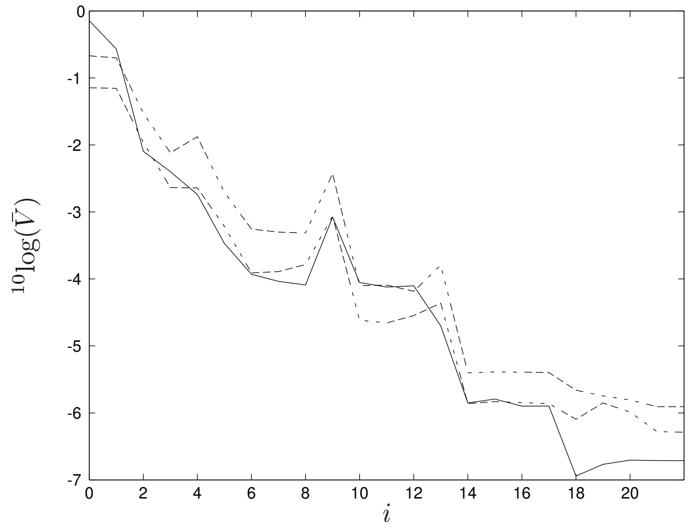

(b) Solid line(—) represents $\bar{V}_1$, dashed-dotted $(-\cdot)$ $\bar{V}_2$ and dashed $(--)$ $\bar{V}_3$.

Figure 3.4 *The history of the logarithm of the cost function values.*

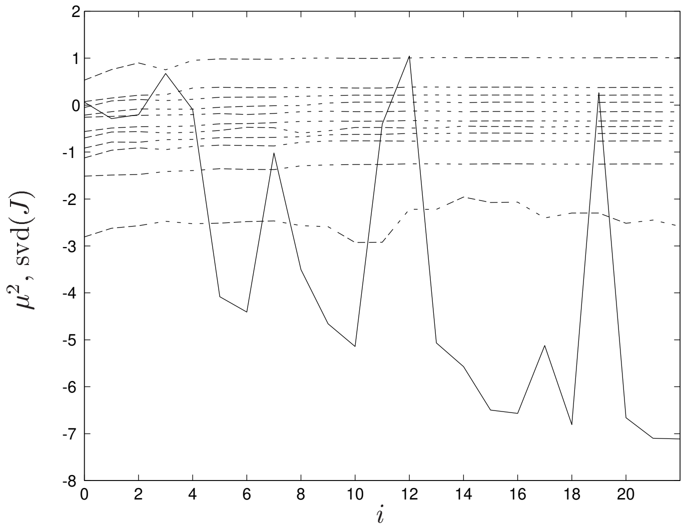

(a) Solid line (—) represents the value of regularization term μ, dashed line (– –) represents the singular values of J.

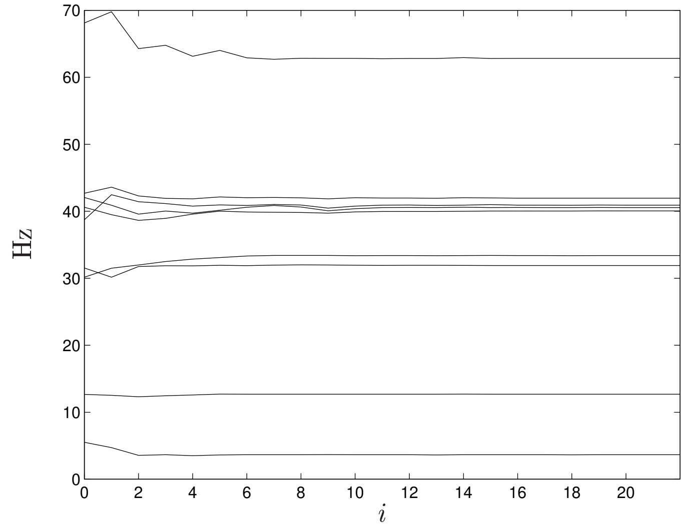

(b) The history of the generalized resonance frequencies $\bar{\omega}_i$.

Figure 3.5 *(a) the history of the regularization term* μ *and the singular values of the Jacobian* J*. (b) the history of the generalized resonance frequencies* $\bar{\omega}_i$*.*

Fig. 3.5(b). Even if there are several multiple modes around 41 Hz, the crossings of the resonance frequencies only occur in the first iteration. This is the advantage of using the generalized resonance frequencies instead of the computed resonance frequencies of the FE model and the traditional mode pairing formulations.

In Example 3.3, the sensitivity w.r.t. not cleanly excited modes are investigated. It is found that for a not to ill-conditioned parameterization as in (3.135), the parameter convergence properties are sufficiently good. Notice that for an ill-conditioned parameterization as in (3.134), the convergence properties may be bad.

Example 3.3 *Let the Garteur model in Appendix A be parameterized by θ in (3.135). Let $\mathcal{U}_1$ denote the updating when the actuators are given by $\mathcal{A}_1$ in (3.136), and $\mathcal{U}_2$ when the actuators are given by $\mathcal{A}_2$ in (3.136). In Fig. 3.6 the parameter history for the two different actuator positions are shown.*

The maximum parameter bias are

$$\begin{aligned} \mathcal{U}_1 &: \quad \max_k \{\tilde{\theta}_k / \theta_k^{ref}\} = 0.0013 \\ \mathcal{U}_2 &: \quad \max_k \{\tilde{\theta}_k / \theta_k^{ref}\} = 0.0389 \end{aligned} \tag{3.139}$$

The relative cost function reductions are

$$\begin{aligned} \mathcal{U}_1 &: \quad \bar{V}(\hat{\theta}) = 5.5{\cdot}10^{-6} \cdot \bar{V}(\theta^{init}) \\ \mathcal{U}_2 &: \quad \bar{V}(\hat{\theta}) = 6.7{\cdot}10^{-5} \cdot \bar{V}(\theta^{init}) \end{aligned} \tag{3.140}$$

For a reasonably well-conditioned parameterization, the mode-pairing free cost function seems to have the ability to decrease the cost function considerably. From an application point of view, the question if $\hat{\theta} = \check{\theta}$ is not as important as if $\hat{\theta} \approx \check{\theta}$ and $V(\hat{\theta}) \ll V(\theta^{init})$ (under the condition that V reflects the important properties of the model/structure).

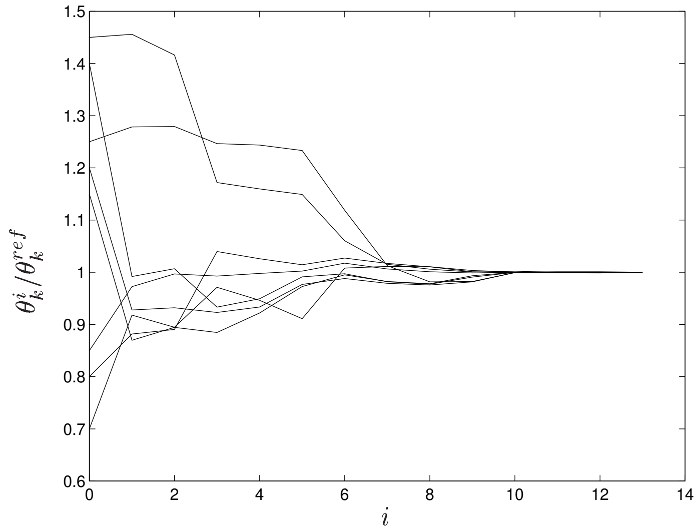

(a) Model updating task $\mathcal{U}_1$

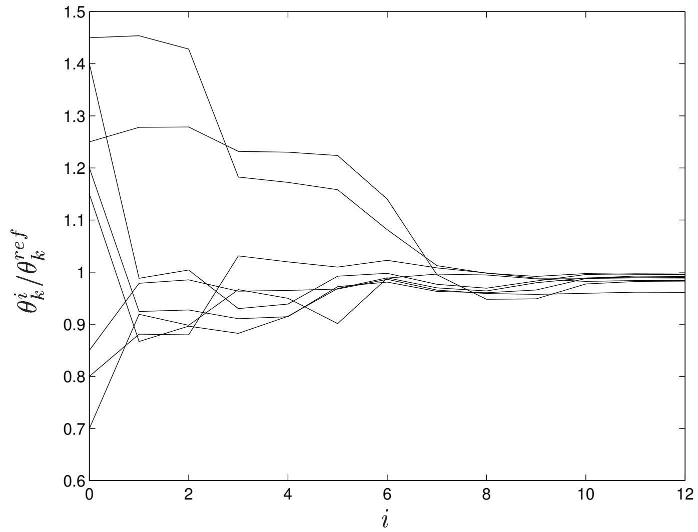

(b) Model updating task $\mathcal{U}_2$

Figure 3.6 *The parameter trajectories of Example 3.3.*

3.9 A Convergence Analysis

In [1], a covariance expression for the parameters θ of the model is derived.

Let $\check{\theta}$ denote the minimizing argument of the cost function V when the measurements are corrupted by noise. Let $V_\star(\theta) = v_\star^T(\theta)v_\star(\theta)$ denote the corresponding cost function for noise-free measurements and let $\check{\theta}_\star$ be its minimizing argument. Then it follows that

$$\epsilon = v_\star(\check{\theta}_\star) - v(\check{\theta}_\star) \tag{3.141}$$

is the vector of measurement noise. Let ξ denote the deviation between the minimizing arguments, $\xi = \check{\theta} - \check{\theta}_\star$. The mean value theorem then yields

$$0 = V'(\check{\theta}_\star + \xi) = V'(\check{\theta}) + V''(\bar{\theta})\xi \tag{3.142}$$

where $\bar{\theta}$ is between $\check{\theta}_\star$ and $\check{\theta}$. From (3.142) we have that

$$\begin{aligned} \xi =& -(V''(\bar{\theta}))^{-1}V'(\check{\theta}_\star) \\ \check{\theta} =& \check{\theta}_\star - (V''(\bar{\theta}))^{-1}V'(\check{\theta}_\star) \end{aligned} \tag{3.143}$$

where

$$V'(\check{\theta}_\star) = 2v'(\check{\theta}_\star)^T v(\check{\theta}_\star) = 2v_\star'(\check{\theta}_\star)^T(\epsilon + v_\star(\check{\theta}_\star)) = 2v_\star'(\check{\theta}_\star)^T\epsilon \tag{3.144}$$

In (3.144) the second equality follows from that measurement noise are independent of θ, and the third equality from $V_\star'(\check{\theta}_\star) = 0$.

The statistical variability of ξ, and therefore also of $\check{\theta}$ can thus be quantified by

$$\begin{aligned} \lim_{\sigma^2\to 0}\frac{E\xi\xi^T}{\sigma^2} =& \lim_{\sigma^2\to 0}\frac{4}{\sigma^2}E\{(V_\star''(\bar{\theta}))^{-1}v_\star(\check{\theta}_\star)^T\epsilon\epsilon^T v_\star(\check{\theta}_\star)(v_\star''(\bar{\theta}))^{-T}\} \\ =& 4(V_\star''(\check{\theta}_\star))^{-1}v_\star'(\check{\theta}_\star)^T v_\star'(\check{\theta}_\star)(V_\star''(\check{\theta}_\star))^{-T} \end{aligned} \tag{3.144}$$

where σ^2 is the noise variance of the measurements. The expression in (3.144) can be simplified if $\mathcal{M}^x \in \mathcal{M}^\theta$. Then

$$V_\star''(\check{\theta}_\star) = 2v_\star'(\check{\theta}_\star)^T v_\star'(\check{\theta}_\star) \tag{3.145}$$

since $v_\star(\check{\theta}_\star) = 0$. The approximate covariance expression $\text{Cov}[\check{\theta}]$ for $\check{\theta}$ is thus given by

$$\text{Cov}[\check{\theta}] \approx 4\sigma^2\left(v_\star'(\check{\theta}_\star)^T v_\star'(\check{\theta}_\star)\right)^{-1} \tag{3.146}$$

where $\check{\theta}_\star$ may be estimated by $\check{\theta}$ since $\check{\theta} \to \check{\theta}_\star$, as $\sigma^2 \to 0$. In practice the derivatives in (3.146) are computed using numerical difference quotient approximations, see (3.7) and (3.8).

The covariance expression above is based on the assumption that the measurements noise variance σ^2 is low. Recall from Section 3.1 that the low noise assumption is valid in most model updating applications based on frequency domain measurements. Covariance expressions for the estimate of parameters based on time domain measurements can be found in [25], where the assumption of a large number of time domain measurements N_x^t is made. Notice that the frequency domain measurements are obtained from time domain measurements, where the measurements are collected during a long time period. Therefore, the assumption made about the frequency domain measurements is similar to the assumption made about the time domain measurements,

$$\sigma^2 \to 0 \quad \Leftrightarrow \quad N_x^t \to \infty \tag{3.147}$$

3.10 Additional Notes on the Design Variables

Here some guidelines for the choice of the design variables inherent in the updating formulations are discussed. To ensure a successful model updating these choices are very important.

3.10.1 Choice of Cost Function

A cost function V may be interpreted as a scalar measure of the deviation between the model $\mathcal{M}$ and the structure $\mathcal{M}^x$. If the cost function is to be valid (yielding valid models), it is crucial to incorporate the important properties of $\mathcal{M}$ and $\mathcal{M}^x$ in the cost function. Here, a model is considered as valid if the agreement between the model output and the measurements are sufficiently good, assuming that the measurements are good enough. One can also verify a model through the parameter bias, but in practice $\check{\theta}$ is unknown. Without going into details, measurements of mechanical structures must include information about the dominating vibrations of the structure to be sufficiently good.

The most important property of a cost function V is good convergence properties, i.e., a large domain of attraction $\check{\Theta}$ to the global minimum $\check{\theta}$. Therefore the main goal when choosing the cost function is to enhance the convergence properties in order to reduce the existence of local minima.

Logarithmic Cost Functions

In [3], the cost function V_{LogLS} is proposed in favor of V_{LS}, see (3.21) and (3.20). However, V_{LogLS} can have severe drawbacks compared to V_{LS}. For instance, assume that the measured frequency response function G^x equals

$$G^x(\omega) = G(\check{\theta}^\star, \omega) + G^n(\omega) \tag{3.148}$$

where G^n denotes the measurement noise, and where $\check{\theta}^\star$ is the parameter estimate given noise-free measurements. Then it holds that,

$$\check{\theta} \to \check{\theta}^\star, \quad \text{as} \quad \|G^n(\omega)\| \to 0 \tag{3.149}$$

where $\breve{\theta}$ is the parameters minimizing the cost function. Denoting G_{kl} as the frequency response function from input l to output k of the frequency response function G, V_{LogLS} has the following property:

$$
\begin{aligned}
V_{LogLS} &= \sum_k \sum_l |\log G_{kl}(\theta, \omega) - \log G^x_{kl}(\omega)| \\
&= \sum_k \sum_l \Big| \log\Big(\frac{G_{kl}(\bar{\theta}, \omega) + G^n_{kl}(\omega)}{G_{kl}(\theta, \omega)} \Big) \Big| \\
&\to \sum_k \sum_l \Big| \log\Big(1 + \frac{G^n_{kl}(\omega)}{G_{kl}(\bar{\theta}, \omega)} \Big) \Big|, \quad \text{as} \quad \breve{\theta} \to \bar{\theta}
\end{aligned}
\tag{3.150}
$$

However, if anti-resonances (some $|G_{kl}| = 0$) are measured,

$$
V_{LogLS} \to \infty, \quad \text{as} \quad |G_{kl}(\breve{\theta})| \to 0, \quad \text{for some } k,\, l \tag{3.151}
$$

even for low levels of noise, and measured anti-resonances. Because the parameters θ are computed in order to minimize the cost function it follows that

$$
\breve{\theta} \nrightarrow \breve{\theta}^{\star}, \quad \text{as} \quad |G_{kl}(\breve{\theta})| \to 0 \tag{3.152}
$$

since (3.151) holds. Thus, the cost function V_{LogLS} is sensitive to noise if anti-resonances are measured.

Moreover, if the intermediate parameter estimate θ^{i+1} is computed from θ^i using the cost function $V_{LogLS}(\theta)$, it should hold that

$$
V_{LogLS}(\theta^{i+1}) < V_{LogLS}(\theta^i) \tag{3.153}
$$

for every iteration step i, $i = 1, \dots, \infty$. Noticing the property of V_{LogLS} in (3.151), it should hold that

$$
|G_{kl}(\theta^i, \omega)| \not\approx 0, \quad \forall k,\, \forall l,\, \forall \omega,\, \forall i \tag{3.154}
$$

if the parameter estimation is to be consistent, $\hat{\theta} \to \breve{\theta}$. Therefore, in order for (3.153) to hold, anti-resonances should not appear in the model during the model updating. If the condition in (3.153) is relaxed, anti-resonances must not appear in a sequence of iterations since the property (3.153) is crucial for a successful model updating.

Measured anti-resonances can always be excluded in the model updating formulation so that $|G_{kl}(\bar{\theta}, \omega)| \not\approx 0$. However, an initial exclusion of the $|G_{kl}(\theta^i, \omega)|$ corresponding to the anti-resonances in the model, emerging during the model updating, is not a feasible task (since this corresponds to a change of the cost function). Therefore additional local minima may be introduced by the use of the V_{LogLS} compared to V_{LS}.

The unavoidable presence of anti-resonances in a mechanical model together with (3.151), (3.153), and (3.154) suggests that the cost function V_{LogLS} is not a noise-robust optimization criterion.

Choice of Input Error or Output Error Equations

The properties of the input error equations in (3.18), or the output error equations in (3.19), are not fully investigated. Here the influence of noise on the cost function will be discussed.

Assume that $y^x(\omega) = y^x_\star(\omega) + y^n(\omega)$, where $y^x_\star(\omega)$ denotes the noise-free measurements, and that the measured noise $y^n(\omega)$ can be modeled as

$$y^n(\omega) = y^{mn}(\omega) + y^{pn}(\omega), \quad y^{pn}(\omega) = G^{pn}(\omega)u^{pn}(\omega) \tag{3.155}$$

where $y^{mn}(\omega)$ is the measured sensor noise, and $y^{pn}(\omega)$ is the measured process noise. In (3.155), $G^{pn}(\omega)$ denotes the frequency response function from the noise sources $y^{pn}(\omega)$ to the sensors. Compare this with the noise model in Section 3.5. Assume also that the commanded input signal $u^x(\omega)$ is noise-free.

Let $N_{IE}(\omega)$ and $N_{OE}(\omega)$ denote the noise contributions to the input error/output error equations:

$$v_{IE}(\theta) = u^x(\omega) - G^{-1}(\theta,\omega)y^x_\star(\omega) + N_{IE}(\omega) \tag{3.156a}$$

$$v_{OE}(\theta) = y^x_\star(\omega) - G(\theta,\omega)u^x(\omega) + N_{OE}(\omega) \tag{3.156b}$$

respectively. The noise contributions then become

$$N_{IE}(\omega) = G^{-1}(\theta,\omega)y^{mn}(\omega) + G^{-1}(\theta,\omega)G^{pn}(\omega)u^{pn}(\omega) \tag{3.157a}$$

$$N_{OE}(\omega) = y^{mn}(\omega) + G^{pn}(\omega)u^{pn}(\omega) \tag{3.157b}$$

where the noise model of the input error formulation is parameter varying. In order to compute the sequence of parameter estimates $\hat{\theta}^i$ properly, a parameter-varying cost function $V = V_i(\theta^i)$ is needed, compare with (3.50) in Section 3.7. However, a parameter-varying cost function V_i introduces difficulties when comparing $V_i(\theta_i)$ with $V_{i+1}(\theta^{i+1})$ in the optimization algorithm, see (3.68).

Furthermore, an anti-resonance of the model, $|G_{kl}| \approx 0$ yields a high noise contribution to the cost function based on the input error equations, since the variance of the measured sensor noise $y^{mn}(\omega)$ is assumed to be independent of $G(\omega)$. If $|G^{-1}_{kl}(\omega)| \approx 0$ and $|G^{pn}_{kl}(\omega)| \not\approx 0$, the contribution from $u^{pn}(\omega)$ in $N_{IE}(\omega)$ may also be critical. The conclusion is that the input-error equations is not an appropriate choice for model updating, since an increase of the cost function not necessarily corresponds to a worse model. This contradicts the idea behind the minimization of the cost function and introduces unnecessary difficulties in the optimization method.

3.10.2 Choice of Parameterization

The parameterization of the model is critical for an updating of a model to be successful. There are several aspects on the choice of parameterization, and some important ones are discussed here. The general rule to follow is that the parameterization of the model should reflect the uncertainties/errors of the model.

If the parameterization does not reflect the major errors in the model, the deviation $\min \|\mathcal{M}^{\theta} - \mathcal{M}^{x}\|$ may be large, or the parameters may take physically unrealistic values in order to compensate for a poor choice of parameterization.

If the parameters are to be *estimable*, i.e., possible to be consistently determined, then the following condition is necessary:

$$C_\theta : \quad \left\{ \frac{\partial M}{\partial \theta_k}, \frac{\partial L}{\partial \theta_k}, \frac{\partial K}{\partial \theta_k} \right\} \Bigg|_{\theta=\theta^*} \neq \left\{ \frac{\partial M}{\partial \theta_l}, \frac{\partial L}{\partial \theta_l}, \frac{\partial K}{\partial \theta_l} \right\} \Bigg|_{\theta=\theta^*}, \quad \forall k \neq l, \ \forall \theta^* \in \Theta \tag{3.158}$$

where Θ denotes the feasible values of θ.

If the condition C_θ in (3.158) does not hold for θ_i and θ_j, then θ_i and θ_j are not distinguishable. For instance, $\theta_i = G$ and $\theta_j = J$ in (2.28) are not distinguishable. The condition C_θ is often easily fulfilled, since the parameterization $m = m(\theta)$, and $k = k(\theta)$ for every finite element of the model is available in symbolic form, compare with (2.29) and (2.28). However, the insight gained by (3.158) is useful. For instance, letting $\theta_i = A$, and $\theta_j = \rho$ may create problems since their influence on (2.28) and (2.29) can be regarded as rather similar.

If the parameters are not estimable, the Jacobian J will be rank deficient. Numerically, rank deficiency corresponds to an ill-conditioned Jacobian. One could therefore let the condition number of $(J^TJ)^{-1}$ for the initial model,

$$\frac{1}{\kappa(J^TJ)} \tag{3.159}$$

guide the choice of parameterization.

Some methods have been proposed for so-called error localization, i.e., methods pointing out where the errors of the model are located. One of these methods is the COMAC in Section 3.6.2, correlating the measured dof of the structure with the corresponding dof of the model. In [12] it is pointed out that a low C_k may be used to detect errors in the model.

3.10.3 Choice of Frequency Points in the Measured FRF

The question of which frequency points of G^x to include in the cost function is discussed in [22]. The reason for not including the FRF in all frequency points is redundancy in the data and the assumption of more data than treatable are available. It is also discussed that data collected near the resonance frequencies and near anti-resonances are less accurate due to leakage and noise, respectively.

The redundancy of the spatial information in the data is obvious, but necessary from a statistical viewpoint in order to estimate the parameters accurately. The relatively large amount of noise in the anti-resonances is not more critical than in any other frequency point and spatial position if a valid noise model is used.

The computation of the normal modes ϕ_i for complex structures is much more time consuming than the computation of the parameter $\hat{\theta}^i$ whenever $\hat{v}_i^a(\theta)$ is available. Therefore no measurements should be left out due to the complexity of the parameter estimate algorithm.

In order to detect all major deviations between the model and the structure, the dominating vibrations of the structure should be included. This incorporates measurements of the vibrations in a frequency region around the resonance frequencies. For the same reason, measurements of vibrations in frequency regions away from the resonance frequencies should also be included. Otherwise a resonance frequency of the model in these frequency regions might not be accounted for in the model updating, yielding an invalid model.

In Section 3.8.1 it was mentioned that the maximum likelihood (ML) estimate corresponds to the minimization of the FRF. It was also mentioned that this estimate is the best if the measurements are corrupted with Gaussian distributed noise. However, if not all frequency points of the FRF is included in the cost function, the minimization of the FRF corresponds no longer to the ML-estimate. The fewer frequency points that are included in the cost function, the less is the minimization of the FRF corresponding to the ML-estimate. This discussion suggests that all frequency points of the FRF should be included in the cost function.

3.11 Summary

Updating of FE models is important for aviation/aerospace applications, where accurate models may be used to minimize the economic expenses of vibrational and/or wind-tunnel experiments. If the initial FE model of the structure is parameterized, one may estimate the values of the parameters in order to minimize the deviation between the parameterized model output and the measurements. However, there are many requirements that must be fulfilled for a model updating formulation to be appropriate for updating FE models of large, flexible structures. The major requirements are on the computational expenses, convergence properties of the parameter estimation, and reliability of the optimization method. A computationally cheap, general procedure for updating FE models was proposed, where a basis of reduction and a linearization are re-used in several iterations. The convergence properties of the cost function were addressed. It was found that cost functions combining modal domain data and frequency domain data have good convexity properties. In order to reduce the effects of the traditional mode-pairing, a novel mode-pairing free cost function was presented. In order to solve highly non-linear, ill-conditioned problems, a reliable optimization for the general model updating procedure method was discussed. Finally, notes on the important choice of cost function, parameterization, and measurements points of the FRF were discussed.

4

Actuator and Sensor Placement

Locating actuators and sensors on a mechanical structure in order to measure its behavior form an important part of the experimental design. It has often been done by the engineer using his/her experience and skills. With high-performing computers available it is possible to compute actuator and sensor locations for a large structure using its nominal model in order to increase the quality of the measurements. In this chapter the topic of actuator and sensor placement will be treated. First, in Section 4.1 an introduction is given, and in Section 4.2 a general analysis of the complexity of locating actuator and sensor is presented. After some introductory remarks in 4.3, placement for the purpose of modal analysis and model updating are discussed and analyzed in Sections 4.4 and 4.5, respectively. Finally, in Section 4.6, validation and comparison of actuator and sensor placements are discussed.

4.1 Introduction

The placement of actuators and sensors on a structure is a part of the pre-test planning, and is made in advance of the measuring. Since the measuring of large complex structures is expensive and/or difficult, the importance of the pre-test planning cannot be underestimated. Therefore, a well performed actuator/sensor placement is necessary in order to obtain high quality measurements to a reasonably low cost.

Actuator and Sensor Placement Objectives

The objective of actuator and sensor placement may be to minimize the number of actuators and sensors used during the measuring, or to achieve measurements of highest possible quality. Here, it is assumed that a specified number of actuators m, and sensors p are to be placed on a flexible structure. The task is to locate the actuators and sensors in order to achieve good measurements. However, a reconstruction of the algorithms in order to minimize the number of actuators and sensors are straightforward and will not be further treated here.

Basically there are three different purposes for collecting measurements: experimental modal analysis, model updating, and control. Experimental modal analysis is a wide and very important area. Traditionally, the dynamics of a designed flexible structure is verified through experimental modal analysis, i.e., through the analysis of measured resonance frequencies, mode shapes and damping. The objective for placement of actuators and sensors for modal analysis is therefore to be able to estimate the modal parameters from measurements of the structure accurately. Actuator and sensor placement for the purpose of model updating is probably the least studied of the three categories above for several reasons, e.g., the modal analysis is often considered to be more important, model updating formulations are commonly based on modal measurements and modal correlation techniques. However, the need for good updating increases and the placement for model updating is therefore believed to become more important, e.g., in aviation applications, where accurate models are of high interest. Actuator and sensor placement for control of highly flexible structures is common in some applications, e.g., in aerospace industry where the structures are extremely flexible due to their construction.

Optimality, Sub-optimality and Trade-offs

The placement of actuators and sensors in order to obtain *optimal* measurements from the structure is a very complex problem. The complexity of the problem arises mainly from the complexity of the model, but also from the question of optimality: what is optimal for a specific application? How to formulate a valid criterion to optimize? These questions depend on the use of the measurements and must therefore be studied every time measurements are to be collected from a structure. For instance, measurements are often used for both experimental modal analysis and model updating. How to formulate the criterion yielding actuator/sensor positions with the desired properties?

Moreover, the optimal placement of actuators and sensors is not only dependent on the properties of the structure, it is also dependent on the type of input (and/or disturbance) signals exciting the structure. The choice of input signals and placement of actuators and sensors then become a coupled problem yielding an optimization problem of extremely high complexity. If the input signal is known beforehand, it is recommended to include this information in the criterion. In [46] the input signal is designed for measuring the modes of the structure. General strategies for designing input signals for the purpose of identification are given in [13]. However, the input signals applied to the real structure are usually tuned during the measuring and therefore not exactly known when computing the positions of the actuators and sensors. One must also keep in mind that the nominal model used to compute the actuator/sensor positions may not be valid in all aspects. Therefore the question of robustness against errors in the nominal model is of vital importance.

Algorithms placing actuators and sensors on dynamical structures of industrial size will always be sub-optimal in some way. To begin with, the modeling of a structure as a finite-dimensional FE model introduces sub-optimality since the finite element in itself is an approximation. Moreover, FE models have only a finite number of positions available for the actuators/sensors (if linear combinations between dof of immediate grid points of the model are disregarded). Models of complex structures may also be very large and one must therefore use sub-optimal algorithms in order to reduce the computation time. To fulfill the time requirements on the algorithm, one may divide the combined task of sensor/actuator placement into two separate problems by computing the actuator and sensor positions separately. Let

$$\mathcal{A}, \quad \mathcal{S} \tag{4.1}$$

denote the sets of actuators and sensors, respectively. Then a *set of artificial actuators* $\mathcal{A}_a$ must be specified in order to compute the sensor positions, and a *set of artificial sensors* $\mathcal{S}_a$ must be specified in order to compute the actuator positions if the criterion is I/O-dependent. The artificial sets of actuators $\mathcal{A}_a$ and sensors $\mathcal{S}_a$ are intermediate sets needed for the computation of the *resulting set of actuators* $\mathcal{A}_r$ and the *resulting set of sensors* $\mathcal{S}_r$.

Another aspect on the complexity is in which order $\mathcal{A}_r$ and $\mathcal{S}_r$ should be computed, since the total computational cost mostly differs. However, in most cases the computation of $\mathcal{A}_r$ in advance of $\mathcal{S}_r$ is less expensive.

Exciting and measuring rotational dof is hard in practice, and the rotational dof may therefore be omitted as candidate positions of sensors and actuators. All translational dof may not be available for measuring due to the geometry of the structure. Moreover, if the forces from the actuators are large, the strength of the structure against the applied forces must also be considered. Taking all these kinds of restrictions into consideration, the actuators and sensors must be chosen from some *candidate sets* $\mathcal{A}_c$ and $\mathcal{S}_c$ containing the feasible actuators and sensors positions, respectively. However, for complex structures, even $\mathcal{A}_c$ and $\mathcal{S}_c$ may be too large and smaller feasible subsets must be constructed in order to fulfill time and memory requirements on the algorithms. These smaller subsets of candidate actuator/sensor positions are preferably constructed by the engineer. One possibility is to simply pick a number of feasible dof such that $\mathcal{A}_c$ and $\mathcal{S}_c$ are evenly distributed on the structure. Another possibility is to use a computationally inexpensive algorithm in order to construct $\mathcal{A}_c$ and $\mathcal{S}_c$ of feasible size. There are thus many trade-offs between optimality and computation complexity one must deal with in order to achieve reasonable algorithms for placement of actuators and sensors.

Robustness Issues

Actuator and sensor placement are based on the nominal model of the structure. It is assumed that for a sufficiently good nominal model, the actuator and sensor positions will yield good measurements of the real structure. Therefore a more important question than optimality is robustness against errors in the nominal model. These (and other) robustness properties are very hard to analyze analytically, basically due to the complexity of the models and the non-convexity of the formulated optimization problems. However, an indication of the robustness against errors in the nominal model can always be achieved by computing actuator and sensor positions for a perturbed, parameterized nominal model, assuming that the errors in the model can be approximated/represented by such perturbations.

A General Method

Distinctions between a *method* and an *algorithm* are made. Here, a method is defined as a strategy to solve a problem, while an algorithm in general has a more formal definition. Loosely speaking, an algorithm needs some input variables, and computes an output in finite time. The major demand on an algorithm is thus to ensure termination.

In Method 4.1 the strategy used to compute the actuator/sensor positions is presented.

Method 4.1 (Strategy for computing actuator/sensor positions.)

1. *Given a criterion $P_{\mathcal{A}}$, compute the actuator positions $\mathcal{A}_r$ using a candidate set of actuators $\mathcal{A}_c$, and the artificial set of sensors $\mathcal{S}_a = \mathcal{S}_c$.*
2. *Given a criterion $P_{\mathcal{S}}$, compute the sensor positions $\mathcal{S}_r$ using a candidate set of sensors $\mathcal{S}_c$, and the artificial set of actuators $\mathcal{A}_a = \mathcal{A}_r$ computed in 1.*
3. *If $\mathcal{A}_r$ and $\mathcal{S}_r$ are considered to be inappropriate, then let $\mathcal{S}_a = \mathcal{S}_r$ and start from 1.*

4.2 Complexity Analysis and Placement Algorithms

Formally, the objective of actuator and sensor placement is to compute the set of resulting actuator positions $\mathcal{A}_r$ and the set of resulting sensor positions $\mathcal{S}_r$ such that a scalar cost function P is maximized,

$$\{\mathcal{A}_r, \mathcal{S}_r\} = \underset{\substack{|\mathcal{A}|=m,\, \mathcal{A}\subset\mathcal{A}_c \\ |\mathcal{S}|=p,\, \mathcal{S}\subset\mathcal{S}_c}}{\arg\max} \; P(\mathcal{A}, \mathcal{S}) \tag{4.2}$$

where $\mathcal{A}_c$ and $\mathcal{S}_c$ are the candidate sets of actuator and sensor positions, respectively. $|\{\cdot\}|$ denotes the number of elements in the set $\{\cdot\}$, and m and p denotes the number of actuators and sensors to be placed, respectively. Henceforth, the conditions $\mathcal{A}_r \subset \mathcal{A}_c$ and $\mathcal{S}_r \subset \mathcal{S}_c$ in (4.2) is tacitly understood, and these conditions will be omitted.

Since the discrete maximization problem formulated in (4.2) in general is non-convex, a full search among $\mathcal{A}_c$ and $\mathcal{S}_c$ is assumed to be required if the optimal solution is to be guaranteed. Therefore, assuming that P has to be computed for every combination of actuators and sensors, $\mathcal{C}_{as}$ evaluations of $P(\circ)$ is needed:

$$\mathcal{C}_{as} = \binom{|\mathcal{A}_c|}{m} \cdot \binom{|\mathcal{S}_c|}{p} = \frac{|\mathcal{A}_c|!}{m!(|\mathcal{A}_c| - m)!} \cdot \frac{|\mathcal{S}_c|!}{p!(|\mathcal{S}_c| - p)!} \tag{4.3}$$

where $\mathcal{C}_{as}$ is rapidly increasing with $|\mathcal{A}_c|$, $|\mathcal{S}_c|$, since typically, $|\mathcal{A}_c| \gg m$ and $|\mathcal{S}_c| \gg p$.

Notice that determining $\{\mathcal{A}_r, \mathcal{S}_r\}$ using (4.2) may be expensive even if $\mathcal{A}_c$ and $\mathcal{S}_c$ are small. The combinatorial complexity is reduced substantially if the combined problem of determining sensors and actuators is separated. Then the actuators and sensors may be determined if an artificial set of actuators $\mathcal{A}_a$ and an artificial set of sensors $\mathcal{S}_a$ are constructed. Suitable choices are $\mathcal{S}_a = \mathcal{S}_c$ and $\mathcal{A}_a = \mathcal{A}_r$ if the actuator positions are computed in advance of the sensor positions. Thus, separating the actuator and sensor placement, the formal objective in (4.2) may be altered to:

$$\mathcal{A}_r = \arg\max_{|\mathcal{A}|=m} P(\mathcal{A} \,|\, \mathcal{S}_a) \tag{4.4a}$$

$$\mathcal{S}_r = \arg\max_{|\mathcal{S}|=p} P(\mathcal{S} \,|\, \mathcal{A}_a) \tag{4.4b}$$

yielding $\mathcal{A}_r$ and $\mathcal{S}_r$ with highly reduced computation time compared to (4.2). Now the computational complexity is reduced to

$$\mathcal{C}_a = \binom{|\mathcal{A}_c|}{m} = \frac{|\mathcal{A}_c|!}{m!(|\mathcal{A}_c| - m)!} \tag{4.5a}$$

$$\mathcal{C}_s = \binom{|\mathcal{S}_c|}{p} = \frac{|\mathcal{S}_c|!}{p!(|\mathcal{S}_c| - p)!} \tag{4.5b}$$

evaluations of P, respectively.

If the computation of P is expensive even (4.4) may be too time consuming. Then a sub-optimal iterative search (i.s.) of actuator and sensor positions among $\mathcal{A}_c$ and $\mathcal{S}_c$ must be introduced. One solution is to pick the single actuator position maximizing the specified criterion P in an iterative manner, adding it to the intermediate set $\mathcal{A}_r^k$ of actuator positions:

$$\mathcal{A}_r^k = \{\mathcal{A}_r^{k-1}, a_k\}, \quad a_k = \arg\max_{a \in \mathcal{A}_c \setminus \mathcal{A}_r^{k-1}} P(\{\mathcal{A}_r^{k-1}, a\} \,|\, \mathcal{S}_a), \quad \mathcal{A}_r^0 = \emptyset \tag{4.6}$$

for $k = 1, \ldots, m$, and finally, letting $\mathcal{A}_r = \mathcal{A}_r^m$. In (4.6), the $\setminus$ denotes set-subtraction and $\emptyset$ the null-set. This strategy needs

$$\mathcal{C}_{a|i.s.} = m \left(|\mathcal{A}_c| - \frac{m-1}{2} \right) \tag{4.6}$$

evaluations of P. The corresponding strategy for sensor placement is

$$\mathcal{S}_r^k = \{\mathcal{S}_r^{k-1},\, s_k\}, \quad s_k = \underset{s \in \mathcal{S}_c \setminus \mathcal{S}_r^{k-1}}{\arg\max}\, P(\{\mathcal{S}_r^{k-1}, s\} \,|\, \mathcal{A}_a), \quad \mathcal{S}_r^0 = \emptyset \tag{4.7}$$

for $k = 1, \dots, p$, and $\mathcal{S}_r = \mathcal{S}_r^p$, which needs

$$\mathcal{C}_{s|i.s.} = p\left(|\mathcal{S}_c| - \frac{p-1}{2}\right) \tag{4.8}$$

evaluations of P.

The algorithm of picking the single actuator (sensor) a_k (s_k) and adding it to the set of resulting actuators (sensors) $\mathcal{A}_r$ ($\mathcal{S}_r$) as in (4.6) and (4.7) can be formulated as an algorithm, see Algorithm 4.1 where $\{\mathcal{X},\, x_k,\, k_{max}\}$ equals $\{\mathcal{A},\, a_k,\, m\}$ or $\{\mathcal{S},\, s_k,\, p\}$. The algorithm is sub-optimal, though.

Algorithm 4.1 (Algorithm for picking actuator/sensor position.)

Input: $\mathcal{X}_c$, k_{max}, P

Output: $\mathcal{X}_r$

1. *Let* $k = 0$, $\mathcal{X}_r = \emptyset$, *and* $\bar{\mathcal{X}}_c = \mathcal{X}_c$.
2. *Let* $k = k + 1$. *Determine* $x_k = \underset{x \in \bar{\mathcal{X}}_c}{\arg\max}\, P(\{\bar{\mathcal{X}}_c, x\})$.
   Let $\mathcal{X}_r = \{\mathcal{X}_r,\, x_k\}$ *and* $\bar{\mathcal{X}}_c = \bar{\mathcal{X}}_c \setminus x_k$
3. *If* $k < k_{max}$: *go to 2.*

It is easily seen that Algorithm 4.1 terminates since a finite number of actuator (sensor) positions are chosen from a finite set of candidate positions.

For some sensor (actuator) placement criteria the corresponding method of deleting a single sensor s_k in $\mathcal{S}_c$ (a_k in $\mathcal{A}_c$) is more appropriate, i.e.,

$$\mathcal{S}_c^k = \mathcal{S}_c^{k-1} \setminus s_k, \quad s_k = \underset{s \in \mathcal{S}_c^{k-1}}{\arg\max}\, P(\{\mathcal{S}_c^{k-1} \setminus s\} \,|\, \mathcal{A}_a), \quad \mathcal{S}_c^0 = \mathcal{S}_c \tag{4.9}$$

for $k = 1, \dots, |\mathcal{S}_c| - p$. The resulting set of sensors $\mathcal{S}_r = \mathcal{S}_r^{|\mathcal{S}_c|-p}$. The complexity is increased (if $|\mathcal{S}_c|/2 > p$) to

$$\mathcal{C}_{s|i.s.}^d = \frac{1}{2}\left(|\mathcal{S}_c| - p\right)\left(|\mathcal{S}_c| + p - 1\right) \tag{4.9}$$

evaluations of $P(\circ)$. The corresponding expressions for the actuator placement task is obtained by exchanging $\mathcal{S}$ and $\mathcal{A}$, s_k and a_k, and p and m in (4.9) and (4.9). The corresponding algorithm is given below in Algorithm 4.2, where $\{\mathcal{X},\, x_k,\, k_{max}\}$ equals $\{\mathcal{A},\, a_k,\, m\}$ or $\{\mathcal{S},\, s_k,\, p\}$. This algorithm is also sub-optimal.

Algorithm 4.2 (Algorithm for deleting actuator/sensor position.)

Input: $\mathcal{X}_c$, k_{max}, P

Output: $\mathcal{X}_r$

1. *Let* $k = 0$ and $\bar{\mathcal{X}}_c = \mathcal{X}_c$.
2. *Let* $k = k + 1$. *Determine* $x_k = \underset{x \in \bar{\mathcal{X}}_c}{\arg\max}\, P(\{\bar{X}_c \setminus x\})$.
   Let $\bar{\mathcal{X}}_c = \bar{\mathcal{X}}_c \setminus x_k$.
3. *If* $|\bar{\mathcal{X}}_c| - k_{max} > 0$ *: go to 2.*
4. *Let* $\mathcal{X}_r = \bar{\mathcal{X}}_c$.

Algorithms computing $\mathcal{A}_r$ $(\mathcal{S}_r)$ from $\mathcal{A}_c$ $(\mathcal{S}_c)$ as in Algorithm 4.1 or as in Algorithm 4.2, without any final, iterative optimization of $\mathcal{A}_r$, is here called *Primary Algorithms.*

It is readily seen that the complexity of (4.6), (4.7), and (4.9) is considerably lower than (4.5) and especially (4.3), see Example 4.1. The *translational dof* of a grid point represent the translational movements a grid point of the model can do.

Example 4.1 *Assume that 3 actuators and 15 sensors are to be placed on the Garteur model in Appendix A, and that*

$$\mathcal{A}_c = \mathcal{S}_c = \{\,\textit{all translational dof}\}, \quad \Rightarrow \quad |\mathcal{A}_c| = |\mathcal{S}_c| = 84$$

The placement corresponding to (4.2) *requires, according to* (4.3),

$$\mathcal{C}_{as} = \binom{84}{3} \cdot \binom{84}{15} = 95284 \cdot 1.48{\cdot}10^{16} = 1.41{\cdot}10^{21}$$

evaluations of P. Separating the computation of actuator and sensor positions as in (4.4) *the complexity reduces to*

$$\binom{84}{3} + \binom{84}{15} = 95284 + 1.48{\cdot}10^{16} = 1.48{\cdot}10^{16}$$

evaluations of P. Reducing the complexity further using the iterative search in (4.6) *and* (4.7), *the complexity becomes*

$$\mathcal{C}_{s|i.s.} + \mathcal{C}_{a|i.s.} = 249 + 1155 = 1404$$

evaluations of P, which can be considered as feasible.

Adding the single actuator (sensor) position a_k (s_k) as in Algorithm 4.1 is optimal under the constraint that the intermediate set $\mathcal{A}_r^k$ ($\mathcal{S}_r^k$) of actuator (sensor) positions is included in the *optimal sets* of actuator (sensor) positions $\mathcal{A}_o$ ($\mathcal{S}_o$). However, the first position is determined as if there were no other actuators/sensors available. When $\mathcal{A}_r$ ($\mathcal{S}_r$) is computed, one may examine if the first computed position is still the optimal choice under the constraints $\{\mathcal{A}_r \setminus a_1\}$ ($\{\mathcal{S}_r \setminus s_1\}$). Then one may continue to examine a_2 (s_2), etc. The idea behind Algorithm 4.3 below is thus to ensure that every single actuator (sensor) a_k (s_k) is the optimal choice under the condition that $\{\mathcal{A}_r \setminus\} \subset \mathcal{A}_o$:

$$a_k = \bar{a}_k, \quad \bar{a}_k = \underset{\bar{a} \in \mathcal{A}_c \setminus \{\mathcal{A}_r \setminus a_k\}}{\arg\max} \; P(\{\mathcal{A}_r \setminus \bar{a}\} \,|\, \mathcal{S}_a) \tag{4.10a}$$

$$s_k = \bar{s}_k, \quad \bar{s}_k = \underset{\bar{s} \in \mathcal{S}_c \setminus \{\mathcal{S}_r \setminus s_k\}}{\arg\max} \; P(\{\mathcal{S}_r \setminus s_k\} \,|\, \mathcal{A}_a) \tag{4.10b}$$

This iterative improvement of $\mathcal{A}_r$ ($\mathcal{S}_r$) in (4.10) suggests an improved actuator (sensor) placement algorithm, see Algorithm 4.3. The proposed improvement algorithm below is also applicable to actuator (sensor) positions computed by Algorithm 4.2 (or any other algorithm where the actuators (sensors) in $\mathcal{A}_r$ ($\mathcal{S}_r$) are not optimal w.r.t. all other actuators in $\mathcal{A}_r$ ($\mathcal{S}_r$)). In order to formulate an improvement algorithm and verify termination, an ordering of the $\mathcal{A}_r$ ($\mathcal{S}_r$) must be made. This ordering is used to distinguish the sets of actuators (sensors) emerging in the algorithm, if the criterion P cannot make this distinction. In Algorithm 4.3 below, it is tacitly understood that the ordering is implicit in P.

Algorithm 4.3 (Algorithm for improving actuator/sensor positions.)

Input: *$\mathcal{X}_c$, $\mathcal{X}_r$, P, ordering of $\mathcal{X}_c$.*

Output: *$\mathcal{X}_r$ (improved)*

1. *Let $k_{max} = |\mathcal{X}_r|$.*
2. *Let $k = 1$.*
3. *Let $\bar{\mathcal{X}}_r = \mathcal{X}_r \setminus x_k$.*
4. *Determine $\bar{x}_k = \underset{\bar{x} \in \mathcal{X}_c \setminus \bar{\mathcal{X}}_r}{\arg\max} P(\{\bar{\mathcal{X}}, \bar{x}\})$.*
5. *If $\bar{x}_k \neq x_k$: $\mathcal{X}_r = \{\bar{\mathcal{X}}_r, \bar{x}_k\}$, go to 2.*
   Else if $k = k_{max}$: end.
   Else : let $k = k + 1$, go to 3.

Proof of termination of Algorithm 4.3:
If

- C1) the elements in $\mathcal{X}_c$ is ordered, such that for all sets $\mathcal{X}_r^1$ and $\mathcal{X}_r^2$, where $\mathcal{X}_r^1 \neq \mathcal{X}_r^2$ the ordering introduces a scalar criteria P_o, $P_o(\mathcal{X}_r^1) \neq P_o(\mathcal{X}_r^2)$,
- C2) $\mathcal{X}_c$ is finite,
- C3) P has a maximum value,
- C4) P is not dependent on the ordering of the elements in $\mathcal{X}_c$,
- C5) P_o is not depending on the order of appearance of the elements x_k in $\mathcal{X}_r$,

then since,

- P1) P is not decreasing in any iteration,
- P2) P_m may take the same value in maximally $k_{max} - 1$ succeeding iterations,

the Algorithm 4.3 terminates (in finite time). To see this, define $\bar{P} = (P, P_o)$, where P is the objective criterion, and P_o the ordering criterion used to distinguish $\mathcal{X}_r^1$ from $\mathcal{X}_r^2$ whenever $P(\mathcal{X}_r^1) = P(\mathcal{X}_r^2)$. In the algorithm above $P = \bar{P}$. If C1) to C5) above is fulfilled, the criterion P has the properties: non-decreasing, increasing in at least every k_{max}-th iteration, and having a finite number of values. Since P1) and P2) are properties of the algorithm, Algorithm 4.3 terminates. □

Notice, the ordering of the actuator/sensor positions should be chosen with care, since it may have an influence on the resulting actuator/sensor positions. However, the ordering is not further considered here. In the subsequent examples, the ordering is : 1_x, 1_y, 1_z, $2_x, \ldots, 28_z$. Thus, $P_o(\{26_z, 1_x\}) > P_o(\{1_y, 2_z\}) > P_o(\{1_z, 2_x\})$.

One can also turn Method 4.1 into a formal algorithm, see Algorithm 4.4 below.

Algorithm 4.4 (Combined Actuator and Sensor Placement Algorithm.)

Input: $\mathcal{A}_c$, $\mathcal{S}_c$, m, p
Ordering of $\mathcal{A}_c$ *and* $\mathcal{S}_c$.
$P_{\mathcal{A}}$ *: actuator placement criterion,*
$P_{\mathcal{S}}$ *: sensor placement criterion,*
PA : Primary actuator placement algorithm,
PS : Primary sensor placement algorithm.

Output: $\mathcal{A}_r$, $\mathcal{S}_r$

1. *Let* $\mathcal{S}_a = \mathcal{S}_c$. *Compute* $\mathcal{A}_r$ *using PA, and the criterion* $P_{\mathcal{A}}$.
2. *Let* $\mathcal{A}_a = \mathcal{A}_r$. *Compute* $\mathcal{S}_r$ *using PS, and the criterion* $P_{\mathcal{S}}$.
3. *Let* $\mathcal{A}_r^p = \mathcal{A}_r$, $\mathcal{S}_a = \mathcal{S}_r$. *Improve* $\mathcal{A}_r$ *using Algorithm 4.3, and the criterion* $P = P_{\mathcal{A}} \cdot P_{\mathcal{S}}$.
4. *Let* $\mathcal{S}_r^p = \mathcal{S}_r$, $\mathcal{A}_a = \mathcal{A}_r$. *Improve* $\mathcal{S}_r$ *using Algorithm 4.3, and the criterion* $P = P_{\mathcal{A}} \cdot P_{\mathcal{S}}$.
5. *If* $\mathcal{A}_r^p = \mathcal{A}_r$, $\mathcal{S}_r^p = \mathcal{S}_r$ *: End.*
   Else : Let $\mathcal{A}_r = \mathcal{A}_r^p$, $\mathcal{S}_r = \mathcal{S}_r^p$, *and go to 3.*

Proof of termination of Algorithm 4.4:
The termination of step 1. and 2. are properties inherent in algorithms PA and PS. The termination of 3. and 4. is a property of Algorithm 4.3. Then, a similar construction of the proof of Algorithm 4.3 proves Algorithm 4.4, since $P = P_{\mathcal{A}} \cdot P_{\mathcal{S}}$ is non-decreasing and the ordering introduces a ordering criterion P_o compare with the proof of Algorithm 4.3. □

Algorithms 4.1-4.4 above are all sub-optimal. However, we have found that the improved actuator (sensor) positions are near optimal in simulations, see Section 4.6.

Notice that the sub-optimality of the algorithms depends on the criteria used for the placement of actuators and/or sensors. If the actuator and sensor placement criteria are independent, an algorithm performing (4.4) will not introduce extra sub-optimality compared to (4.2). A criterion being I/O-dependent will thus end up in a relatively “more” suboptimal algorithm.

4.3 Prerequisites

The model used in the examples is the reference Garteur model in Appendix A reduced with a modal basis consisting of the 9 non-rigid, low-frequency modes, see Section 3.4. The reference model is used instead of the initial model due to the near multiple modes in the reference model. In the following, it will be assumed that 3 actuators and 15 sensors are to be placed on the Garteur model. A proportional damping with damping ratios $\xi_i = 0.01$ are used.

It is important to notice that the Garteur model in Appendix A is symmetric in all aspects w.r.t. the fuselage. A set of actuators $\mathcal{A}_r$, or a set of sensors $\mathcal{S}_r$ will never be totally unique, since there always is a mirrored set $\mathcal{A}_r^m$ and/or $\mathcal{S}_r^m$ with exactly the same properties, i.e., $P(\mathcal{A}_r, \mathcal{S}_r) = P(\mathcal{A}_r^m, \mathcal{S}_r^m)$.

The candidate sets of actuators $\mathcal{A}_c$ and sensors $\mathcal{S}_c$ equal both the set {all translational dof} in the examples below. When necessary, the artificial set of sensors $\mathcal{S}_a =$ {all translational dof}, and the artificial set of actuators $\mathcal{A}_a$ is specified.

The actuator and sensor positions are denoted by x_k, where x denotes the grid point of the model, and where subscript k denotes the direction of the applied input force or the direction of the measured displacement. See Fig. A.1 in Appendix A.

No attention is paid to the practical feasibility of the mutual actuator/sensor positions. For instance, it is in practice customary to not allow the actuators to be placed too close each other, since otherwise they may interfere.

The combined actuator/sensor placement algorithm proposed in Algorithm 4.4 is not used. Instead the combined actuator and sensor placement are separated (one may say that Algorithm 4.4 is used without doing the possible iteration introduced in step 5.).

The actuator positions $\mathcal{A}_r = \{a_1, a_2, a_3\}$ computed by Algorithm 4.1, and the improved actuator positions $\mathcal{A}_r$ computed by Algorithm 4.3 are given. The presented sensor positions are given by the improved set $\mathcal{S}_r$ computed by Algorithm 4.3.

4.4 Placement for Modal Analysis

Previously it was mentioned that the objective of placement for modal analysis is to placed actuators and sensors in order to estimate the modal parameters of the structure accurately. The resonance frequencies $\hat{\omega}_i^x$ are estimated as the frequency of the sinusoidal input force when the structure is vibrating in resonance. Assuming proportional damping, the damping ratios $\hat{\xi}_i^x$ may be estimated from the frequency response function (FRF) in (2.60). However, the main goal in practice is to achieve accurate estimates $\hat{\phi}_i^x$ of the "true" mode shapes ϕ_i^x.

4.4.1 Actuator Placement based on the Multivariate Mode Indicator Function

In Section 3.3, the Multivariate Mode Indicator Function (MMIF) was presented. It is used in experimental modal analysis to indicate (multiple) modes of the structure. It is also used to determine an input force pattern to excite a single target mode of a structure. However, in order to excite the single modes of a structure, an appropriate set of actuator positions must be chosen. Using the nominal model together with specified actuator and sensor positions, one may simulate measurements of the structure. Using these simulated measurements together with the MMIF, it is possible to determine whether the specified actuator/sensor position combination is appropriate for collecting measurements from the real structure.

In the school of experimental modal analysis it is of vital importance that the modes $\hat{\phi}_i^x$ of the structure are accurately estimated, see [10]. For many model updating formulations it is also known that the mode pairing of estimated modes $\hat{\phi}_i^x$ of the structure with the normal modes ϕ_i of the model is crucial for a successful model updating, see Section 3.8.4. Notice also the construction of the proposed reduction basis $\bar{\Phi}_r$ in Section 3.8.5, which is also dependent on good mode estimates.

Thus, for experimental modal analysis purposes, the actuators must be able to excite a single target mode, even if near multiple modes are present. It is also desirable to place the actuators so that the measured responses have a high Signal-to-Noise Ratio (SNR). In order to estimate the modes $\hat{\phi}_i^x$ of the structure, the actuators must be able to excite the modes $\hat{\phi}_i^x$ properly. A criterion for actuator placement based on the ability to excite the single target modes of the structure is therefore desirable.

A criterion for actuator placement based on the MMIF is proposed in [19]. Here, a generalization of the criterion in [19] is constructed. However, the main result is the noise-robust MMIF criterion for actuator placement. Using the MMIF, and a measurement/process noise model, an actuator placement criterion is developed. The proposed criterion is capable to place actuators such that the single modes are excited with a high SNR, even when near multiple modes are present.

The Actuator Placement MMIF Criterion

For proportionally, lowly damped structures the modes ϕ_i can be estimated by

$$\hat{\phi}_i^d = \operatorname{Im}\{\bar{Y}(\omega_i)\} \tag{4.11}$$

where ω_i is the resonance frequency of the target mode ϕ_i. In (4.11), superscript d denotes damping, since one may view $\hat{\phi}_i^d$ as the estimate of the normal mode ϕ_i when damping are present in the model.

Defining the dMAC (damped Modal Assurance Criterion) as the corresponding MAC in (3.43) between the normal mode ϕ_i of the model and the estimate $\hat{\phi}_j^d$ of ϕ_j,

$$\text{dMAC:} \qquad \mathsf{M}_{ij}^d = \frac{|\phi_i^T \hat{\phi}_j^d|^2}{|\phi_i|^2 |\hat{\phi}_j^d|^2} \tag{4.12}$$

a criterion correlating the modes $\hat{\phi}_j^d$ of the damped I/O-model and the normal modes ϕ_i of the FE model is obtained. Henceforth, M_i^d will denote M_{ii}^d.

The dMAC-values for the actuators and sensors in Example 3.1 are computed can now be computed as follows, see Example 4.2 below.

Example 4.2 *Continuing Example 3.1 in Section 3.3, the dMAC-values are shown in Table 4.1 where it is seen that all modes cannot be perfectly estimated using 3 actuators positioned to*

$$\mathcal{A}_r = \{13_x, 14_z, 15_z\}$$

and 15 sensors positioned to

$$\mathcal{S}_r = \{12_x, 13_x, 14_x, 21_y, 22_y, 23_y, 27_y, 5_z, 6_z, 9_z, 10_z, 12_z, 13_z, 14_z, 15_z\}$$

The reasons for the un-perfectly excited modes are due to the damping and the near multiplicity of modes $\phi_5 - \phi_8$. In general it holds that the higher the damping of a mode ϕ_l is, and the closer in resonance frequencies other modes ϕ_i are, the harder is an appropriate excitation of the mode ϕ_l, $i \neq l$ to be obtained. This is seen in (2.66) *for displacement measurements:*

$$G(\omega) = \sum_i \frac{C\phi_i\phi_i^T B}{\omega_i^2 - \omega^2 + j2\xi_i\omega_i\omega} \tag{4.13}$$

where the damping ratio ξ_i highly affects the FRF in the resonance frequencies, i.e., when $\omega = \omega_i$. Recall the estimation of a mode in (4.11). *A higher damping ratio ξ_l reduces mode ϕ_l's influence on $|G(\omega_l)|$ compared to the other modes ϕ_i, $i \neq l$, giving the effect that other modes more corrupts the estimate of ϕ_l. It can also be seen in* (4.13) *that the closer in resonance frequency a modes ϕ_k is to ϕ_l, the more is the estimate of ϕ_l corrupted by ϕ_k.*

Table 4.1 *The dMAC-values of example 4.2.*

Mode	1	2	3	4	5	6	7	8	9
M_i^d	1	1	.999	.999	1	1	.972	.990	1

The proposed criterion for actuator placement is

$$P^d = \|W\bar{\mathsf{M}}^d\|_b \tag{4.14}$$

where $1 \leq b \leq \infty$, W is a (diagonal) weighting matrix, and $\bar{\mathsf{M}}^d$ is the vector of the square root of the dMAC-values,

$$\bar{\mathsf{M}}^d = \left[\left(\mathsf{M}_1^d\right)^{1/2}, \ldots, \left(\mathsf{M}_{N_{tm}}^d\right)^{1/2}\right]^T \tag{4.15}$$

where N_{tm} denotes the number of target modes of the model. Compare this with (4.11), and (4.12). The previous mentioned criterion for actutator placement in [19] can be found to correspond to (4.14) when $W = I$, and $b = 2$.

There are many design variables that must be chosen properly, e.g., the damping of the structure must be designed/estimated, the weight matrix W, and the norm b in (4.14) must be chosen. The exact damping of the structure is never known but often the engineer has a good insight into the damping of the structure using knowledge from earlier measurements of similar structures.

In Example 4.3, the computed actuator positions for different values of the norm b are shown. We have found that non-equal weights can be used if different norms of b fail to yield a satisfactory actuator placement. How to choose the norm b in order to get good results, i.e., high dMAC-values, are explored in Example 4.3.

Example 4.3 *Table 4.2 presents the computed actuator positions using Algorithm 4.1. The corresponding M_i^d-values are also given. It is readily seen that the choice of b when $W = I$ is not obvious, but $b = 1$ and $b = 2$ seem to be appropriate choices, whereas $b = 4$ is not suitable.*

Table 4.2 *The actuator positions and the dMAC-values for different choices of norm b.*

Norm	Actuator Positions $\mathcal{A}_r$	Mode/dMAC								
b	a_1, a_2, a_3	1	2	3	4	5	6	7	8	9
1	22_x, 13_z, 17_z	1	1	1	1	.997	.997	.998	.998	1
2	22_x, 13_z, 17_z	1	1	1	1	.997	.997	.998	.998	1
4	12_y, 10_x, 14_z	1	1	1	1	.998	.922	.948	.999	1
8	12_y, 6_x, 15_z	1	1	1	1	.998	.929	.959	.999	1
16	21_x, 11_z, 12_z	1	1	1	1	.998	.994	.997	.998	1

Introducing a diagonal weighting matrix W_i in the i-th iteration (when determining a_i), where

$$\begin{aligned} W_1 &= \mathrm{diag}(0,0,0,0,0,1,1,0,0) \\ W_2 &= \mathrm{diag}(0,0,1,1,1,1,1,1,1) \\ W_3 &= \mathrm{diag}(1,1,1,1,1,1,1,1,1) \end{aligned}$$

the actuator positions become

$$\mathcal{A}_r = \{14_z,\ 14_y,\ 18_z\}$$

and the dMAC-values

$$1,\ 1,\ 1,\ 1,\ 1,\ .99,\ 1,\ .99,\ 1$$

for $b = 4$. This indicates that if the norm b fails to return good actuator positions, then the weighting matrix W in (4.14) can be used as a design variable.

Improving the actuator positions with Algorithm 4.3, the actuator positions become $\mathcal{A}_r = \{13_z, 17_z, 22_x\}$ or its mirrored set $\mathcal{A}_r^m = \{12_z, 17_z, 21_x\}$ for $b = 1, 2, 4, 8, 16$.

The Noise Robust Actuator Placement MMIF Criterion

The criterion based on the dMAC-values in (4.12) aims at maximizing the correlation between the normal modes ϕ_i of the model and their estimates $\hat{\phi}_i^d$ from simulated measurements. Thus, only robustness against (proportional) damping is considered.

However, it is not only the damping that makes the estimation $\hat{\phi}_i^d$ of the normal modes ϕ_i difficult. Noise can also cause problems, especially if the response in comparison with the noise level is low, i.e., if the SNR is low. If the robustness against noise is not considered, the mode estimates $\hat{\phi}_i^d$ may be poor even for low levels of noise. A criterion, where also robustness against noise is considered, will promote actuator positions yielding measurements with higher SNR.

There are mainly two types of modeled noise (errors), measurement and process noise. The measurement noise is generated by the sensors and are assumed to be pure measurement errors. The process noise are disturbances generated by sources acting on the structures as "actuators" with more or less known positions, and with an unknown input force.

It is assumed that the normal modes ϕ_i are corrupted with errors $\tilde{\phi}_i^d$ corresponding to the damping, measurement noise $\tilde{\phi}_i^{mn}$, and the process noise $\tilde{\phi}_i^{pn}$, i.e.,

$$\phi_i^{nd} = \phi_i + \tilde{\phi}_i^d + \tilde{\phi}_i^{mn} + \tilde{\phi}_i^{pn} \tag{4.16}$$

where superscript nd denotes noise-damping. Using a proportional model of damping in the structure, and a model of the measurement/process noise, the noise-damping disturbed estimate $\hat{\phi}_i^{nd}$ of ϕ_i can be written

$$\hat{\phi}_i^{nd} = \hat{\phi}_i^d + \hat{\phi}_i^{mn} + \hat{\phi}_i^{pn} \tag{4.17}$$

where $\hat{\phi}_i^d$ is defined in (4.11), and where $\hat{\phi}_i^{mn}$ and $\hat{\phi}_i^{pn}$ are the modeled measurement noise and process noise, respectively.

The effect of measurement noise $\tilde{\phi}_i^{mn}$ on ϕ_i^{nd} can be modeled as a vector $\hat{\phi}_i^{mn}$ of random variables, where the measurement noise in one sensor s_j is represented by an independent random variable $\hat{\phi}_{i,j}^{mn} = x_{i,j}^{mn}$. This is a common assumption made about the measurement noise, and is valid in most applications.

Noise models were discussed in Section 3.5. If the process noise sources can be modeled as discrete actuators a_k^{pn}, the effect of $\tilde{\phi}_{i,k}^{pn}$ on the mode estimates $\hat{\phi}_i^{nd}$ may be estimated via the frequency response output function $\bar{Y}_{i,k}^{pn}$,

$$\bar{Y}_{i,k}^{pn} = G_k^{pn}(\omega_i)\bar{U}_{i,k}^{pn} \tag{4.18}$$

where $\bar{U}_{i,k}^{pn}$ is the input force pattern from noise source a_k^{pn} at resonance frequency ω_i, see Section 3.3. Denoting

$$\tilde{\phi}_i^{pn} = \sum_k \tilde{\phi}_{i,k}^{pn}, \quad \tilde{\phi}_{i,k}^{pn} = \mathrm{Im}\{\bar{Y}_{i,k}^{pn}\} \tag{4.19}$$

the effect of the process noise on the mode estimate $\hat{\phi}_i^{nd}$ can be modeled. If the input noise forces $U_{i,k}^{pn}$ from a_k^{pn} are modeled as independent random variables for every process noise source, then the effect of the process noise $\tilde{\phi}_i^{pn}$ can be estimated. The assumptions made about the process noise model are: (a) the process noise sources can be modeled as actuators, and if so, (b) the positions of the major process noise sources are known, and (c) the power from the noise sources can be estimated. The case of two or more mutually dependent process noise sources is implicitly included in (4.18), (4.19), since two correlated noise sources may be turned into an equivalent single noise source (due to the construction of $\hat{\phi}_{i,k}^{pn}$ via G^{pn}).

In (4.20)-(4.22), a fairly general noise model is proposed, including both measurement and process noise.

Noise Model $\mathcal{N}$:
Assuming that the measurement errors $\tilde{\phi}_i^{mn}$ are unbiased and independent between the sensors, it can be modeled as a normally distributed random vector of zero-mean and variance $(\sigma_i^{mn})^2$, i.e.,

$$\hat{\phi}_i^{mn} = [\ldots, x_{i,j}^{mn}, \ldots], \quad x_{i,j}^{mn} \sim \mathrm{N}(0, \sigma_i^{mn}) \tag{4.20a}$$

$$x_{i,j_1}^{mn}, x_{i,j_2}^{mn} \quad \text{independent} \quad \forall i,\ \forall j_1 \neq j_2 \tag{4.20b}$$

Moreover, if the positions of the process noise sources a_k^{pn} are known, the FRF from the process noise sources to the sensors G^{pn}, can be computed. Assuming that the input forces from the noise sources are unbiased and independent, we arrive at the process noise model $\hat{\phi}_i^{pn}$

$$\hat{\phi}_i^{pn} = \sum_{k=1}^{N_{pn}} \hat{\phi}_{i,k}^{pn} = \sum_{k=1}^{N_{pn}} \phi_{i,k}^{pn} x_{i,k}^{pn}, \quad x_{i,k}^{pn} \sim \mathrm{N}(0, \sigma_{i,k}^{pn}) \tag{4.21a}$$

$$x_{i,k_1}^{pn}, x_{i,k_2}^{pn} \quad \text{independent} \quad \forall i,\ \forall k_1 \neq k_2 \tag{4.21b}$$

where $(\sigma_{i,k}^{pn})^2$ are the variance of the force from a_k^{pn} at resonance frequency ω_i. We also assume that the measurement noise and the process noise are independent,

$$x_{i,j}^{mn}, x_{i,k}^{pn} \quad \text{independent} \quad \forall i,\ \forall j, k \tag{4.22}$$

In order to construct a suitable correlation criterion ndMAC between ϕ_i and the random vector $\hat{\phi}_j^{nd}$, corresponding to the MAC in (3.43), a probabilistic framework must be used, see [34] for an introduction to random variables. A generalization of the dMAC in (4.12) is

$$\text{ndMAC:} \qquad \mathsf{M}_{ij}^{nd} = \mathrm{E}\left[\frac{|\phi_i^T \hat{\phi}_j^{nd}|^2}{|\phi_i|^2 |\hat{\phi}_j^{nd}|^2}\right] \tag{4.23}$$

where E denotes expectation. Henceforth, M_i^{nd} denotes M_{ii}^{nd}. However, the computation of M_i^{nd} in (4.23) is tricky and may therefore be approximated.

Let $\mathsf{M}_{*,i}^{nd}$ denote an approximation of M_i^{nd}. The noise-robust MMIF-based actuator placement criterion P^{nd} can now be formulated. Let

$$P^{nd} = \|W \bar{\mathsf{M}}_{*,i}^{nd}\|_b \tag{4.24}$$

where $1 \leq b \leq \infty$, W is a weighting matrix, and where $\bar{\mathsf{M}}_{*,i}^{nd}$ in (4.24) is

$$\bar{\mathsf{M}}_{*,i}^{nd} = \left[\left(\mathsf{M}_{*,1}^{nd}\right)^{1/2}, \dots, \left(\mathsf{M}_{*,N_{tm}}^{nd}\right)^{1/2}\right]^T \tag{4.25}$$

where N_{tm} denotes the number of target modes. In (4.24) and (4.25), $\mathsf{M}_{*,i}^{nd}$ may equal any approximation of M_i^{nd}.

In Appendix B two proposals for an approximation of the M_i^{nd} are given, the $\mathsf{M}_{a,i}^{nd}$ and $\mathsf{M}_{b,i}^{nd}$. The approximation of M_i^{nd} should fulfill some conditions in order to be valid, namely

$$\text{C1:} \qquad \mathsf{M}_{*,i}^{nd} \leq 1 \tag{4.23}$$

$$\text{C2a:} \qquad \frac{\partial\ \mathsf{M}_{*,i}^{nd}}{\partial\ (\sigma_i^{mn})^2} < 0,\ \forall i \tag{4.24a}$$

$$\text{C2b:} \qquad \frac{\partial\ \mathsf{M}_{*,i}^{nd}}{\partial\ (\sigma_{i,k}^{pn})^2} < 0,\ \forall i,\ k \tag{4.24b}$$

$$\text{C3a:} \qquad \lim_{(\sigma_i^{mn})^2 \to \infty} \mathsf{M}_{*,i}^{nd} = \varepsilon_i^{mn} \ll 1,\ \forall i \tag{4.25a}$$

$$\text{C3b:} \qquad \lim_{(\sigma_{i,k}^{pn})^2 \to \infty} \mathsf{M}_{*,i}^{nd} = \varepsilon_{i,k}^{pn} \ll 1,\ \forall i, \forall k \tag{4.25b}$$

$$\text{C4:} \qquad \lim_{\substack{(\sigma_i^{mn})^2 \to 0 \\ (\sigma_{i,k}^{pn})^2 \to 0, \forall k}} \mathsf{M}_{*,i}^{nd} = \mathsf{M}_i^d, \quad \forall i \tag{4.26}$$

The formulated conditions in (4.23)-(4.26) can be motivated intuitively as follows

C1) The ndMAC-values in (4.23) are always less than 1.

C2) The ndMAC-values should not be favoured by increased noise levels.

C3) For high noise levels, the ndMAC-values should be low.

C4) Low noise levels should not significantly affect the dMAC-values.

In Appendix B.2, the $\mathsf{M}_{a,i}^{nd}$ and some of its properties are presented. The case with no modeled process noise, $\mathsf{M}_{a,i}^{nd}$ equals:

$$\boxed{\mathsf{M}_{a,i}^{md} = \frac{|\phi_i^T \hat{\phi}_i^d|^2 + |\phi_i|^2 (\sigma_i^{mn})^2}{|\phi_i|^2 |\hat{\phi}_i^d|^2 + \bar{p}|\phi_i|^2 (\sigma_i^{mn})^2} - \frac{2|\phi_i|^4 (\sigma_i^{mn})^4 + 4|\phi_i|^2 |\phi_i^T \hat{\phi}_i^d|^2 (\sigma_i^{mn})^2}{\left(|\phi_i|^2 |\hat{\phi}_i^d|^2 + \bar{p}|\phi_i|^2 (\sigma_i^{mn})^2\right)^2} \quad (4.27)}$$

where superscript md denotes measurement noise-damping.

The criterion $\mathsf{M}_{a,i}^{md}$ in (4.27) fulfills the conditions C1-C4 above under the additional condition in (B.31):

$$\bar{p} \geq 4, \quad \text{and} \quad \frac{|\phi_i^T \hat{\phi}_i^d|^2}{|\phi_i|^2 |\hat{\phi}_i^d|^2} > \frac{1}{\bar{p}} + \frac{(\sigma_i^{mn})^2}{|\hat{\phi}_i^d|^2}, \quad \forall\, i \tag{4.28}$$

which is easily fulfilled since $\bar{p}$ typically is large, and the measured noise variance from one sensor $(\sigma_i^{mn})^2$ typically is a lot less than the measured power $|\hat{\phi}_i^d|^2$ from the structure, generated by the set of specified actuators, see Appendix B.

In Example 4.4, the design of the noise variance levels are discussed.

Example 4.4 *The choice of noise variance levels may be seen as a design variable and has to be chosen properly. One approach is to set the measurement noise levels $(\sigma_i^{mn})^2$ and the process noise levels $(\sigma_{i,k}^{pn})^2$ as a fraction of a (simulated) measured response. Define, $\bar{\mathcal{P}}_i$ as the mean power measured by the sensors,*

$$\bar{\mathcal{P}}_i(\mathcal{A}_t, \mathcal{S}_t) = \frac{1}{|\mathcal{A}_t|} \sum_{k=1}^{|\mathcal{A}_t|} \mathcal{P}_{i,k}, \quad \mathcal{P}_{i,k}(a_k, \mathcal{S}_t) = \frac{|\hat{\phi}_i^d(a_k)|^2}{|\mathcal{S}_t|}, \quad a_k \in \mathcal{A}_t \tag{4.29}$$

where $|\hat{\phi}_i^d(a_k)|^2$ is the measured power for a single actuator a_k in a specified test set of actuators $\mathcal{A}_t$ exciting the structure, and for a test set of sensors $\mathcal{S}_t$. Similar, $\mathcal{P}(a_k, \mathcal{S}_t)$ is the measured power in mean for actuator a_k and for the sensors defined by $\mathcal{S}_t$. The measurement noise levels $\{\sigma_l^{mn}, \sigma_m^{mn}, \sigma_h^{mn}\}$ (low, medium, high) are related to $\bar{\mathcal{P}}_i$ as,

$$\sigma_l^{mn} \quad \Leftrightarrow \quad \frac{\bar{\mathcal{P}}_i}{(\sigma_i^{mn})^2} = 10^4 \quad \leftrightarrow \quad 40 \text{ } dB \text{ } SNR \tag{4.30a}$$

$$\sigma_m^{mn} \quad \Leftrightarrow \quad \frac{\bar{\mathcal{P}}_i}{(\sigma_i^{mn})^2} = 10^3 \quad \leftrightarrow \quad 30 \text{ } dB \text{ } SNR \tag{4.30b}$$

$$\sigma_h^{mn} \quad \Leftrightarrow \quad \frac{\bar{\mathcal{P}}_i}{(\sigma_i^{mn})^2} = 10^2 \quad \leftrightarrow \quad 20 \text{ } dB \text{ } SNR \tag{4.30c}$$

The measurement noise variance levels in (4.30) are in the examples defined for

$$\mathcal{A}_t = \mathcal{S}_t = \{ \text{ all transl. dof } \}$$

Notice that the power $\bar{\mathcal{P}}_i$ is averaged over a set of actuators where

$$\max_k \mathcal{P}_i(a_k, \mathcal{S}_t) / \min_k \mathcal{P}_i(a_k, \mathcal{S}_t) \gg 1$$

The measured power levels may differ a lot between different actuators, and the SNR will therefore be higher in mean for $\mathcal{A}_r$ than for a random set of actuators.

Another approach is to define a level of the measurement noise variance related to the maximum response, e.g.,

$$(\sigma_i^{mn})^2 = \frac{1}{\alpha}\max_k \mathcal{P}_i(a_k, \mathcal{S}_t), \quad a_k \in \mathcal{A}_t \tag{4.31}$$

for some α defining the SNR.

Including errors from process noise sources, the design of process noise variance is more simple. One approach is to let the process noise variance be a fraction of the square of the commanded input force, i.e., $(\sigma_{i,k}^{pn})^2 = |\bar{U}_i|^2/m/\alpha$ for some α defining the SNR. However, the process noise will not be accounted for in the examples and is therefore not further considered here.

The actuator positions using Algorithms 4.1 and 4.3 are presented in the following example.

Example 4.5 *Using Algorithm 4.1, criterion P^{nd} with norm $b = 1$, damping ratio $\xi = 0.01$, the actuator positions as a function of variance $(\sigma_i^{mn})^2$ are shown in Table 4.3. Choosing $b = 2$ may also be appropriate, although $b = 1$ gives actuator positions with slightly better properties in this particular case. The errors corresponding to the process noise sources is assumed to be negligible, i.e., $(\sigma_{i,k}^{pn})^2 = 0$, and the levels of measurement noise variance, $(\sigma_i^{mn})^2$ are defined in Example 4.4.*

Table 4.3 *Actuator positions using Algorithm 4.1, criterion P^{nd}, and norm $b = 1$, as a function of variance $(\sigma^{mn})^2$.*

Variance	$\mathcal{A}_r$	Mode $i/\mathsf{M}_i^d/\mathsf{M}_{a,i}^{md}$								
σ^{mn}	a_1, a_2, a_3	1	2	3	4	5	6	7	8	9
σ_l^{mn}	$21_x, 12_z, 11_z$	1	1	1	1	.999	.994	.997	.998	1
		1	1	1	1	.998	.993	.996	.998	.999
σ_m^{mn}	$22_z, 15_z, 21_z$	1	1	1	1	1	.999	.985	.986	.999
		1	.998	.999	.979	1	.997	.980	.985	1
σ_h^{mn}	$7_z, 4_x, 15_z$	1	1	1	1	1	.928	.969	.999	1
		.999	.995	.998	.998	.991	.925	.960	.997	.985

As expected, in Table 4.3 it is shown that when the noise levels σ_i^{mn} are increased from σ_l^{mn} to σ_m^{mn} and from σ_l^{mn} to σ_h^{mn}, both the criteria $\mathsf{M}_i^d/\mathsf{M}_{a,i}^{md}$ decrease. This is clear from the fact that the resulting actuators are determined to excite the modes accurately, even when noise are present. This robustness against noise must be payed with sub-optimality (lower dMAC-values) when no noise are present. However, it is interesting to see that the set of resulting actuators $\{22_z, 15_z, 21_z\}$ determined for the noise level σ_m^{mn} seems to be sub-optimal compared to the set $\{12_z, 15_y, 15_z\}$ determined for the noise level σ_h^{mn}.

An improvement of the actuator positions only appeared for $\sigma^{mn} = \sigma_h^{mn}$, see Table 4.4.

Table 4.4 *Actuator positions using Algorithm 4.3 and $\mathcal{A}_r$ according to Table 4.3.*

Variance σ^{mn}	Improved $\mathcal{A}_r$	Mode $i/\mathsf{M}_i^d/\mathsf{M}_{a,i}^{md}$								
		1	2	3	4	5	6	7	8	9
σ_h^{mn}	12_z, 15_y, 15_z	1	1	1	1	1	.999	.984	.987	1
		1	.999	.999	.998	.998	.999	.983	.986	.999

A robustness test against noise can now be performed. By computing the ndMAC-values for the actuators in Tables 4.3 and 4.4, robustness against higher (and lower) noise levels are achieved. Table 4.5 shows the mean of the dMAC-values and the mean of the ndMAC-values for the computed actuator positions. Even a low variance in the design gives actuators with a highly improved robustness against noise. Moreover, a high level of noise do not significantly reduce the corresponding noise-free objective. The conclusion is that robustness against noise does not contradicts the possibility to obtain accurate mode estimates, and that the actuator positions computed for no designed noise have bad robustness properties against noisy measurements.

Table 4.5 *Robustness against various levels of noise.*

Design Variance	Improved $\mathcal{A}_r$	$\frac{1}{N_{tm}}\sum_{i=1}^{N_{tm}} \mathsf{M}_{a,i}^{md}$			
		$\sigma^{mn} = 0$	$\sigma^{mn} = \sigma_l^{mn}$	$\sigma^{mn} = \sigma_m^{mn}$	$\sigma^{mn} = \sigma_h^{mn}$
$\sigma^{mn} = 0$	13_z, 17_z, 22_x	.999	.997	.984	.869
$\sigma^{mn} = \sigma_l^{mn}$	11_z, 12_z, 21_x	.999	.998	.995	.962
$\sigma^{mn} = \sigma_m^{mn}$	15_z, 21_z, 22_z	.997	.996	.993	.966
$\sigma^{mn} = \sigma_h^{mn}$	12_z, 15_y, 15_z	.996	.996	.996	.989

4.4.2 The Method of Effective Independence, EI-method

In [21], the Method of Effective Independence for sensor placement is presented. It is developed in order to accurately identify and correlate a number of target modes measured from highly flexible structures, e.g., large space structures. Its first intended use is to provide a set of sensor positions for identification and correlation of modes of a large space structure in orbit. However, the intended use of the method does not distinguish it from other proposed methods for sensor placement for the purpose of modal analysis. We will here derive the Method of Effective Independence from a different viewpoint than in [21].

From the I/O-relation (2.64) the noise-disturbed output y_n can be at any time instant t written as

$$y_n(t) = y(t) + n(t), \quad y(t) = \Phi_s q_r(t) \tag{4.32}$$

where $\Phi_s = C\Phi_r$, compare with (2.64). In (4.32), the columns of Φ_r are the target modes of the modeled structure, q_r the corresponding generalized coordinates and n the additive measurement noise of the sensors. Assume that the zero-mean noise vector n has the property

$$\mathrm{E}\left[nn^T\right] = \sigma^2 I \tag{4.33}$$

where E denotes the expectation operator, and where I denotes the identity matrix. Thus, the measurement noise n of the sensors are uncorrelated and of equal variance σ^2.

If the number of sensors p in (4.32) is larger than the number of target modes N_{tm}, the estimation of q_r is an over-determined (least-squares) problem. An unbiased estimate of q_r can thus be obtained as

$$\hat{q}_r = (\Phi_s^T \Phi_s)^{-1} \Phi_s^T y_n \tag{4.34}$$

since Φ_s is assumed to have full rank N_{tm}. An estimate $\hat{y}$ of y can be obtained as

$$\hat{y} = \mathsf{P} y_n, \quad \mathsf{P} = \Phi_s (\Phi_s^T \Phi_s)^{-1} \Phi_s^T \tag{4.35}$$

The covariance matrix of the estimate error $\tilde{y} = y - \hat{y}$ is

$$\mathrm{Cov}[\tilde{y}] = \mathrm{E}[\tilde{y}\tilde{y}^T] = (I - \mathsf{P})\sigma^2 \tag{4.36}$$

since $\tilde{y} = \Phi_s(q_r - \hat{q}_r) - n$, and $\mathsf{P}\mathsf{P}^T = \mathsf{P}$.

The objective is to choose the set of sensor positions $\mathcal{S}_r$ from the candidate set of sensor positions $\mathcal{S}_c$ such that the covariance matrix $\mathrm{Cov}[\tilde{y}]$ is minimized,

$$\mathcal{S}_r = \underset{|\mathcal{S}_r|=p}{\arg\min}\ P\big(\mathrm{Cov}[\tilde{y}]\big) \tag{4.37}$$

In order to minimize $\mathrm{Cov}[\tilde{y}]$ in (4.36) using (4.37), an iterative search has to be performed since $|\mathcal{S}_c|$ is often too large for a complete search for the optimal sensor positions as in (4.4b). Therefore, $\mathcal{S}_c$ is reduced with the sensor s_k corresponding to the smallest diagonal element in P,

$$s_k : \quad k = \arg\max_i \mathsf{P}_{ii} \tag{4.38}$$

where k denotes the index of the largest diagonal element in P. The complexity of the Method of Effective Independence is therefore proportional to

$$\mathcal{C}_{EI} = |\mathcal{S}_c| - p \tag{4.39}$$

evaluations of P in (4.34). Since P in (4.35) is inexpensive to compute, the Method of Effective Independence becomes extremely fast/inexpensive.

The use of the diagonal elements may be motivated by the fact that $\text{rank}\,(\mathsf{P}) = \text{tr}\,(\mathsf{P}) = N_{tm}$. Removing the sensors s_k in the criterion (4.38) aims to keep those sensors with the smallest contribution to the trace of $(I - \mathsf{P})$ in $\mathcal{S}_r$. Recall that $I - \mathsf{P}$ corresponds to the covariance matrix of the estimate error. The diagonal elements of P is the so-called effective independence of each sensor.

Example 4.6 *The sensor positions obtained by using the Method of Effective Independence for the reference Garteur model in Appendix A are presented in Table 4.6. It is readily seen that the sensors mainly are placed at the wings in the z-direction, but also in the x-direction, and at the tail in the y-direction.*

Table 4.6 *Sensor positions on the reference Garteur model using the Method of Effective Independence.*

Improved $\mathcal{S}_r$
5_z, 6_z, 7_z, 9_z, 10_z, 11_z, 12_x, 12_x, 12_z, 13_x, 14_z, 15_z, 21_y, 22_y, 23_y

The advantage with the EI-method is the inexpensive computation of a single sensor position. Only one computation of P is needed in an iteration. Thus, only $|\mathcal{S}_c| - p$ evaluations of P in (4.37) are needed. A drawback with the EI-method may be the fact that not all prior knowledge of the structure is used in the criterion, e.g., the prior knowledge about resonance frequencies and the damping.

4.4.3 Placement Based on the Controllability and Observability Gramians

One may argue that the modes must be observable in order to be measured by the sensors and controllable in order to be excited by the actuators. Therefore, using a scalar measure of how controllable (observable) the modeled structure is, a criterion for the placement of actuators (sensors) may be obtained.

For time-discrete control purposes, many actuator placement criteria have been presented recently. For instance, in [16] an actuator placement criterion for the control of time-discrete systems is presented, and applied to an optimal fuel control problem. However, the modal analysis properties of the actuator placement based on the controllability Gramian have not been fully investigated. We will therefore study some criteria based on the controllability/observability Gramians for the placement of actuators/sensors on FE modeled structures. A comparison with the actuator/sensor criteria for model updating is also made in Section 4.6.

One of the drawbacks with the EI-method in Section 4.4.2 is that not all prior knowledge of the structure is taken care of, e.g., the resonance frequencies and the damping are not included in the criterion. Therefore, a criterion based on the observability Gramian may be used to place sensors on the structure, since the prior knowledge of the resonance frequencies and the damping is inherent in the A-matrix of the state space model in (2.67).

For the time-invariant linear state-space model in (2.67), the controllability Gramian $\mathcal{W}_c$ is defined as the solution to

$$A_s\mathcal{W}_c + \mathcal{W}_c A_s^T + B_s B_s^T = 0 \tag{4.40}$$

and the observability Gramian $\mathcal{W}_o$ as the solution to

$$A_s^T\mathcal{W}_o + \mathcal{W}_o A_s + C_s^T C_s = 0 \tag{4.41}$$

see [38]. For a similarity transformation $z = T\bar{z}$, and the corresponding state space realization in (2.69) the Gramians become

$$\begin{aligned}\bar{\mathcal{W}}_c &= T\mathcal{W}_c T^T\\ \bar{\mathcal{W}}_o &= T^{-T}\mathcal{W}_o T^{-1}\end{aligned} \tag{4.42}$$

In [30] three proposals for determining the degrees of controllability and observability and their physical interpretation are presented. They are all based on the Gramians $\mathcal{W}_c$ and $\mathcal{W}_o$ in (4.40) and (4.41):

$$\tau_1\left(\mathcal{W}_*\right) = \det\left(\mathcal{W}_*\right) \tag{4.43a}$$

$$\tau_2\left(\mathcal{W}_*\right) = \lambda_{\min}\left(\mathcal{W}_*\right) \tag{4.43b}$$

$$\tau_3\left(\mathcal{W}_*\right) = \frac{1}{\operatorname{tr}\left(\mathcal{W}_*^{-1}\right)} \tag{4.43c}$$

where $*$ can be interpreted as either c or o. In order to use τ_i, $i = \{1, 2, 3\}$ in (4.43) as a criterion for actuator and sensor placement, $\mathcal{A}_r$ and $\mathcal{S}_r$ must be unique, i.e., they must be independent of similarity transformations. For actuator placement based on the controllability Gramian this uniqueness requirement can be stated as

$$\begin{gathered}\tau_i\left(\mathcal{W}_c(A_s, B_{s,1})\right) > \tau_i\left(\mathcal{W}_c(A_s, B_{s,2}\right)\\ \Leftrightarrow\\ \tau_i\left(\mathcal{W}_c(T^{-1}A_sT, T^{-1}B_{s,1})\right) > \tau_i\left(\mathcal{W}_c(T^{-1}A_sT, T^{-1}B_{s,2})\right)\end{gathered} \tag{4.44}$$

where $\mathcal{W}_c = \mathcal{W}_c(A_s, B_s)$, is a function of the matrices A_s and B_s in (2.67). Notice that B_s represents the actuator positions. The corresponding uniqueness requirement is also imposed on the observability Gramian,

$$\begin{gathered}\tau_i\left(\mathcal{W}_o(A_s, C_{s,1})\right) > \tau_i\left(\mathcal{W}_o(A_s, C_{s,2})\right)\\ \Leftrightarrow\\ \tau_i\left(\mathcal{W}_o(T^{-1}A_sT, C_{s,1}T)\right) > \tau_i\left(\mathcal{W}_o(T^{-1}A_sT, C_{s,2}T)\right)\end{gathered} \tag{4.45}$$

where $\mathcal{W}_o = \mathcal{W}_o(A_s, C_s)$ is a function of the matrices A_s and C_s in (2.67). Here C_s represents the sensor positions.

For τ_1 the uniqueness requirements in (4.44) and (4.45) are easily fulfilled since for a fixed T_*,

$$\det\left(\bar{\mathcal{W}}_*\right) = \det\left(T_* \mathcal{W}_* T_*^T\right) = \det\left(T_*\right)^2 \det\left(\mathcal{W}_*\right) \tag{4.46}$$

where $T_* = T$ if $* = c$, and $T_* = T^{-T}$ if $* = o$. The uniqueness requirements (4.44) and (4.45) are thus verified for τ_1 in (4.43a). However, τ_2 and τ_3 in (4.43b) and (4.43c) do not satisfy (4.44) or (4.45), which is shown in Example 4.7.

Example 4.7 *Consider the system matrices*

$$A_s = \begin{bmatrix} -0.087 & 0.018 \\ -0.149 & -0.041 \end{bmatrix}, \quad B_{s,1} = \begin{bmatrix} 1.334 \\ 0.698 \end{bmatrix}, \quad B_{s,2} = \begin{bmatrix} -0.315 \\ 1.547 \end{bmatrix} \tag{4.47}$$

and the similarity transformation

$$T = \begin{bmatrix} 0.554 & 0.015 \\ -0.053 & -0.022 \end{bmatrix} \tag{4.48}$$

Then we have that (4.44) *is not fulfilled for* τ_2 *or* τ_3*, since*

$$\begin{aligned} \tau_2\left(\mathcal{W}_{c,1}\right) &= 8.8363, & \tau_2\left(T\mathcal{W}_{c,1}T^T\right) &= 0.0057 \\ \tau_2\left(\mathcal{W}_{c,2}\right) &= 0.5255, & \tau_2\left(T\mathcal{W}_{c,2}T^T\right) &= 0.0121 \end{aligned}$$

and

$$\begin{aligned} \tau_3\left(\mathcal{W}_{c,1}\right) &= 23.5936, & \tau_3\left(T\mathcal{W}_{c,1}T^T\right) &= 2.9976 \\ \tau_3\left(\mathcal{W}_{c,2}\right) &= 30.4731, & \tau_3\left(T\mathcal{W}_{c,2}T^T\right) &= 0.1805 \end{aligned}$$

where $\mathcal{W}_{c,i} = \mathcal{W}(A_s, B_{s,i})$.

It can be shown that $\mathcal{W}_c\left(A_s, B_s\right) = \mathcal{W}_o\left(A_s^T, C_s = B_s^T\right)$*, so that* (4.45) *is not fulfilled for* τ_2 *and* τ_3.

Since the eigenvalues of the product

$$\mathcal{W}_{co} = \mathcal{W}_c \mathcal{W}_o \tag{4.49}$$

are invariant under similarity transformations, i.e.,

$$\lambda_i\left(\bar{\mathcal{W}}_c \bar{\mathcal{W}}_o\right) = \lambda_i\left(\mathcal{W}_c \mathcal{W}_o\right) \tag{4.50}$$

the criteria τ_2 and τ_3 for actuator/sensor placement can be formed on $\mathcal{W}_{co}$, in (4.43b) and (4.43c).

The criteria for actuator and sensor placement thus become

$$P_1^{ma} = \tau_1(\mathcal{W}_*)\,, \quad * \in \{c, o, co\} \tag{4.51a}$$
$$P_2^{ma} = \tau_2(\mathcal{W}_{co}) \tag{4.51b}$$
$$P_3^{ma} = \tau_3(\mathcal{W}_{co}) \tag{4.51c}$$

where τ_i is defined in (4.43).

Notice that if the balanced realization of the state space model is chosen, then the criteria τ_2 and τ_3 may be formed on $\mathcal{W}_c$ and $\mathcal{W}_o$, since then $\mathcal{W}_o = \mathcal{W}_c = \Sigma = \mathrm{diag}(\sigma_1, \ldots, \sigma_n)$, where σ_i are the square roots of the eigenvalues of $\mathcal{W}_{co}$. See [48] for a presentation of the balanced realization.

In Example 4.8 the actuator positions obtained by the criteria in (4.51) are presented.

Example 4.8 *Using Algorithm 4.1, Algorithm 4.3, and the criteria* P_i^{ma}, $i = 1, 2, 3$, *the resulting actuator positions for the reference Garteur model are shown in Table 4.7. All actuators are placed at the wings. The improved actuator positions are closer to the end of the wings, than the actuator positions determined by the primary algorithm. The results are not totally different w.r.t. to the criteria: one of the actuators is placed to the middle of a wing in the* z*-direction, one to the end of a wing in the* x*-direction and one in the* z*-direction for the primary position, while the improved positions have two actuators in the* z*-direction, and a third actuator in either the* x*-direction or the* y*-direction. The artificial set of sensors is* $\mathcal{S}_a = \{$*all transl. dof*$\}$.

Table 4.7 *Actuator positions* $\mathcal{A}_r$ *for the reference Garteur mode based on the controllability Gramian* $\mathcal{W}_c$.

Criterion P	Primary $\mathcal{A}_r$ a_1, a_2, a_3	Improved $\mathcal{A}_r$
P_1^{ma}	$10_z, 15_z, 13_x$	$6_z, 12_x, 14_z$
P_2^{ma}	$6_z, 4_x, 12_z$	$9_z, 13_y, 13_z$
P_3^{ma}	$6_z, 4_x, 14_z$	$5_z, 12_x, 12_z$

A validation of the actuator positions in Table 4.7 w.r.t. the critria P_i^{ma} *in (4.51) can be made. Table 4.8 shows the values of the criterions for the computed actuator positions. Notice that the criteria are normalized such that the largest value of each row equals 1. For this case it is seen that the actuator positions maximizes the corresponding criterion, which indicates that the sub-optimality of Algorithm 4.3 is not critical. It is hard to point out the criterion* P_i^{ma} *having the best properties.*

Table 4.8 *A validation of the actuator positions based on the controllability Gramian.*

Design Criterion	Improved $\mathcal{A}_r$	Validation Criterion		
		P_1^{ma}	P_2^{ma}	P_3^{ma}
P_1^{ma}	6_z, 12_x, 14_z	1	.506	.891
P_2^{ma}	9_z, 13_y 13_z	$4 \cdot 10^{-5}$	1	.801
P_1^{ma}	5_z, 12_x, 12_z	$2 \cdot 10^{-3}$	.834	1

In Example 4.9 the sensor positions using the criteria in (4.51) are presented.

Example 4.9 *Using Algorithm 4.1, and Algorithm 4.3, the sensor positions for the reference Garteur model are shown in Table 4.9 for the criteria P_i^{ma}, $i = 1, 2, 3$. Studying Table 4.9 it can be seen that the criteria P_1^{ma}, P_2^{ma} and P_3^{ma} mainly place the sensors at the wings in the z-direction, but also in the x-direction. There exist differences: criterion P_1^{ma} places several sensors at the tail in the y-direction, while criterion P_2^{ma} does not place any sensor in the y-direction at all. The criterion P_3^{ma} has only placed one sensor in the y-direction. The artificial sets of actuators for computing the sensors using P_2^{ma} and P_3^{ma} are the actuators for the corresponding criterion in Table 4.7.*

Table 4.9 *Sensor positions for the reference Garteur model based on the observability Gramian $\mathcal{W}_o$.*

Criterion P	Improved $\mathcal{S}_r$
P_1^{ma}	5_z, 6_z, 9_z, 10_z, 12_z, 13_x, 13_z, 14_x, 14_z, 15_x, 15_z, 20_y, 21_y, 22_y, 28_y
P_2^{ma}	5_z, 6_z, 9_z, 10_z, 12_x, 12_z, 13_x, 13_y, 13_z, 14_x, 15_x, 21_z, 22_z, 25_x, 26_x
P_3^{ma}	5_z, 6_z, 8_x, 9_z, 10_z, 12_x, 12_z, 13_z, 14_x, 14_z, 25_z, 21_z, 22_z, 25_x, 27_y

---

The computation of $\mathcal{W}_c$ and $\mathcal{W}_o$ can be made by solving the set of linear equations:

$$\mathsf{A}x = \mathsf{d}, \quad x = (\mathsf{A})^{-1}\mathsf{d} \tag{4.52}$$

where x are the entries of either $\mathcal{W}_c$ or $\mathcal{W}_o$. In (4.52), the vector d is a function of the actuator/sensor positions. Since A is determined from the constant matrix A_s

in (2.67), the computation of $\mathcal{W}_c$ ($\mathcal{W}_o$) is extremely inexpensive when A is obtained. A, b in (4.52) can be computed as

$$\mathcal{W}_c \;:\; \mathsf{A} = I \otimes A_s + A_s \otimes I, \quad \mathsf{d} = -\operatorname{vec}(B_s B_s^T) \tag{4.53a}$$

$$\mathcal{W}_o \;:\; \mathsf{A} = I \otimes A_s^T + A_s^T \otimes I, \quad \mathsf{d} = -\operatorname{vec}(C_s^T C_s) \tag{4.53b}$$

for $\mathcal{W}_c$ and $\mathcal{W}_o$, respectively. In (4.53), $\otimes$ denotes the Kronecker product, and vec denotes the construction of $\mathcal{W}_c$ ($\mathcal{W}_o$) into a vector, see [15].

4.5 Placement for Model Updating

Model updating is the common name of tuning dynamical (FE) models to measurements of mechanical structures. A successful model updating will thus yield an updated model with properties with a high correlation with the measurements. One approach to update FE models is to parameterize expected uncertainties in the model, and then estimate the values of these parameters using the measurements of the structure. In Sections 3.1 and 3.8 it was stressed that a cost function with good convergence properties is the single most important issue in order to update a model accurately. However, it is not only the properties of the cost function that affects the outcome of the model updating. High quality measurements are necessary in order to minimize the errors of the parameter estimates.

In order to achieve a valid model the parameters of the parameterized model should be estimated as accurate as possible, i.e., the bias and the covariance matrix of the parameter estimates should be minimized. Neglecting the bias term, the most natural objective of actuator/sensor placement for model updating is to place actuators and sensors in order to minimize the covariance matrix of the parameter estimates. In Section 3.9 the covariance matrix $\operatorname{Cov}[\theta]$ for a general cost function $V(\theta) = v(\theta)^T v(\theta)$ was presented, repeated here for convenience,

$$\operatorname{Cov}[\theta] \approx \sigma^2 \left(v'(\theta)^T v'(\theta)\right)^{-1} \tag{4.53}$$

where σ^2 is the variance of the zero-mean measured noise, independent between the measurement points, and where $v' = \partial v / \partial \theta$. Using the cost function V, and a parameterization θ of the initial model, the actuator and sensor positions can be computed in order to minimize the covariance matrix $\operatorname{Cov}[\theta]$ in (4.53).

In [40], the time domain cost function

$$V(\theta) = \sum_{i=1}^{p} \int_0^T \nu_i(t) \left(y_i(t,\theta) - y_i^x(t)\right)^2 dt \tag{4.54}$$

is to used to compute the sensor positions in order to minimize the corresponding covariance matrix. This idea is here generalized for a general cost function. The minimization of the covariance expression in (4.53) is proposed as a criterion for actuator and sensor placement.

The computation of $v'(\theta)$ in (4.53) is often very expensive, due to the size of the model N_{dof}, and the number of parameters N_θ, but also due to the size of the candidate set $|\mathcal{A}_c|$ of actuators and the candidate set $|\mathcal{S}_c|$ of sensors. It is therefore motivated to separate the actuator and sensor position algorithms in order to achieve a computationally reasonable algorithm.

Three candidates for the minimization of the covariance matrix $\mathrm{Cov}[\theta]$ w.r.t. actuator and sensor positions are investigated:

$$P_1^{mu}(\mathrm{Cov}[\theta]) = 1/\det(\mathrm{Cov}[\theta]) \tag{4.55a}$$
$$P_2^{mu}(\mathrm{Cov}[\theta]) = 1/\lambda_{\max}(\mathrm{Cov}[\theta]) \tag{4.55b}$$
$$P_3^{mu}(\mathrm{Cov}[\theta]) = 1/\operatorname{tr}(\mathrm{Cov}[\theta]) \tag{4.55c}$$

where $\mathrm{Cov}[\theta]$ denotes the covariance matrix of the parameters θ.

In Example 4.10 and 4.11 below, the used cost function is

$$V = \sum_{i=1}^{N_\omega} \left\| G(\omega_{R,i}^x, \theta) - G^x(\omega_{R,i}^x) \right\|_{Fro}, \qquad \omega_R^x = \{\omega \,|\, 2 \le \omega \le 80\} \text{ Hz} \tag{4.56}$$

where ω_R^x denotes the frequency points of the "measured" FRF. The parameterization $\theta = \{\theta_1, \ldots, \theta_{12}\}$ is given in Appendix A.2, and the parameter values correspond to the reference Garteur model in Appendix A.

In Example 4.10, the actuator positions using Algorithms 4.1 and 4.3 for the parameterization in Section A.2 in Appendix A are presented.

Example 4.10 *Using Algorithm 4.1 the actuator positions $\mathcal{A}_r$ are shown in Table 4.10. Criterion P_1^{mu} favors actuators placed at the wings in the z-direction, while criteria P_2^{mu} and P_3^{mu} yield two actuators in the z-direction and one in the x-direction, all three placed at the wings.*

Table 4.10 *Actuator positions $\mathcal{A}_r$ computed using the criteria P_i^{mu} in* (4.55).

Criterion P	Primary $\mathcal{A}_r$ a_1, a_2, a_3	Improved $\mathcal{A}_r$
P_1^{mu}	10_z, 15_z, 6_z	6_z, 10_z, 15_z
P_2^{mu}	12_z, 14_z, 10_z	10_z, 12_z, 13_z
P_3^{mu}	12_z, 10_z, 13_z	10_z, 12_z, 13_z

A validation of the actuator positions can be made if the criteria in (4.55) *are used for the actuator positions in Table 4.10,*

$$\begin{aligned} &P_1^{mu}(\{6_z, 10_z, 15_z\}) = 1, && P_1^{mu}(\{10_z, 12_z, 13_z\}) = 0.056 \\ &P_2^{mu}(\{6_z, 10_z, 15_z\}) = 0.720, && P_2^{mu}(\{10_z, 12_z, 13_z\}) = 1 \\ &P_3^{mu}(\{6_z, 10_z, 15_z\}) = 0.748, && P_3^{mu}(\{10_z, 12_z, 13_z\}) = 1 \end{aligned}$$

where the values of the criteria are normalized such that the largest criterion of each "row" equals 1. This validation seems not to be sufficient to determine which criterion P_i^{mu} is the best. However, the minor sub-optimality of Algorithm 4.3 is once again indicated.

In Example 4.11, the sensor positions using Algorithms 4.1 and 4.3 for the parameterization in Section A.2 are presented.

Example 4.11 *Using the criteria in (4.55) the sensor positions $\mathcal{S}_r$ are shown in Table 4.11. The criteria P_1^{mu}, P_2^{mu} and P_3^{mu} yield nearly equal sensor positions. The sensors are mainly placed at the wings and the stabilizers in the z-direction and the y-direction. The conclusion is that the choice of criterion P_i^{mu} seems to be of rather low importance.*

Table 4.11 *Sensor positions $\mathcal{S}_r$ computed using the criteria P_i^{mu} in (4.55).*

Criterion P	Improved $\mathcal{S}_r$
P_1^{mu}	5_z, 6_z, 7_z, 9_z, 10_z, 11_z, 12_z, 13_z, 14_z, 15_z, 20_y, 21_y, 21_z, 22_y, 28_y
P_2^{mu}	5_z, 6_z, 7_z, 9_z, 10_z, 11_z, 12_z, 13_z, 14_z, 15_z, 19_y, 21_z, 22_z, 23_y, 27_y
P_3^{mu}	5_z, 6_z, 7_z, 9_z, 10_z, 11_z, 12_z, 13_x, 13_z, 14_z, 15_x, 15_z, 23_y, 26_x, 27_y

When placing actuators and sensors for model updating it is not only robustness in $\mathcal{A}_r$ and $\mathcal{S}_r$ against errors in the initial model that has to be examined. Also, the robustness against parameterization deviation is also of interest, i.e., robustness against a change of parameterization when subsequently updating the model. This is especially interesting since the parameterization is partly based on the emerging deviation between the measurements and the model, i.e., the parameterization may not be exactly known when determining the sensor and actuator positions.

In Example 4.12 the actuator positions minimizing the variances of the single parameters are computed.

Example 4.12 *In Table 4.12, the actuator positions minimizing the variance of the single parameters of the parameterization in Appendix A.2 are presented. It is seen that the actuator positions are mainly placed on the wings in the z-direction, and on the tail in the x-direction. The physical interpretation of the parameters are presented in Table A.7, see Section A.2.*

4.6 Comparison and Validation

In applications of industrial size there are a lot of trade-offs and sub-optimalities introduced in order to obtain algorithms of sufficiently low complexity. Therefore

Table 4.12 *The actuator positions minimizing the variance of the single parameters.*

$\mathcal{A}_r$	Parameter θ_i											
a_k	θ_1	θ_2	θ_3	θ_4	θ_5	θ_6	θ_7	θ_8	θ_9	θ_{10}	θ_{11}	θ_{12}
a_1	10_z	21_y	6_z	15_z	10_z	6_z	22_y	6_z	6_z	6_z	6_z	22_y
a_2	6_z	22_y	10_z	26_z	6_z	10_z	21_y	10_z	10_z	10_z	10_z	21_y
a_3	22_y	20_y	7_z	8_z	5_z	13_z	20_y	15_x	12_z	5_z	14_z	20_y

the validation of $\mathcal{A}_r$ and $\mathcal{S}_r$ are important, i.e., the judgment whether the resulting actuator/sensor positions are appropriate or not. The validation may be hard to perform properly based on engineering skills due to the complexity of the structures. However, the engineering insights are believed to be important in validation procedure.

Moreover, $\mathcal{A}_r$ and $\mathcal{S}_r$ should not only maximize the criterion used in the algorithms, they should also yield good properties for other criteria that are considered to be important for the application in question. However, if $\mathcal{A}_r$ and $\mathcal{S}_r$ do not fulfill the specified properties, a judgment of every step inherent in the used algorithm has to be made, i.e., a validation of the trade-offs and sub-optimality inherent in the algorithms. For instance, the candidate sets of actuators $\mathcal{A}_c$ and sensors $\mathcal{S}_c$ must be properly constructed, the optimization criterion must be formed to maximize the objective, no unnecessary sub-optimality should be introduced into the algorithms, the number of actuators m and sensors p used during the measurements should be sufficiently large, etc. Taking all these (kind of) aspects into consideration, the computed actuator and sensor positions should be able to give measurements of sufficiently high quality.

We have found that the actuator positions should be determined with care. Otherwise important aspects on the properties of the actuator positions may not be fulfilled. In practice there are often several purposes for the measuring e.g., experimental modal analysis and model updating. The actuators must then be able to excite the structure such that the modes are appropriately estimated and the parameters of the model are estimated accurately. This can become critical due to the complexity of the structure and the often low number of actuators available for placement. If there may be several purposes for collecting measurements, e.g., both for model updating and experimental modal analysis. Then one may construct a single criterion that fulfills all the aspects on the measurements through

$$\bar{P} = \prod_i P_i \tag{4.57}$$

where P_i is a valid criterion for a single aspect.

The sensor positions seems to be less critical than the actuator positions. Often the number of sensors is very large. It is therefore not critical if a low number of sensors are not placed optimally. One can also make another distinction between the actuators and the sensors: the actuators are active and the sensors are passive in the sense that the sensors are measuring the vibrations obtained by the actuators. On one hand, if the modes of the structure are not appropriately excited, the experimental modal analysis/model updating may be affected no matter how optimal the sensors are placed. On the other hand, if the modes are accurately excited the sensors will measure the modes appropriately if the SNR is sufficiently high.

The sensor placement task is therefore not as critical as the actuator placement task. Moreover, the computation of the sensor positions are more expensive. An inexpensive algorithm for sensor placement combined with a more expensive actuator placement algorithm may yield good measurements for a totally low cost.

The sensor positions in Tables 4.6, 4.9, and 4.11 is not validated in the same fashion as the actuators. However, one may draw the conclusion that the sensors are mainly placed on the wings in the z-direction, on the wing-tips in the x-direction, and on the tail in the y-direction, where the response of the structure is relatively high.

The actuator positions computed by the algorithms in Section 4.4 and 4.5 are shown in Table 4.13. It is indicated that maximizing the controllability Gramian and the $\mathsf{M}_{a,i}^{md}$-values for a “high” level of noise variance yields good actuator positions with good overall properties. Moreover, maximizing the M_i^d-values and the $\mathsf{M}_{a,i}^{md}$-values for a “low” level of noise variance is found to give less good actuator positions. It is also found that the objective to minimize the covariance matrix of $\mathrm{Cov}[\theta]$ may suffer from a non-negligible level of sub-optimality, but still the overall properties are acceptable.

Example 4.13 *In Table 4.13 the actuator positions computed by the criteria in Section 4.4 and 4.5 are summarized. In Table 4.14 a comparison of the actuator positions in the examples of Section 4.4 and 4.5 is made.*

The (N) in Table 4.14 denotes that the values of the corresponding rows are normalized such that the highest value equals 1, and the other values equals the fraction of the maximum value. The highest value of each row is marked ?. If a value is marked ?, then the corresponding $\mathcal{A}_r$ is sub-optimal (among $\mathcal{A}_r^i$).

Notice that neither $\min(\mathsf{M}_i^d)$ *nor* $\min(\mathsf{M}_{a,i}^{md})$ *are used for computing actuator positions. They are shown here for indicating robustness properties against worst-case mode excitation. It is seen that the expected set of actuators $\mathcal{A}_r$ with one exception minimizes the corresponding criterion used in the algorithm. This is due to the sub-optimality of Algorithm 4.1. However, the sub-optimality is not found to be critical, due to the near-optimality of the values of the corresponding criterion. A more interesting aspect is to study the properties of the actuator positions w.r.t. other criteria. It can be seen that the criteria P_i^{ma} based on the controllability Gramian yields actuator positions with overall good properties. In particular, the*

Table 4.13 *The actuator positions using Algorithm 4.3, and the criteria in Section 4.4 and 4.5.*

Notation	Actuator Positions	Criterion	References
$\mathcal{A}_r^1$	6_z, 12_x, 14_z	P_1^{ma}	(4.51a)
$\mathcal{A}_r^2$	9_z, 13_y, 13_z	P_2^{ma}	(4.51b)
$\mathcal{A}_r^3$	5_z, 12_x, 12_z	P_3^{ma}	(4.51c)
$\mathcal{A}_r^4$	13_z, 17_z, 22_x	P^d	(4.14)
$\mathcal{A}_r^5$	11_z, 12_z, 21_x	P^{nd}, σ_l^{mn}	(4.24), (4.30a)
$\mathcal{A}_r^6$	15_z, 21_z, 22_z	P^{nd}, σ_m^{mn}	(4.24), (4.30b)
$\mathcal{A}_r^7$	12_z, 15_y, 15_z	P^{nd}, σ_h^{mn}	(4.24), (4.30c)
$\mathcal{A}_r^8$	6_z, 10_z, 15_z	P_1^{mu}	(4.55a)
$\mathcal{A}_r^9$	10_z, 12_z, 13_z	P_2^{mu}	(4.55b)
$\mathcal{A}_r^{10}$	10_z, 12_z, 13_z	P_3^{mu}	(4.55c)

criterion P_1^{ma} has good overall properties. The criterion P^{nd} for a high level of noise variance yields actuator positions with very good modal analysis properties. Moreover, the robustness against noise is not critical in order to obtain high ndMAC-values for low levels of noise. The criterion P_1^{mu} minimizing the covariance matrix has for the parameterization in Appendix A.2 good parameter estimate properties, and also good overall properties. However, P_2^{mu} and P_3^{mu} may not be as good as P_1^{mu}, compare $\det(\mathrm{Cov}[\theta])$, and their worst-case mode excitation properties $\min(\mathsf{M}_{a,i}^{md})$.

From Table 4.14 one may draw the conclusion that the criterion P_1^{ma} based on the controllability Gramian has very good overall properties, i.e., the ability to provide actuator positions for both model updating and experimental modal analysis. A high level of modeled noise gives actuator positions that have good mode excitation properties. The criterion P_1^{mu} seems to have the best parameter estimation properties.

4.7 Summary

The placement of actuators and sensors on a large flexible mechanical structure is a part of the experimental design. It is made in advance of the vibrational experiments to ensure that high quality measurements are obtained. It is stressed that the size of the FE models, the large number of sensors (actuators), and the non-convexity of the optimization problems require sub-optimal algorithms to be practical. The sub-optimality of the most common algorithms are reduced via a combined actuator/sensor placement algorithm that iteratively improves the set of actuators and sensors. A novel noise-robust actuator placement criterion was presented. Simulations show that the prize paid for the robustness property is negligible. It is also found that the controllability Gramian has good overall actuator placement properties. A generalized actuator/sensor placement criterion for model updating was also presented.

Table 4.14 Comparison of the actuator positions $\mathcal{A}_r^i$ given in Table 4.13.

	$\mathcal{A}_r^1$	$\mathcal{A}_r^2$	$\mathcal{A}_r^3$	$\mathcal{A}_r^4$	$\mathcal{A}_r^5$	$\mathcal{A}_r^6$	$\mathcal{A}_r^7$	$\mathcal{A}_r^8$	$\mathcal{A}_r^9$	$\mathcal{A}_r^{10}$
$\det(\mathcal{W}_c)$ (N)	1	$4\cdot10^{-5}$	$2\cdot10^{-3}$	$2\cdot10^{-18}$	$1\cdot10^{-8}$	$2\cdot10^{-9}$	$3\cdot10^{-8}$	$6\cdot10^{-2}$	$3\cdot10^{-4}$	$3\cdot10^{-4}$
$\lambda_{\min}(\mathcal{W}_{co})$ (N)	.506	1	.834	.017	.105	.036	.094	.024	.011	.011
$1/\operatorname{tr}(\mathcal{W}_{co}^{-1})$ (N)	.891	.801	1	.035	.188	.082	.199	.062	.030	.030
$\frac{1}{N_q}\sum_{i=1}^{N_q} \mathsf{M}_i^d$	.984	.984	.984	.999	.999	.997	.996	.982	.945	.945
$\frac{1}{N_q}\sum_{i=1}^{N_q} \mathsf{M}_{a,i}^{md},\ \sigma^{mn}=\sigma_l^{mn}$	.984	.984	.984	.997	.998	.996	.996	.982	.944	.944
$\frac{1}{N_q}\sum_{i=1}^{N_q} \mathsf{M}_{a,i}^{md},\ \sigma^{mn}=\sigma_m^{mn}$	.983	.981	.983	.984	.995	.993	.996	.979	.940	.940
$\frac{1}{N_q}\sum_{i=1}^{N_q} \mathsf{M}_{a,i}^{md},\ \sigma^{mn}=\sigma_h^{mn}$	.979	.952	.979	.869	.962	.966	.989	.954	.918	.918
$1/\det(\mathrm{Cov}[\theta])$ (N)	.736	.022	.016	$1\cdot10^{-9}$	$5\cdot10^{-5}$	$9\cdot10^{-6}$	$4\cdot10^{-5}$	1	.056	.056
$1/\lambda_{\max}(\mathrm{Cov}[\theta])$ (N)	.593	.530	.537	.343	.465	.345	.658	.720	1	1
$\operatorname{tr}(\mathrm{Cov}[\theta])$ (N)	.626	.552	.561	.346	.488	.360	.675	.748	1	1

$\min(\mathsf{M}_i^d)$	.911	.918	.910	.997	.994	.985	.984	.911	.522	.522
$\min(\mathsf{M}_{a,i}^{md}),\ \sigma^{mn}=\sigma_l^{mn}$	.911	.912	.911	.996	.993	.984	.984	.911	.910	.910
$\min(\mathsf{M}_{a,i}^{md}),\ \sigma^{mn}=\sigma_m^{mn}$	.911	.918	.911	.967	.982	.979	.983	.910	.519	.519
$\min(\mathsf{M}_{a,i}^{md}),\ \sigma^{mn}=\sigma_h^{mn}$	.910	.829	.909	.762	.883	.826	.981	.732	.304	.304

5

Conclusions

In industrial applications it is of vital importance that methods are reliable, efficient, and easy to apply. All these aspects on a method for solving a problem of high complexity may be hard to fulfill. Depending on the application, the importance of the aspects differs. A goal for this thesis has been to construct efficient and reliable methods that solve the specific tasks of model updating and actuator/sensor placement in applications of industrial complexity.

For aviation/aerospace applications, accurate models are valuable. In order to reduce the expenses for the measuring task, simulations using accurate models can be made. However, FE modeling of the structures does not always yield as accurate models as desired. It is therefore of interest to improve/update an initial model. The most common approach is to construct a parameterization of the model and then estimate the values of these parameters from measurements. However, the major obstacle of model updating is the numerous local minima of the cost function in the parameter space. Another crucial issue is the computational expenses of the model updating task as well as the reliability of the optimization methods. These three considerations must be taken care of in a proper way for a successful model updating to be accomplished.

The existence of local minima can be reduced with a combined modal domain/frequency domain cost function, see Section 3.8.4. However, the use of traditional mode pairing in the cost functions leads to a combinatorial optimization as well as to local minima. The critical mode pairing is circumvented with the novel mode pairing free cost function in Section 3.8.5, which in simulations is found to have very good parameter convergence properties. The drawback of this cost function is comes as parameter bias if the modes of the structure are not appropriately estimated. The computational expenses are reduced via the proposed model updating procedure in Section 3.8.2, where a semi-fixed reduction basis reduces the number of times the normal modes of the model are computed. It is also stressed that the single most important design variable of the optimization method is the regularization term. If the regularization is not appropriately made, the optimization algorithm typically end up in an undesired local minimum. An extensive motivation for the choice of the regularization term is made. In simulations the presented strategy of adaptively determining the regularization term is shown to be successful.

In order to measure the behavior of mechanical structures, actuators and sensors must be located on the structure. The purpose of the measuring may be for experimental modal analysis, model updating or for the eventual combination of these two tasks. Since the FE model is a spatially discrete model, locating actuators/sensors on a mechanical structure becomes a discrete optimization problem. Furthermore, the optimization problem is in general non-convex, and the task to compute the optimal actuator/sensor positions is not practical. One must therefore use sub-optimal algorithms in order to fulfill the time and memory requirements. An actuator/sensor placement algorithm improving the results of the most common algorithms is proposed in Section 4.2. It is in simulations found that the desired properties of these improved actuator/sensor positions are significantly enhanced for an acceptable increase of the computational expenses.

For experimental modal analysis, a criterion for the placement of actuators for appropriate excitation of the modes in presence of noise and damping is proposed in Section 4.4.1. It is found that including an appropriate noise model when placing the actuators increases the robustness against noise substantially for a negligible decrease of the corresponding noise-free objective. As a consequence of the noise-robustness, the Signal-to-Noise Ratio (SNR) is improved considerably.

A

The Garteur Model

The Garteur FE model used in the simulation examples is presented here. Its real physical counterpart was developed for the purpose of experimental modal analysis in a Garteur project (Group for Aeronautical Research and Technology in EURope). It was designed to have several near multiple modes in the structure, see Table A.6.

The model is based on the beam element derived in Section 2.2, and eight point masses, see Section 2.3. In Fig. A.1, the model is visualized where circles ($\circ$) denotes a grid point and the lines represent beams in the model. Notice that the properties of the beams are not reflected in Fig. A.1, only their spatial location between the grid points, see Table A.4 for the properties of the reference model.

In Table A.1 the coordinates of the grid points are presented, and in Table A.2 the grid points of the beams in the Garteur model are defined.

There are also "rigid elements" connecting the beams in Table A.2, i.e., five stiff beams of no mass between the grid points {3, 24}, {4, 25}, {8, 26}, {19, 27} and {28, 20}.

The sparsity of the Garteur model is visualized in Fig. A.2. The entries of the mass matrix M, and the stiffness matrix K have structural zeroes (entries being zero due to the structure of the model). The entries of M and K not being zero is marked with a dot ($\cdot$) in Fig. A.2. In the M and K matrices there are 680 and 860 non-zero entries yielding a sparsity of 2.41 % and 3.05 %, respectively. The differences in the structural zeros between the system matrices M and K are due to the rigid elements connecting the beams of the model, since they are modeled as massless.

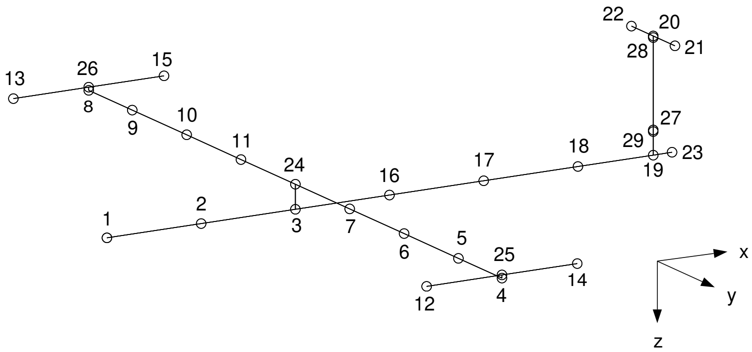

Figure A.1 *The Garteur model.*

A.1 The Reference Garteur Model

In Table A.3, the interpretation of the symbols in Table A.4 are given. The properties of the beams in the initial Garteur model are presented in Table A.4. It is readily seen that the fuselage is stiffer than the wing and the stabilizers. The fuselage is much stiffer in the z-direction than in the y-direction and the wing is much stiffer in the x-direction than in the z-direction. This indicates that the modes will be dominated by the deflections in the wingz (in z-direction) and the stabilizers (in the y-direction).

There are also point masses in the model. These represent concentrated masses such as joints etc. Their location and mass are specified in Table A.5. The modal parameters of the nine low-frequency modes are presented in Table A.6.

Fig. A.3 shows the nine low frequency non-rigid normal modes of the reference Garteur model.

Table A.1 *The coordinates of the grid points in the Garteur model.*

coord-	Grid Point									
inate	1	2	3	4	5	6	7	8	9	10
x	0.00	0.25	0.50	0.50	0.50	0.50	0.50	0.50	0.50	0.50
y	0.00	0.00	0.00	0.95	0.75	0.50	0.25	-0.95	-0.75	-0.50
z	0.38	0.38	0.38	0.30	0.30	0.30	0.30	0.30	0.30	0.30

coord-	Grid Point									
inate	11	12	13	14	15	16	17	18	19	20
x	0.50	0.30	0.30	0.70	0.70	0.75	1.00	1.25	1.45	1.45
y	-0.25	0.95	-0.95	0.95	-0.95	0.00	0.00	0.00	0.00	0.00
z	0.30	0.29	0.29	0.29	0.29	0.38	0.38	0.38	0.38	0.00

coord-	Grid Point								
inate	21	22	23	24	25	26	27	28	29 (ref. grid)
x	1.45	1.45	1.50	0.50	0.50	0.50	1.45	1.45	1.45
y	0.10	-0.10	0.00	0.00	0.95	-0.95	0.00	0.00	0.00
z	0.00	0.00	0.38	0.30	0.29	0.29	0.38	0.05	0.30

Table A.2 *The beams of the Garteur model. The gid points defines their locations.*

Beam	Grid Points
Fuselage	1, 2, 3, 16, 17, 18, 19, 23
Wing	4, 5, 6, 7, 8, 9, 10, 11
Wing Tips (Right and Left)	13, 15, 26 and 12, 14, 25
Vertical Stabilizer	27, 28
Horizontal Stabilizer	20, 21, 22

A.2 The Parameterization of the Garteur model

The general parameterization of the Garteur model is shown in Table A.7. The actual parameterization and the values of quotient $\theta^{init}/\theta^{ref}$ of the parameters are presented in connection to the examples.

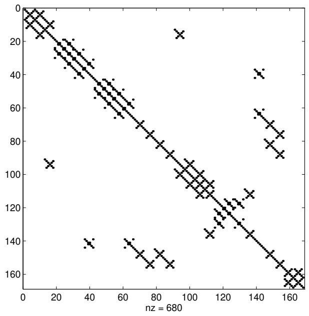

(a) The non-zero entries of the M matrix.

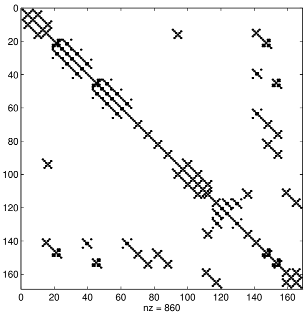

(b) The non-zero entries of the K matrix.

Figure A.2 *The sparsity of the system matrices of the Garteur model. A non-zero entry in the system matrices is marked with a dot* $(\cdot)$. *The mass matrix* M *have 2.41% non-zero entries and the stiffness matrix* K *have 3.05% non-zero entries.*

Table A.3 *The physical interpretation of the symbols defining the properties of the beam.*

Property	Description
E	Young's modulus
ρ	Material density
G	Shear modulus
J	Torsional moment of inertia
I_x	Moment of inertia of the cross section in x-direction
I_y	Moment of inertia of the cross section in y-direction
A	Cross section area

Table A.4 *Properties of the beams in the reference model.*

Property	Fuselage	Wing	Wing Tips	Stabilizers	Rigid Elements
E	$7.2 \cdot 10^{10}$	$7.2 \cdot 10^{10}$	$7.2 \cdot 10^{10}$	$7.2 \cdot 10^{10}$	$7.2 \cdot 10^{10}$
ρ	$2.7 \cdot 10^{3}$	$2.7 \cdot 10^{3}$	$2.7 \cdot 10^{3}$	$2.7 \cdot 10^{3}$	0
G	$2.769 \cdot 10^{10}$	$2.769 \cdot 10^{10}$	$2.769 \cdot 10^{10}$	$2.769 \cdot 10^{10}$	$2.769 \cdot 10^{10}$
J	$1.562 \cdot 10^{-5}$	$1.0 \cdot 10^{-6}$	$8.4167 \cdot 10^{-7}$	$8.4167 \cdot 10^{-7}$	$1.0 \cdot 10^{-4}$
I_x	$1.562 \cdot 10^{-6}$	$8.333 \cdot 10^{-9}$	$8.333 \cdot 10^{-9}$	$8.333 \cdot 10^{-6}$	$1.0 \cdot 10^{-4}$
I_y	$1.406 \cdot 10^{-5}$	$8.333 \cdot 10^{-7}$	$8.333 \cdot 10^{-6}$	$8.333 \cdot 10^{-9}$	$1.0 \cdot 10^{-4}$
A	$7.5 \cdot 10^{-3}$	$1.0 \cdot 10^{-3}$	$1.0 \cdot 10^{-3}$	$1.0 \cdot 10^{-3}$	0.1

Table A.5 *The point masses of the Garteur model.*

Grid Point	Mass
4, 8	0.135
3, 12, 13, 14, 15, 20	2.0

Table A.6 *Modal parameters of the reference model.*

Modal Parameter	Mode i								
	1	2	3	4	5	6	7	8	9
ω_i	3.66	12.70	31.90	33.39	40.05	40.56	40.92	41.96	62.82
ξ_i	0.030	0.015	0.010	0.008	0.009	0.012	0.006	0.007	0.005

Table A.7 *The parameterization of the Garteur model, and the parameter values of the initial Garteur model related to the values of the reference model.*

Parameter	Description	$\theta^{init}/\theta^{ref}$
1	ρ in the fuselage	0.70
2	J in the fuselage	0.60
3	I_x in the fuselage	1.30
4	I_y in the fuselage	0.90
5	ρ in the wings, wing tips and the stabilizers	1.20
6	J in the wings	1.25
7	I_x in the wings	1.15
8	I_y in the wings	0.85
9	A in the wings	1.05
10	Point masses in grid points 12 and 13	1.30
11	Point masses in grid points 14 and 15	0.80
12	Point mass in grid points 20	1.40

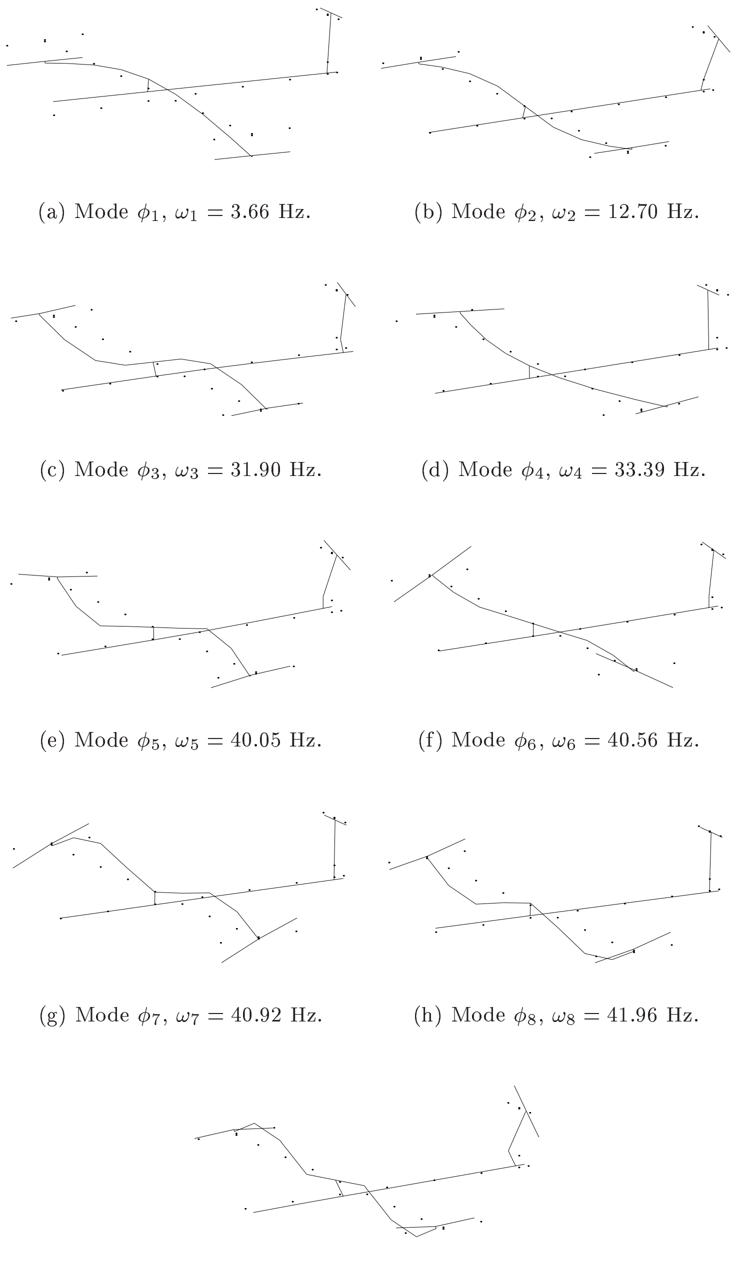

(a) Mode ϕ_1, $\omega_1 = 3.66$ Hz.

(b) Mode ϕ_2, $\omega_2 = 12.70$ Hz.

(c) Mode ϕ_3, $\omega_3 = 31.90$ Hz.

(d) Mode ϕ_4, $\omega_4 = 33.39$ Hz.

(e) Mode ϕ_5, $\omega_5 = 40.05$ Hz.

(f) Mode ϕ_6, $\omega_6 = 40.56$ Hz.

(g) Mode ϕ_7, $\omega_7 = 40.92$ Hz.

(h) Mode ϕ_8, $\omega_8 = 41.96$ Hz.

(i) Mode ϕ_9, $\omega_9 = 62.82$ Hz.

Figure A.3 *The modes of the reference Garteur model. The dots represent the grid points of the model.*

B

Properties of the Approximated ndMAC

Here two proposals for the approximation of M_i^{nd} in (4.23) in Section 4.4.1 are derived, $\mathsf{M}_{a,i}^{nd}$ and $\mathsf{M}_{b,i}^{nd}$. Some of the properties of $\mathsf{M}_{a,i}^{nd}$ and $\mathsf{M}_{b,i}^{nd}$ as actuator placement criterions are also presented.

B.1 Prerequisitities

In (4.20)-(4.22) the noise model $\mathcal{N}$ is presented, shortly repeated here for convenience. Let $\hat{\phi}_i^{mn}$ denote the measurement noise model for mode ϕ_i, and let $\hat{\phi}_i^{pn}$ denote the corresponding process noise model:

$$\hat{\phi}_i^{mn} = \left[\ldots, x_{i,j}^{mn}, \ldots\right]^T, \qquad x_{i,j}^{mn} \sim \mathrm{N}(0, \sigma_i^{mn}) \tag{B.1a}$$

$$\hat{\phi}_i^{pn} = \sum_{k=1}^{N_{pn}} \hat{\phi}_{i,k}^{pn} = \sum_{k=1}^{N_n} \phi_{i,k}^{pn} x_{i,k}^{pn}, \quad x_{i,k}^{pn} \sim \mathrm{N}(0, \sigma_{i,k}^{pn}) \tag{B.1b}$$

where N_{pn} denotes the number of process noise sources. The random variables in (B.1) are assumed to be independent,

$$x_{i,j_1}^{mn}, x_{i,j_2}^{mn} \quad \text{independent} \quad \forall i, \forall j_1 \neq j_2 \tag{B.2a}$$

$$x_{i,k_1}^{pn}, x_{i,k_2}^{pn} \quad \text{independent} \quad \forall i, \forall k_1 \neq k_2 \tag{B.2b}$$

$$x_{i,j}^{mn}, x_{i,k}^{pn} \quad \text{independent} \quad \forall i, \forall j, \forall k \tag{B.2c}$$

Compare this with the noise model $\mathcal{N}$ in Section 4.4.1, and with the noise model in Section 3.5.

For independent, Gaussian distributed random variables $x_i \sim \mathrm{N}(0, \sigma_i)$ of zero mean, the following property holds

$$\mathrm{E}\Big[\prod_j x_{i_j}\Big] \neq 0, \quad \text{if and only if} \quad \prod_j x_{i_j} = \prod_l x_l^{2k_l} \tag{B.3}$$

for some i, j, k, l. Moreover,

$$\mathrm{E}\big[x_i^2\big] = \sigma_i^2, \quad \mathrm{E}\big[x_i^4\big] = 3\sigma_i^4 \tag{B.4}$$

and for sums of the independent Gaussian variables x_i, the following holds

$$X = \sum_i a_i x_i, \quad \Rightarrow \quad X \sim \mathrm{N}(0, \sigma_X) \quad \text{where} \quad \sigma_X^2 = \sum_i a_i^2 \sigma_i^2 \tag{B.5}$$

where σ_i^2 is the variance of x_i, and where the $a_i \in \mathbb{R}$ are constant values.

The ndMAC in (4.23) is defined as

$$\text{ndMAC:} \qquad \mathsf{M}_i^{nd} = \mathrm{E}\left[\frac{|\phi_i^T \hat{\phi}_i^{nd}|^2}{|\phi_i|^2 |\hat{\phi}_i^{nd}|^2}\right] \tag{B.6}$$

where

$$\hat{\phi}_i^{nd} = \hat{\phi}_i^d + \hat{\phi}_i^{mn} + \hat{\phi}_i^{pn} \tag{B.7}$$

is an estimate of mode ϕ_i. Compare this with (4.16) and (4.17) in Section 4.4.1.

Denoting $|\phi_i|^2 = \phi_i^T \phi_i$, and suppressing the i-dependency of T_r and D_s we get

$$\left(\frac{T}{D}\right)_i = \frac{|\phi_i^T \hat{\phi}_i^{nd}|^2}{|\phi_i|^2 |\hat{\phi}_i^{nd}|^2} = \frac{\sum_{r=1}^6 T_r}{\sum_{s=1}^6 D_s} \tag{B.8}$$

In (B.8) the numerator terms T_r are

$$T_1 = |\phi_i^T \hat{\phi}_i^d|^2, \qquad T_2 = |\phi_i^T \hat{\phi}_i^{mn}|^2 \tag{B.9 a,b}$$

$$T_3 = \Big|\sum_k \phi^T \hat{\phi}_{i,k}^{pn}\Big|^2, \qquad T_4 = 2(\phi_i^T \hat{\phi}_i^d)(\phi_i^T \hat{\phi}_i^{mn}) \tag{B.9 c,d}$$

$$T_5 = 2\phi_i^T \hat{\phi}_i^d \sum_k \phi_i^T \hat{\phi}_{i,k}^{pn}, \quad T_6 = 2\phi_i^T \hat{\phi}_i^{mn} \sum_k \phi_i^T \hat{\phi}_{i,k}^{pn} \tag{B.9 e,f}$$

and the denominator terms D_s are

$$D_1 = |\phi_i|^2 |\hat{\phi}_i^d|^2, \qquad D_2 = |\phi_i|^2 |\hat{\phi}_i^{mn}|^2 \tag{B.10 a,b}$$

$$D_3 = |\phi_i|^2 \Big|\sum_k \hat{\phi}_{i,k}^{pn}\Big|^2, \qquad D_4 = 2|\phi_i|^2 (\hat{\phi}_i^d)^T \hat{\phi}_i^{mn} \tag{B.10 c,d}$$

$$D_5 = 2|\phi_i|^2 \sum_k (\hat{\phi}_i^d)^T \hat{\phi}_{i,k}^{pn}, \quad D_6 = 2|\phi_i|^2 \sum_k (\hat{\phi}_i^{mn})^T \hat{\phi}_{i,k}^{pn} \tag{B.10 e,f}$$

The computation of the M_i^{nd} in (B.6) is hard. An approximation $\mathsf{M}_{*,i}^{nd}$ of M_i^{nd} is therefore inevitable. In order for an approximation of M_i^{nd} to be valid as a criterion for actuator placement, some conditions should be fulfilled:

$$\text{C1:} \qquad \mathsf{M}_{*,i}^{nd} \leq 1, \quad \forall i \tag{B.11}$$

$$\text{C2a:} \qquad \frac{\partial \mathsf{M}_{*,i}^{nd}}{\partial (\sigma_i^{mn})^2} < 0, \ \forall i \tag{B.12a}$$

$$\text{C2b:} \qquad \frac{\partial \mathsf{M}_{*,i}^{nd}}{\partial (\sigma_{i,k}^{pn})^2} < 0, \ \forall i, \forall k \tag{B.12b}$$

$$\text{C3a:} \qquad \lim_{(\sigma_i^{mn})^2 \to \infty} \mathsf{M}_{*,i}^{nd} = \varepsilon_i^{mn} \ll 1, \ \forall i \tag{B.13a}$$

$$\text{C3b:} \qquad \lim_{(\sigma_{i,k}^{pn})^2 \to \infty} \mathsf{M}_{*,i}^{nd} = \varepsilon_{i,k}^{pn} \ll 1, \ \forall i, \forall k \tag{B.13b}$$

$$\text{C4:} \qquad \lim_{\substack{(\sigma_i^{mn})^2 \to 0 \\ (\sigma_{i,k}^{pn})^2 \to 0, \forall k}} \mathsf{M}_{*,i}^{nd} = \mathsf{M}_i^{d}, \quad \forall i \tag{B.14}$$

see Section 4.4.1 where the conditions C1-C4 above are motivated intuitively. Even if some of the conditions C1-C4 above are not fulfilled, a valid actuator placement criterion may be obtained anyway, although, it is less likely.

In order to get a deeper feeling for the expressions arising below, the physical interpretation of some of the variables may be helpful:

$\bar{p}$:	the number of modeled sensors used for actuator placement
$(\sigma_i^{mn})^2$:	the measurement noise variance from a sensor, measuring mode ϕ_i.
$\bar{p} \cdot (\sigma_i^{mn})^2$:	total amount of measured (measurement) noise variance for mode ϕ_i.
$(\sigma_{i,k}^{pn})^2$:	input force noise variance from noise source a_k^{pn} for mode ϕ_i.
$\sum_k \lvert\phi_{i,k}^{pn}\rvert^2 (\sigma_{i,k}^{pn})^2$:	total amount of measured process noise variance.
$\lvert\hat{\phi}_i^d\rvert^2$:	total amount of measured power of mode ϕ_i originating from the actuators.

Notice that variance equals power in a probabilistic framework.

B.2 Properties of the $\mathsf{M}_{a,i}^{nd}$

It can be shown that

$$\frac{|\phi_i^T \hat{\phi}_i^{nd}|^2}{|\phi_i|^2 |\hat{\phi}_i^{nd}|^2} = \frac{|a+s|}{|b+t|} \tag{B.15}$$

for some random variables s, t and for some positive real-valued constants a, b. It is easily seen that the statistics of s and t are determined by the random vectors $\hat{\phi}_i^{mn}$ and $\hat{\phi}_i^{pn}$ in (B.1). Since $\hat{\phi}_i^{mn}$ and $\hat{\phi}_i^{pn}$ are zero-mean and Gaussian, the statistics of s and t are determined by σ_i^{mn} and $\sigma_{i,k}^{pn}$. Consider

$$\frac{a+s}{b+t} \tag{B.16}$$

A Taylor expansion of the numerator around its expected value becomes

$$\frac{a+s}{b+t} = \frac{a+s}{b+\mathrm{E}[t]} \sum_{l=0}^{\infty} (-1)^l \left(\frac{t-\mathrm{E}[t]}{b+\mathrm{E}[t]} \right)^l \tag{B.17}$$

where it is assumed that $|(t-\mathrm{E}[t])/(b+\mathrm{E}[t])| < 1$ holds. Restricting the Taylor expansion to the first two terms:

$$\frac{a+s}{b+\mathrm{E}[t]} \left(1 - \frac{t-\mathrm{E}[t]}{b+\mathrm{E}[t]} \right) \tag{B.18}$$

a linearization of (B.16) is obtained. Since

$$\mathrm{E}\big[(t-\mathrm{E}[t])^2\big] \to 0 \quad \Rightarrow \quad \sigma_i^{mn} \to 0,\ \sigma_{i,k}^{pn} \to 0 \tag{B.19}$$

also the higher order moments goes to zero,

$$\mathrm{E}\big[(t-\mathrm{E}[t])^l\big] \to 0, \quad \forall l > 2 \tag{B.20}$$

as $\mathrm{E}\big[(t-\mathrm{E}[t])^2\big] \to 0$. An asymptotically unbiased approximation of the expectation of (B.16) therefore is

$$\mathrm{E}\left[\frac{a+s}{b+t}\right] \to \mathrm{E}\left[\frac{a+s}{b+\mathrm{E}[t]} \left(1 - \frac{t-\mathrm{E}[t]}{b+\mathrm{E}[t]} \right)\right], \quad \text{as} \quad \mathrm{E}\left[\left(\frac{t-\mathrm{E}[t]}{b+\mathrm{E}[t]}\right)^2\right] \to 0 \tag{B.21}$$

Notice that it is henceforth assumed that the probabilities $\mathsf{P}(a \gg s) \approx 1$ and $\mathsf{P}(b \gg t) \approx 1$ hold, i.e., the probability that the quotient (B.16) is greater than zero is very likely (≈ 1).

An approximation of (B.8) may then be performed as

$$\begin{aligned} \left(\frac{T}{D}\right)_i \approx \left(\frac{T}{D}\right)_{i,a} &= \mathrm{E}\left[\frac{T_1}{D_1 + \sum_{s=2}^{6} \mathrm{E}[D_s]} \left(1 + \frac{\sum_{r=2}^{6} T_r}{T_1}\right) \left(1 - \frac{\sum_{s=2}^{6} (D_s - \mathrm{E}[D_s])}{D_1 + \sum_{s=2}^{6} \mathrm{E}[D_s]}\right)\right] \\ &= \frac{T_1 + \sum_{r=2}^{6} \mathrm{E}[T_r]}{D_1 + \sum_{s=2}^{6} \mathrm{E}[D_s]} - \frac{\sum_{r=2}^{6} \sum_{s=2}^{6} \mathrm{E}[T_r (D_s - \mathrm{E}[D_s])]}{\big(D_1 + \sum_{s=2}^{6} \mathrm{E}[D_s]\big)^2} \end{aligned} \tag{B.22}$$

since T_1 and D_1 are deterministic.

Defining $\mathsf{M}_{a,i}^{nd}$ as the asymptotical unbiased, expected value of M_i^{nd},

$$\mathsf{M}_{a,i}^{nd} = \mathrm{E}\left[\left(\frac{T}{D}\right)_{i,a}\right] \tag{B.23}$$

we can obtain an approximation of M_i^{nd}.

Using (B.3), (B.4) and (B.5), the expected mean values of T_r and D_s become

$$\mathrm{E}[T_2] = |\phi_i|^2(\sigma_i^{mn})^2, \qquad \mathrm{E}[D_2] = \bar{p}|\phi_i|^2(\sigma_i^{mn})^2 \tag{B.24 a,b}$$

$$\mathrm{E}[T_3] = \sum_k |\phi_i^T \phi_{i,k}^{pn}|^2(\sigma_{i,k}^{pn})^2, \quad \mathrm{E}[D_3] = |\phi_i|^2 \sum_k |\phi_{i,k}^{pn}|^2(\sigma_{i,k}^{pn})^2 \tag{B.24 c,d}$$

$$\mathrm{E}[T_r] = 0,\ r = 4,\,5,\,6, \qquad \mathrm{E}[D_s] = 0,\ s = 4,\,5,\,6 \tag{B.24 e,f}$$

Proof of (B.24b):

$$\mathrm{E}[D_2] = \mathrm{E}\big[|\phi_i|^2|\hat{\phi}_i^{mn}|^2\big] = |\phi_i|^2\,\mathrm{E}\left[\sum_{k,\,l}^{\bar{p}} x_{i,k}^{mn} x_{i,l}^{mn}\right] = \bar{p}|\phi_i|^2(\sigma_i^{mn})^2 \qquad \square$$

In the same manner, the non-zero terms of $\mathrm{E}[T_r(D_s - \mathrm{E}[D_s])]$ become

$$\mathrm{E}[T_2(D_2 - \mathrm{E}[D_2])] = 2|\phi_i|^4(\sigma_i^{mn})^4 \tag{B.25a}$$

$$\mathrm{E}[T_3(D_3 - \mathrm{E}[D_3])] = 2|\phi_i|^2 \sum_k \sum_l (\phi_{i,k}^{pn})^T \phi_{i,l}^{pn} (\phi_i^T \phi_{i,k}^{pn})(\phi_i^T \phi_{i,l}^{pn})(\sigma_{i,k}^{pn})^2(\sigma_{i,l}^{pn})^2 \tag{B.25b}$$

$$\mathrm{E}[T_4 D_4] = 4|\phi_i|^2|\phi_i^T \hat{\phi}_i^d|^2(\sigma_i^{mn})^2 \tag{B.25c}$$

$$\mathrm{E}[T_5 D_5] = 4|\phi_i|^2 \phi_i^T \hat{\phi}_i^d \sum_k (\phi_i^T \phi_{i,k}^{pn})(\hat{\phi}_i^d)^T \phi_{i,k}^{pn}(\sigma_{i,k}^{pn})^2 \tag{B.25d}$$

$$\mathrm{E}[T_6 D_6] = 4|\phi_i|^2 \sum_k |\phi_i^T \phi_{i,k}^{pn}|^2(\sigma_i^{mn})^2(\sigma_{i,k}^{pn})^2 \tag{B.25e}$$

Proof of (B.25b):

$$
\begin{aligned}
\mathrm{E}[T_3 \cdot D_3] &= \mathrm{E}\left[\left| \sum_k \phi_i^T \phi_{i,k}^{pn} x_k^{pn} \right|^2 \cdot |\phi_i|^2 \left| \sum_r \phi_{i,r}^{pn} x_r^{pn} \right|^2 \right] \\
&= |\phi_i|^2\, \mathrm{E}\left[\left(\sum_{k,l} (\phi_i^T \phi_{i,k}^{pn})(\phi_i^T \phi_{i,l}^{pn}) x_{i,k}^{pn} x_{i,l}^{pn} \right) \cdot \left(\sum_{r,\, s} (\phi_{i,r}^{pn})^T \phi_{i,s}^{pn} x_{i,r}^{pn} x_{i,s}^{pn} \right) \right] \\
&= |\phi_i|^2\, \mathrm{E}\left[\sum_{k,\, l,\, r,\, s} (\phi_i^T \phi_{i,k}^{pn})(\phi_i^T \phi_{i,l}^{pn})(\phi_{i,r}^{pn})^T \phi_{i,s}^{pn} x_{i,k}^{pn} x_{i,l}^{pn} x_{i,r}^{pn} x_{i,s}^{pn} \right] \\
&= |\phi_i|^2\, \mathrm{E}\Bigg[\Bigg(\sum_k |\phi_i^T \phi_{i,k}^{pn}|^2 |\phi_{i,k}^{pn}|^2 (x_{i,k}^{pn})^4 + \sum_{\substack{k,\, r \\ k \neq r}} |\phi_i^T \phi_{i,k}^{pn}|^2 |\phi_{i,r}^{pn}|^2 (x_{i,k}^{pn})^2 (x_{i,r}^{pn})^2 \\
&\qquad + 2 \sum_{\substack{k,\, r \\ k \neq r}} (\phi_i^T \phi_{i,k}^{pn})(\phi_i^T \phi_{i,r}^{pn})(\phi_{i,r}^{pn})^T \phi_{i,s}^{pn} (x_{i,k}^{pn})^2 (x_{i,r}^{pn})^2 \Bigg) \Bigg] \\
&= |\phi_i|^2 \Bigg(\sum_{k,\, r} |\phi_i^T \phi_{i,k}^{pn}|^2 |\phi_{i,r}^{pn}|^2 (\sigma_{i,k}^{pn})^2 (\sigma_{i,r}^{pn})^2 \\
&\qquad + 2 \sum_{k,\, r} (\phi_i^T \phi_{i,k}^{pn})(\phi_i^T \phi_{i,r}^{pn})(\phi_{i,r}^{pn})^T \phi_{i,s}^{pn} (\sigma_{i,k}^{pn})^2 (\sigma_{i,r}^{pn})^2 \Bigg) \\
&\Rightarrow \text{(B.25b)} \qquad \square
\end{aligned}
$$

Thus, the asymptotic expected mean of the $\mathsf{M}_{a,i}^{nd}$ in (B.6) equals

$$
\boxed{
\begin{aligned}
\mathsf{M}_{a,i}^{nd} = &\frac{|\phi_i^T \hat{\phi}_i^d|^2 + |\phi_i|^2 (\sigma_i^{mn})^2 + \sum_k |\phi_i^T \phi_{i,k}^{pn}|^2 (\sigma_{i,k}^{pn})^2}{|\phi_i|^2 |\hat{\phi}_i^d|^2 + \bar{p} |\phi_i|^2 (\sigma_i^{mn})^2 + |\phi_i|^2 \sum_k |\phi_{i,k}^{pn}|^2 (\sigma_{i,k}^{pn})^2} \\
&- \frac{2|\phi_i|^2 \sum_k \sum_l (\phi_{i,k}^{pn})^T \phi_{i,l}^{pn} (\phi_i^T \phi_{i,k}^{pn})(\phi_i^T \phi_{i,l}^{pn})(\sigma_{i,k}^{pn})^2 (\sigma_{i,l}^{pn})^2}{\left(|\phi_i|^2 |\hat{\phi}_i^d|^2 + \bar{p} |\phi_i|^2 (\sigma_i^{mn})^2 + |\phi_i|^2 \sum_k |\phi_{i,k}^{pn}|^2 (\sigma_{i,k}^{pn})^2 \right)^2} \\
&- \frac{4|\phi_i|^2 |\phi_i^T \hat{\phi}_i^d|^2 (\sigma_i^{mn})^2 + 4|\phi_i|^2 \phi_i^T \hat{\phi}_i^d \sum_k (\phi_i^T \phi_{i,k}^{pn})(\hat{\phi}_i^d)^T \phi_{i,k}^{pn} (\sigma_{i,k}^{pn})^2}{\left(|\phi_i|^2 |\hat{\phi}_i^d|^2 + \bar{p} |\phi_i|^2 (\sigma_i^{mn})^2 + |\phi_i|^2 \sum_k |\phi_{i,k}^{pn}|^2 (\sigma_{i,k}^{pn})^2 \right)^2} \\
&- \frac{2|\phi_i|^4 (\sigma_i^{mn})^4 + 4|\phi_i|^2 \sum_k |\phi_i^T \phi_{i,k}^{pn}|^2 (\sigma_i^{mn})^2 (\sigma_{i,k}^{pn})^2}{\left(|\phi_i|^2 |\hat{\phi}_i^d|^2 + \bar{p} |\phi_i|^2 (\sigma_i^{mn})^2 + |\phi_i|^2 \sum_k |\phi_{i,k}^{pn}|^2 (\sigma_{i,k}^{pn})^2 \right)^2}
\end{aligned}
} \qquad \text{(B.26)}
$$

• Condition C1:
If the process noise are negligible,

$$
\sigma_{i,k}^{pn} = 0, \quad \forall\, i, \forall\, k \qquad \text{(B.27)}
$$

then the $\mathsf{M}_{a,i}^{nd}$ has unitary upper bound,

$$\mathsf{M}_{a,i}^{nd} \leq 1, \quad \forall\ i \tag{B.28}$$

Proof of (B.28):

$$\begin{aligned}
(\sigma_{i,k}^{pn})^2 =& 0 \quad \forall i, \forall k \quad \Rightarrow \\
\mathsf{M}_{a,i}^{nd} =& \frac{|\phi_i^T \hat{\phi}_i^d|^2 + |\phi_i|^2 (\sigma_i^{mn})^2}{|\phi_i|^2 |\hat{\phi}_i^d|^2 + \bar{p}|\phi_i|^2 (\sigma_i^{mn})^2} \\
& - \frac{2|\phi_i|^4 (\sigma_i^{mn})^4 + 4|\phi_i|^2 |\phi_i^T \hat{\phi}_i^d|^2 (\sigma_i^{mn})^2}{\left(|\phi_i|^2 |\hat{\phi}_i^d|^2 + \bar{p}|\phi_i|^2 (\sigma_i^{mn})^2\right)^2} \leq 1
\end{aligned}$$

since the following inequalities hold:

$$\begin{aligned}
|\phi_i|^2 |\hat{\phi}_i^d|^2 - |\phi_i^T \hat{\phi}_i^d|^2 \geq& 0 \\
\bar{p}|\phi_i|^2 (\sigma_i^{mn})^2 - |\phi_i|^2 (\sigma_i^{mn})^2 \geq& 0 \\
\frac{2|\phi_i|^4 (\sigma_i^{mn})^4 + 4|\phi_i|^2 |\phi_i^T \hat{\phi}_i^d|^2 (\sigma_i^{mn})^2}{\left(|\phi_i|^2 |\hat{\phi}_i^d|^2 + \bar{p}|\phi_i|^2 (\sigma_i^{mn})^2\right)^2} \geq& 0
\end{aligned} \qquad \square$$

Thus: *The* $\mathsf{M}_i^{nd} \leq 1$ *for unmodeled process noise.*

• Condition C2a:
The $\mathsf{M}_{a,i}^{nd}$ is monotonically decreasing in σ_i^{mn}:

$$\frac{\partial\left(\mathsf{M}_{a,i}^{nd}\right)}{\partial(\sigma_i^{mn})^2} < 0, \quad \forall\ i \tag{B.29}$$

if (B.27) holds, and if also

$$|\hat{\phi}_i^d|^2 \left(\bar{p} + 4\right) + \bar{p}\left(\bar{p} - 4\right)(\sigma_i^{mn})^2 > 0, \quad \forall\ i \tag{B.30a}$$

$$\frac{|\phi_i^T \hat{\phi}_i^d|^2}{|\phi_i|^2 |\hat{\phi}_i^d|^2} - \frac{1 + \left(\bar{p} - 4 - 2\bar{p}\frac{(\sigma_i^{mn})^2}{|\hat{\phi}_i^d|^2}\right)\frac{(\sigma_i^{mn})^2}{|\hat{\phi}_i^d|^2}}{\bar{p} + 4 + \bar{p}\left(\bar{p} - 4\right)\frac{(\sigma_i^{mn})^2}{|\hat{\phi}_i^d|^2}} > 0, \quad \forall\ i \tag{B.30b}$$

hold.
Proof of (B.29): define

$$\begin{aligned}
a_1 =& |\phi_i^T \hat{\phi}_i^d|^2 + |\phi_i|^2 (\sigma_i^{mn})^2 \\
a_2 =& 2|\phi_i|^4 (\sigma_i^{mn})^4 + 4|\phi_i|^2 |\phi_i^T \hat{\phi}_i^d|^2 (\sigma_i^{mn})^2 \\
b_d =& |\phi_i|^2 |\hat{\phi}_i^d|^2 + \bar{p}|\phi_i|^2 (\sigma_i^{mn})^2
\end{aligned}$$

which yields

$$\begin{aligned}\frac{\partial a_1}{\partial(\sigma_i^{mn})^2} =& |\phi_i|^2 \\ \frac{\partial a_2}{\partial(\sigma_i^{mn})^2} =& 4|\phi_i|^4(\sigma_i^{mn})^2 + 4|\phi_i|^2|\phi_i^T\hat{\phi}_i^d|^2 \\ \frac{\partial b_d}{\partial(\sigma_i^{mn})^2} =& \bar{p}|\phi_i|^2\end{aligned}$$

Then,

$$\begin{aligned}\frac{\partial \mathsf{M}_{a,i}^{nd}}{\partial(\sigma_i^{mn})^2} =& \frac{b_d^2\dfrac{\partial\ a_1}{\partial(\sigma_i^{mn})^2} - a_1 b_d \dfrac{\partial\ b_d}{\partial(\sigma_i^{mn})^2} - b_d\dfrac{\partial\ a_2}{\partial(\sigma_i^{mn})^2} + 2a_2\dfrac{\partial\ a_1}{\partial(\sigma_i^{mn})^2}}{b_d^4} \\ =& |\phi_i|^6|\hat{\phi}_i^d|^2\Bigg\{|\hat{\phi}_i^d|^2 + \big(\bar{p}-4\big)(\sigma_i^{mn})^2 - 2\bar{p}\frac{(\sigma_i^{mn})^4}{|\hat{\phi}_i^d|^2} \\ & - \frac{|\phi_i^T\hat{\phi}_i^d|^2}{|\phi_i|^2|\hat{\phi}_i^d|^2}\Big(\big(\bar{p}+4\big)|\hat{\phi}_i^d|^2 + \bar{p}\big(\bar{p}-4\big)(\sigma_i^{mn})^2\Big)\Bigg\} < 0\end{aligned}$$

if (B.30a) and (B.30b) holds. $\square$

More convenient, the $\mathsf{M}_{a,i}^{nd}$ is monotonically decreasing in σ_i^{mn}, if (B.27) holds, and if also

$$\bar{p} \geq 4, \quad \text{and} \quad \frac{|\phi_i^T\hat{\phi}_i^d|^2}{|\phi_i|^2|\hat{\phi}_i^d|^2} > \frac{1}{\bar{p}} + \frac{(\sigma_i^{mn})^2}{|\hat{\phi}_i^d|^2}, \quad \forall\ i \tag{B.31}$$

hold.
Proof of (B.31):

$$\big(\bar{p}+4\big)|\hat{\phi}_i^d|^2 + \bar{p}\big(\bar{p}-4\big)(\sigma_i^{mn})^2 > 0 \quad \text{if} \quad \bar{p} \geq 4$$

$$\frac{1 + \Big(\bar{p} - 4 - 2\bar{p}\frac{(\sigma_i^{mn})^2}{|\hat{\phi}_i^d|^2}\Big)\frac{(\sigma_i^{mn})^2}{|\hat{\phi}_i^d|^2}}{\bar{p} + 4 + \bar{p}\big(\bar{p}-4\big)\frac{(\sigma_i^{mn})^2}{|\hat{\phi}_i^d|^2}} < \frac{1}{\bar{p}} + \frac{(\sigma_i^{mn})^2}{|\hat{\phi}_i^d|^2} \qquad \square$$

Thus: *If the process noise are unmodeled: under the conditions in (B.30a) and (B.30b), or under the relaxed conditions in* (B.29)*, the* $\mathsf{M}_{a,i}^{nd}$ *is monotonically decreasing in* σ_i^{mn}*. The relaxed conditions in* (B.29) *are easily fulfilled: the number of modeled sensors* $\bar{p}$ *is often large, and the total amount of measured power* $|\hat{\phi}_i^d|^2$ *generated by the actuators are often considerably higher than the amount of measured noise variance from* $(\sigma_i^{mn})^2$ *for a single sensor.*

• Condition C2b: Is not shown to be fulfilled.

• Condition C3a:
For a high level of measurement noise σ_i^{mn} the $\mathsf{M}_{a,i}^{nd}$ asymptotically converges as

$$\lim_{(\sigma_i^{mn})^2 \to \infty} \mathsf{M}_{a,i}^{nd} = \frac{\bar{p}-2}{\bar{p}^2} < \frac{1}{\bar{p}}, \quad \forall i \tag{B.32}$$

Proof of (B.32): see (B.26). □

Thus: *The* $\mathsf{M}_{a,i}^{nd}$ *is small for high levels of measurement noise, if the numbers of sensors* $\bar{p}$ *is large.*

• Condition C3b:
For a high level of process noise $\sigma_{i,k}^{pn}$, the $\mathsf{M}_{a,i}^{nd}$ asymptotically converges as

$$\lim_{(\sigma_{i,k}^{pn})^2 \to \infty} \mathsf{M}_{a,i}^{nd} = \frac{|\phi_i^T \phi_{i,k}^{pn}|^2 \left(|\phi_i|^2 |\phi_{i,k}^{pn}|^2 - |\phi_i^T \phi_{i,k}^{pn}|^2\right)}{|\phi_i|^4 |\phi_{i,k}^{pn}|^4} \leq \frac{1}{4}, \quad \forall\, i, \forall\, k \tag{B.33}$$

Proof of (B.33): see (B.26). The upper bound follows from the maximum value of $\alpha(1-\alpha) = 1/4$, where $\alpha = |\phi_i^T \phi_{i,k}^{pn}|^2 / |\phi_i|^2 |\phi_{i,k}^{pn}|^2$ in (B.33). □

Thus: *The* $\mathsf{M}_{a,i}^{nd}$ *is small for high levels of process noise.*

• Condition C4:
For low levels of measurement noise and process noise, the $\mathsf{M}_{a,i}^{nd}$ asymptotically converges as

$$\lim_{\substack{(\sigma_i^{mn})^2 \to 0 \\ (\sigma_{i,k}^{pn})^2 \to 0,\ \forall k}} \mathsf{M}_{a,i}^{nd} = \frac{|\phi_i^T \hat{\phi}_i^d|^2}{|\phi_i|^2 |\hat{\phi}_i^d|^2} \tag{B.34}$$

Proof of (B.34): see (B.26). □

Thus: *The* M_a^{nd} *equals the dMAC in* (4.12) *for zero noise levels.*

• Additional property of the $\mathsf{M}_{a,i}^{nd}$:
Define β_i as

$$\beta_i = \min\left\{ \frac{\sum_k |\phi_i|^2 |\phi_{i,k}^{pn}|^2 (\sigma_{i,k}^{pn})^2}{|\hat{\phi}_i^d|^2},\ \frac{\sum_k |\phi_{i,k}^{pn}|^2 (\sigma_{i,k}^{pn})^2}{\bar{p}(\sigma_i^{mn})^2} \right\} \tag{B.35}$$

then

$$\lim_{\substack{\beta_i \to 0 \\ |\phi_i^T \hat{\phi}_i^d| \to 0}} \left|\mathsf{M}_{a,i}^{nd}\right| \leq \frac{\bar{p}+2}{\bar{p}^2} \leq \frac{3}{\bar{p}}, \quad \forall i \tag{B.36}$$

Proof of (B.36): denote,

$$\begin{aligned}\beta_{i,1} =&\frac{\sum_k |\phi_i|^2 |\phi^{pn}_{i,k}|^2 (\sigma^{pn}_{i,k})^2}{|\hat{\phi}^d_i|^2}\\ \beta_{i,2} =&\frac{\sum_k |\phi^{pn}_{i,k}|^2 (\sigma^{pn}_{i,k})^2}{\bar{p}(\sigma^{mn}_i)^2}\\ \varepsilon_i =&\phi_i^T \hat{\phi}^d_i\end{aligned}$$

Assume that $\beta_{i,2} \geq \beta_{i,1}$, then

$$\begin{aligned}\left|\mathsf{M}^{nd}_{a,i}\right| \leq &\frac{\varepsilon_i^2 + |\phi_i|^2(\sigma^{mn}_i)^2 + |\hat{\phi}^d_i|^2\beta_{i,1}}{|\phi_i|^2|\hat{\phi}^d_i|^2 + \bar{p}|\phi_i|^2(\sigma^{mn}_i)^2 + \beta_{i,1}|\hat{\phi}^d_i|^2} +\\ &+ \frac{1}{\left(|\phi_i|^2|\hat{\phi}^d_i|^2 + \bar{p}|\phi_i|^2(\sigma^{mn}_i)^2 + \beta_{i,1}|\hat{\phi}^d_i|^2\right)^2}\Big(2|\phi_i|^4(\sigma^{mn}_i)^4\\ &\quad + 2|\hat{\phi}^d_i|^4\beta_{i,1}^2 + 4|\phi_i|^2(\sigma^{mn}_i)^2\varepsilon_i^2 + 4|\phi_i|^2|\hat{\phi}^d_i|^4\beta_{i,1}\\ &\quad + 4\beta_{i,1}|\phi_i|^2|\hat{\phi}^d_i|^2(\sigma^{mn}_i)^2\Big) \Rightarrow\\ \left|\mathsf{M}^{nd}_{a,i}\right| \to &\frac{|\phi_i|^2(\sigma^{mn}_i)^2}{|\phi_i|^2|\hat{\phi}^d_i|^2 + \bar{p}|\phi_i|^2(\sigma^{mn}_i)^2} + \frac{2|\phi_i|^4(\sigma^{mn}_i)^4}{\left(|\phi_i|^2|\hat{\phi}^d_i|^2 + \bar{p}|\phi_i|^2(\sigma^{mn}_i)^2\right)^2}\\ &\leq \frac{1}{\bar{p}} + \frac{2}{\bar{p}^{\,2}}, \quad \varepsilon_i,\, \beta_{i,1} \to 0\end{aligned} \tag{B.37}$$

Also, assume that $\beta_{i,1} \geq \beta_{i,2}$, then

$$\begin{aligned}\left|\mathsf{M}^{nd}_{a,i}\right| \leq &\frac{\varepsilon_i^2 + |\phi_i|^2(\sigma^{mn}_i)^2 + \bar{p}(\sigma^{mn}_i)^2\beta_{i,2}}{|\phi_i|^2|\hat{\phi}^d_i|^2 + \bar{p}|\phi_i|^2(\sigma^{mn}_i)^2 + \bar{p}(\sigma^{mn}_i)^2\beta_{i,2}} +\\ &+ \frac{1}{\left(|\phi_i|^2|\hat{\phi}^d_i|^2 + \bar{p}|\phi_i|^2(\sigma^{mn}_i)^2 + \bar{p}(\sigma^{mn}_i)^2\beta_{i,2}\right)^2}\Big(\\ &\quad 2|\phi_i|^4(\sigma^{mn}_i)^4 + 2|\phi_i|^2\bar{p}^{\,2}(\sigma^{mn}_i)^4\beta_{i,2}^2 + 4|\phi_i|^2(\sigma^{mn}_i)^2\varepsilon_i^2\\ &\quad + 4\bar{p}|\phi_i|^2(\sigma^{mn}_i)^2\left(|\hat{\phi}^d_i|^2 + (\sigma^{mn}_i)^2\right)\beta_{i,2}\Big) \Rightarrow\\ \left|\mathsf{M}^{nd}_{a,i}\right| \to &\frac{|\phi_i|^2(\sigma^{mn}_i)^2}{|\phi_i|^2|\hat{\phi}^d_i|^2 + \bar{p}|\phi_i|^2(\sigma^{mn}_i)^2} + \frac{2|\phi_i|^4(\sigma^{mn}_i)^4}{\left(|\phi_i|^2|\hat{\phi}^d_i|^2 + \bar{p}|\phi_i|^2(\sigma^{mn}_i)^2\right)^2}\\ &\leq \frac{1}{\bar{p}} + \frac{2}{\bar{p}^{\,2}}, \quad \varepsilon_i,\, \beta_{i,2} \to 0\end{aligned} \tag{B.38}$$

Therefore, since $\beta_i = \min\{\beta_{i,1}, \beta_{i,2}\}$, (B.37) and (B.38) give (B.36). □

Thus: *If β_i in* (B.35) *is small, then the $\mathsf{M}_{a,i}^{nd}$ is also small. For instance, if the total amount of measured measurement noise variance $\bar{p}\cdot(\sigma_i^{mn})^2$ is considerably larger than the total amount of measured process noise variance $\sum_k |\phi_{i,k}^{pn}|^2(\sigma_{i,k}^{pn})^2$, and if $\bar{p}$ is large, then the dMAC is low.*

Notice: The conditions C1-C4 are fulfilled only for unmodeled process noise. For unmodeled process noise, the approximated ndMAC $\mathsf{M}_{a,i}^{nd}$ equals $\mathsf{M}_{a,i}^{md}$:

$$\boxed{\mathsf{M}_{a,i}^{md} = \frac{|\phi_i^T\hat{\phi}_i^d|^2 + |\phi_i|^2(\sigma_i^{mn})^2}{|\phi_i|^2|\hat{\phi}_i^d|^2 + \bar{p}|\phi_i|^2(\sigma_i^{mn})^2} - \frac{2|\phi_i|^4(\sigma_i^{mn})^4 + 4|\phi_i|^2|\phi_i^T\hat{\phi}_i^d|^2(\sigma_i^{mn})^2}{\left(|\phi_i|^2|\hat{\phi}_i^d|^2 + \bar{p}|\phi_i|^2(\sigma_i^{mn})^2\right)^2}} \tag{B.39}$$

B.3 Properties of the $\mathsf{M}_{b,i}^{nd}$

Defining

$$\mathsf{M}_{b,i}^{nd} = \frac{\mathrm{E}[T]}{\mathrm{E}[D]} \tag{B.40}$$

an approximation of the M_i^{nd} in (B.6) is achieved, compare with (B.8). Evaluating (B.40), it is readily seen that

$$\boxed{\mathsf{M}_{b,i}^{nd} = \frac{|\phi_i^T\hat{\phi}_i^d|^2 + |\phi_i|^2(\sigma_i^{mn})^2 + \sum_k |\phi_i^T\phi_{i,k}^{pn}|^2(\sigma_{i,k}^{pn})^2}{|\phi_i|^2|\hat{\phi}_i^d|^2 + \bar{p}|\phi_i|^2(\sigma_i^{mn})^2 + |\phi_i|^2\sum_k |\phi_{i,k}^{pn}|^2(\sigma_{i,k}^{pn})^2}} \tag{B.41}$$

which equals the first term of the $\mathsf{M}_{a,i}^{nd}$ in (B.26).

• Condition C1:
The $\mathsf{M}_{b,i}^{nd}$ has an unitary upper bound,

$$\mathsf{M}_{b,i}^{nd} \leq 1, \quad \forall\, i \tag{B.42}$$

Proof of (B.42): since

$$\begin{aligned}
|\phi_i^T\hat{\phi}_i^d|^2 &\leq |\phi_i|^2|\hat{\phi}_i^d|^2 \\
|\phi_i|^2(\sigma_i^{mn})^2 &\leq \bar{p}|\phi_i|^2(\sigma_i^{mn})^2 \\
\sum_k |\phi_i^T\phi_{i,k}^{pn}|^2(\sigma_{i,k}^{pn})^2 &\leq |\phi_i|^2\sum_k |\phi_{i,k}^{pn}|^2(\sigma_{i,k}^{pn})^2
\end{aligned}$$

the numerator is not greater than the denominator in (B.41). □

Thus: *The upper bound of* $\mathsf{M}_{b,i}^{nd}$ *is unitary.*

• Condition C2a:
If

$$\frac{|\phi_i^T \hat{\phi}_i^d|^2}{|\phi_i|^2 |\hat{\phi}_i^d|^2} > \frac{1}{\bar{p}}\left(1 + \frac{\sum_k |\phi_{i,k}^{pn}|^2 (\sigma_{i,k}^{pn})^2}{|\hat{\phi}_i^d|^2}\right) - \frac{\sum_k |\phi_i^T \phi_{i,k}^{pn}|^2 (\sigma_{i,k}^{pn})^2}{|\phi_i|^2 |\hat{\phi}_i^d|^2} \tag{B.43}$$

then $\mathsf{M}_{b,i}^{nd}$ is monotonically decreasing in σ_i^{mn},

$$\frac{\partial \left(\mathsf{M}_{b,i}^{nd}\right)}{\partial (\sigma_i^{mn})^2} < 0 \tag{B.44}$$

Proof of (B.44):

$$\frac{\partial \mathsf{M}_{b,i}^{nd}}{\partial (\sigma_i^{mn})^2} = \frac{|\phi_i|^2 \left(|\phi_i|^2 |\hat{\phi}_i^d|^2 + (|\phi_i|^2 - \bar{p}) \sum_k |\phi_{i,k}^{pn}|^2 (\sigma_{i,k}^{pn})^2 - \bar{p} |\phi_i^T \hat{\phi}_i^d|^2\right)}{\left(|\phi_i|^2 |\hat{\phi}_i^d|^2 + |\phi_i|^2 \bar{p} (\sigma_i^{mn})^2 + |\phi_i|^2 \sum_k |\phi_{i,k}^{pn}|^2 (\sigma_{i,k}^{pn})^2\right)^2} \Rightarrow$$

$$\frac{\partial \left(\mathsf{M}_{b,i}^{nd}\right)}{\partial (\sigma_i^{mn})^2} < 0 \quad \text{if} \quad \text{(B.43)} \quad \text{holds.}$$ □

Thus: *Under the mild condition in* (B.43) *the* $\mathsf{M}_{b,i}^{nd}$ *is monotonically decreasing in the measurement noise level* σ_i^{mn}*. It is sufficient that the actuators are capable to excite the structure, and that the number of modeled sensors* $\bar{p}$ *only are a fraction of the number of sensor* p *available in the real measurements, for* (B.44) *to hold.*

• Condition C2b:
If

$$\frac{|\phi_i^T \hat{\phi}_i^d|^2}{|\phi_i|^2 |\hat{\phi}_i^d|^2} > \frac{|\phi_i^T \phi_{i,l}^{pn}|^2}{|\phi_i|^2 |\phi_{i,l}^{pn}|^2}\left(1 + \frac{\bar{p}(\sigma_i^{mn})^2}{|\hat{\phi}_i^d|^2} + \frac{\sum_k |\phi_{i,k}^{pn}|^2 (\sigma_{i,k}^{pn})^2}{|\hat{\phi}_i^d|^2}\right) \tag{B.45}$$

then $\mathsf{M}_{b,i}^{nd}$ is monotonically decreasing in $\sigma_{i,l}^{pn}$,

$$\frac{\partial \left(\mathsf{M}_{b,i}^{nd}\right)}{\partial (\sigma_{i,l}^{pn})^2} < 0 \tag{B.46}$$

Proof of (B.46):

$$\frac{\partial\left(\mathsf{M}_{b,i}^{nd}\right)}{\partial(\sigma_{i,l}^{pn})^2} = \frac{1}{\left(|\phi_i|^2|\hat{\phi}_i^d|^2 + \bar{p}|\phi_i|^2(\sigma_i^{mn})^2 + |\phi_i|^2\sum_k |\phi_{i,k}^{pn}|^2(\sigma_{i,k}^{pn})^2\right)^2}\Bigg($$

$$|\phi_i|^2|\phi_i^T\hat{\phi}_i^d|^2|\hat{\phi}_i^d|^2 + \bar{p}|\phi_i|^2|\phi_i^T\phi_{i,l}^{pn}|^2(\sigma_i^{mn})^2$$

$$+ |\phi_i|^2|\phi_i^T\phi_{i,l}^{pn}|^2\sum_k |\phi_{i,k}^{pn}|^2(\sigma_{i,k}^{pn})^2 - |\phi_i|^2|\phi_i^T\hat{\phi}_i^d|^2|\phi_{i,l}^{pn}|^2$$

$$- |\phi_i|^4|\phi_{i,l}^{pn}|^2(\sigma_i^{mn})^2 - |\phi_i|^2|\phi_{i,l}^{pn}|^2\sum_k |\phi_i^T\phi_{i,k}^{pn}|^2(\sigma_{i,k}^{pn})^2\Bigg) \Rightarrow$$

$$\frac{\partial\left(\mathsf{M}_{b,i}^{nd}\right)}{\partial(\sigma_{i,l}^{pn})^2} < 0 \quad \text{if} \quad \text{(B.45)} \quad \text{holds.} \qquad \square$$

Thus: *Under the condition in* (B.45)*, the* $\mathsf{M}_{b,i}^{nd}$ *is monotonically decreasing in the process noise level* $\sigma_{i,k}^{pn}$*. It is sufficient that the actuators are more capable than the process noise sources to excite the structure, and that the total amount of measured noise power is low in comparison with the measured power arising from the actuators.*

• ConditionC3a:
For high measurement noise variance level, the $\mathsf{M}_{b,i}^{nd}$ converges as

$$\lim_{(\sigma_i^{mn})^2\to\infty} \mathsf{M}_{b,i}^{nd} = \frac{1}{\bar{p}}, \quad \forall\, i \tag{B.48}$$

Proof of (B.48): compare with (B.41). □

Thus: *For high noise levels the* $\mathsf{M}_{b,i}^{nd}$ *converges to the low value* $1/\bar{p}$*.*

• Condition C3b:
For high process noise variance level, the $\mathsf{M}_{b,i}^{nd}$ converges as

$$\lim_{(\sigma_{i,k}^{pn})^2\to\infty} \mathsf{M}_{b,i}^{nd} = \frac{|\phi_i^T\phi_{i,k}^{pn}|^2}{|\phi_i|^2|\phi_{i,k}^{pn}|^2}, \quad \forall i, \forall k \tag{B.49}$$

Proof of (B.49): compare with (B.41). □

Thus: *The* $\mathsf{M}_{b,i}^{nd}$ *converges to the dMAC corresponding to the case where the noise sources are viewed as the actuators.*

• Condition C4:
For low noise variance levels, the $\mathsf{M}_{b,i}^{nd}$ converges as

$$\lim_{\substack{(\sigma_i^{mn})^2 \to 0 \\ (\sigma_{i,k}^{pn})^2 \to 0,\ \forall k}} \mathsf{M}_{b,i}^{nd} = \frac{|\phi_i^T \hat{\phi}_i^d|^2}{|\phi_i|^2 |\hat{\phi}_i^d|^2}, \quad \forall i \tag{B.50}$$

Thus: *The* $\mathsf{M}_{b,i}^{nd}$ *equals the dMAC for zero noise levels.*

Notice: in order to secure that the actuator locations are properly chosen, the modeled process noise sources should not be able to excite the mode too accurate, i.e., the limiting value in (B.49), should be

$$\lim_{(\sigma_{i,k}^{pn})^2 \to \infty} \mathsf{M}_{b,i}^{nd} = \frac{|\phi_i^T \phi_{i,k}^{pn}|^2}{|\phi_i|^2 |\phi_{i,k}^{pn}|^2} \not\approx 1, \quad \forall i, \forall k \tag{B.51}$$

Otherwise, a criterion based on the estimate $\hat{\phi}_i^{nd}$ of ϕ_i may determine actuator locations from their ability to cooperate with the modeled process noise sources.

Bibliography

[1] T. Abrahamsson, M. Andersson, and T. McKelvey. A finite element model updating formulation using frequency responses and eigenfrequencies. In *Second International Conference on Structural Dynamics Modelling - Test, Analysis and Correlation*, pages 293–305. DTA/NAFEMS, July 1996.

[2] R. Allemang and D. Brown. A correlation coefficient for modal vector analysis. In *Proc. 1st International Modal Analysis Conference*, pages 110–116, 1982.

[3] E. Balmès. A finite element updating procedure using frequency response functions. Applications to the MIT/SERC interferometer testbed. In *Proceedings of the 11th International Modal Analysis Conference*, pages 176–182, 1993.

[4] K.-J. Bathe. *Finite Element Procedures in Engineering Analysis*. Prentice-Hall, 1982.

[5] Å. Björck. *Numerical Methods for Least Squares Problems*. SIAM, 1996.

[6] T. K. Caughey. Classical normal modes in damped linear dynamic systems. *Journal of Applied Mechanics*, pages 269–271, June 1960.

[7] R. D. Cook, D. S. Malkus, and M. E. Plesha. *Concepts and Applications of Finite Element Modeling*. Wiley, 1989.

[8] E. Dascotte. Applications of finite element model tuning using experimental modal data. *Journal of Sound and Vibration*, June 1991.

[9] L. Eckert and B. Caesar. Model updating under incomplete and noisy modal test data. In *Proc. of 9th International Modal Analysis Conference*, pages 563–571, 1991.

[10] D. J. Ewins. *Modal Testing: Theory and Practice.* Research Studies Press, John Wiley, 1984.

[11] R. Fletcher. *Practical Methods of Optimization.* Wiley, 1987.

[12] M. I. Friswell and J. E. Mottershead. *Finite Element Model Updating in Structural Dynamics.* Kluwer, 1995.

[13] K. Godfrey, editor. *Perturbation Signals for System Identification.* Prentice Hall, 1993.

[14] M. Géradin and D. Rixen. *Mechanical Vibrations - Theory and Application to Structural Dynamics.* Wiley, 1994.

[15] A. Graham. *Kronecker Products and Matrix Calculus: with Applications.* Wiley, 1981.

[16] X. Guangqian and P. M. Bainum. Actuator placement using degree of controllability for discrete-time systems. *Trans. of the ASME*, 114:508–516, September 1992.

[17] R. T. Haftka, Z. Gürdal, and M. P. Kamat. *Elements of Structural Optimization.* Kluwer, 2nd edition, 1989.

[18] T. K. Hasselman. Method for constructing a full modal damping matrix from experimental measurements. *AIAA Journal*, 10(4):526–527, 1972.

[19] P. S. Holmes, J. R. Wright, and J. E. Cooper. Optimum exciter placement for normal mode force appropriation using an a priori model. In *Proc. 14th International Modal Conference*, 1996.

[20] S. R. Ibrahim. Correlation and updating methods: Finite element dynamic model and vibration test data. pages 323–347. DTA/NAFEMS, 1993.

[21] D. C. Kammer. Sensor placement for on-orbit modal identification and correlation of large space structures. *Journal of Guidance, Control and Dynamics*, 14(2):251–259, March-April 1991.

[22] S. Lammens. *Frequency Response Based Validation of Dynamic Structural Finite Element Models.* PhD thesis, Katholieke Universiteit Leuven, Celestijnenlaan 300B, 3001 Leuven (Heverlee), Belgium, September 1995.

[23] P.-O. Larsson and P. Sas. Model updating on forced vibrations testing using numerically stable formulations. In *Proceedings of the 10th International Modal Analysis Conference*, pages 966–974, February 1992.

[24] N. A. J. Lieven. Spatial correlation of mode shapes, the coordinate model assurance criterion. In *Proc. 6th International Modal Analysis Conference*, pages 690–695, February 1988.

[25] L. Ljung. *System Identification - Theory for the User.* Prentice-Hall, 1987.

[26] R. R. Craig, Jr. *Structural Dynamics. An Introduction to Computer Methods.* Wiley, 1981.

[27] T. McKelvey. *Identification of State-Space Models from Time and Frequency Data.* PhD thesis, Linköping University, Dept. of Electr. Eng., Linköping University, 581 83 Linköping, May 1995.

[28] J. J. Moré. Recent developments inalgorithms and software for trust region methods. In A. Bachem, M. Grötchel, and B. Korte, editors, *Mathematical Programming. The State of the Art*, pages 258–287. Springer-Verlag, 1983.

[29] J. E. Mottershead and M. I. Friswell. Model updating in structural dynamics: A survey. *Journal of Sound and Vibration*, 167(2):347–375, 1993.

[30] P. C. Müller and H. I. Weber. Analysis and optimization of certain qualities of controllability and observability for linear dynamical systems. *Automatica*, 8:237–246, 1972.

[31] A. D. Nashif, D. I. G. Jones, and J. P. Henderson. *Vibration Damping.* Wiley, 1985.

[32] J. O'Callahan. Comparison of reduced model concepts. In *Proceedings of the International Modal Analysis Conference*, pages 422–430, 1990.

[33] N. Saabye Ottosen and H. Petersson. *Introduction to the Finite Element Method.* Reprocentralen, Lund University, second edition, 1991.

[34] A. Papoulis. *Probability, Random Variables, and Stochastic Processes.* McGraw-Hill, 3rd edition, 1991.

[35] S. Park, I. Park, and F. Ma. Decoupling approximation of nonclassically damped structures. *AIAA Journal*, 30(9):2348–2351, 1992.

[36] J. Piranda, G. Lallement, and S. Cogan. Parametric correction of finite element models by minimization of an output residual: Improvement of the sensitivity method. In *Proc. of 9th International Modal Analysis Conference*, pages 363–368, 1991.

[37] J. S. Przemieniecki. *Theory of Matrix Structural Analysis.* McGraw-Hill, 1968.

[38] W. J. Rugh. *Linear System Theory, Second Edition.* Prentice Hall, second edition, 1996.

[39] L. E. Scales. *Introduction to Non-Linear Optimization.* Macmillan, 1985.

[40] P. C. Shah and F. E. Udwadia. A methodology for optimal sensor locations for identification of dynamic systems. *Journal of Applied Mechanics*, 45:188–196, March 1978.

[41] J. Sjöberg. *Non-Linear System Identification with Neural Networks.* PhD thesis, Linköping University, Dept. of Electr. Eng., Linköping University, 581 83 Linköping, May 1995.

[42] S. W. Smith and C. A. Beattie. Secant method matrix adjustments for structural models. In *Proceedings of the 30th Structures, Structural Dynamics and Materials Conference*. AIAA, 1989.

[43] M. Soni. Finite element procedure in damping design. In *Proceedings of the 14th Inernational Seminar on Modal Analysis*, pages 8.1.1–8.1.48, Leuven, 1989.

[44] S. P. Timoshenko and J. M. Gere. *Mechanics of Materials.* Van Nostrand Reinhold, 1972.

[45] W. J. Visser. *Updating Structural Dynamic Models using Frequency Response Data.* PhD thesis, Department of Mechanical Engineering, Imperial College of Science, Technology and Medicine, London SW7, England, September 1992.

[46] R. Williams, J. Crowley, and H. Vold. The multivariate mode indicator function in modal analysis. In *Proceedings of the 3rd International Modal Analysis Conference*, pages 66–70, 1985.

[47] M. A. Wolfe. *Numerical Methods for Unconstrained Optimization-an introduction.* Van Nostrand Reinhold, 1978.

[48] K. Zhou, J.C. Doyle, and K. Glover. *Robust and Optimal Cotrol.* Prentice-Hall, 1996.